Effect of Global Sea Level Rise over the Near, Intermediate and Long-Term on Tsunami Waves at the Seal Cove Coast Guard Station in Northwestern British Columbia

Richard Thomson, Alexander Rabinovich, Lauren Lupton, Stephen Mundschutz and Nicky Hastings

Fisheries and Oceans Canada
Institute of Ocean Sciences
9860 West Saanich Road
Sidney, BC V8L 4B2

2023

Canadian Technical Report of
Hydrography and Ocean Sciences 361

Fisheries and Oceans Canada | Pêches et Océans Canada

Canada

Canadian Technical Report of Hydrography and Ocean Sciences

Technical reports contain scientific and technical information of a type that represents a contribution to existing knowledge, but which is not normally found in the primary literature. The subject matter is generally related to programs and interests of the Oceans and Science sectors of Fisheries and Oceans Canada.

Technical reports may be cited as full publications. The correct citation appears above the abstract of each report. Each report is abstracted in the data base Aquatic Sciences and Fisheries Abstracts.

Technical reports are produced regionally but are numbered nationally. Requests for individual reports will be filled by the issuing establishment listed on the front cover and title page.

Regional and headquarters establishments of Ocean Science and Surveys ceased publication of their various report series as of December 1981. A complete listing of these publications and the last number issued under each title are published in the Canadian Journal of Fisheries and Aquatic Sciences, Volume 38: Index to Publications 1981. The current series began with Report Number 1 in January 1982.

Rapport technique canadien sur l'hydrographie et les sciences océaniques

Les rapports techniques contiennent des renseignements scientifiques et techniques qui constituent une contribution aux connaissances actuelles mais que l'on ne trouve pas normalement dans les revues scientifiques. Le sujet est généralement rattaché aux programmes et intérêts des secteurs des Océans et des Sciences de Pêches et Océans Canada.

Les rapports techniques peuvent être cités comme des publications à part entière. Le titre exact figure au-dessus du résumé de chaque rapport. Les rapports techniques sont résumés dans la base de données Résumés des sciences aquatiques et halieutiques.

Les rapports techniques sont produits à l'échelon régional, mais numérotés à l'échelon national. Les demandes de rapports seront satisfaites par l'établissement auteur dont le nom figure sur la couverture et la page de titre.

Les établissements de l’ancien secteur des Sciences et Levés océaniques dans les régions et à l'administration centrale ont cessé de publier leurs diverses séries de rapports en décembre 1981. Vous trouverez dans l'index des publications du volume 38 du Journal canadien des sciences halieutiques et aquatiques, la liste de ces publications ainsi que le dernier numéro paru dans chaque catégorie. La nouvelle série a commencé avec la publication du rapport numéro 1 en janvier 1982.

Canadian Technical Report of
Hydrography and Ocean Sciences 361

2023

EFFECT OF GLOBAL SEA LEVEL RISE OVER THE NEAR, INTERMEDIATE AND LONG-TERM ON TSUNAMI WAVES AT THE SEAL COVE COAST GUARD STATION IN NORTHWESTERN BRITISH COLUMBIA

Richard Thomson[1], Alexander Rabinovich[1], Lauren Lupton[1], Stephen Mundschutz[1], and Nicky Hastings[2]

[1]Fisheries and Oceans Canada
Institute of Ocean Sciences
9860 West Saanich Road
Sidney, BC V8L 4B2

[2]Natural Resources Canada
Geological Survey of Canada - Pacific Division
605 Robson Street
Vancouver, BC V6B 5J3

© His Majesty the King in Right of Canada, as represented by the Minister of the Department of Fisheries and Oceans, 2023

Cat. No.: Fs97-18/361E-PDF ISBN 978-0-660-68319-5 ISSN 1488-5417

Correct citation for this publication:

Thomson, R., Rabinovich, A., Lupton, L., Mundschutz, S., and Hastings, N., 2023. Effect of global sea level rise over the near, intermediate and long-term on tsunami waves at the Seal Cove Coast Guard Station in northwestern British Columbia. Can. Tech. Rep. Hydrogr. Ocean Sci. 361: v + 75 p.

CONTENTS

ABSTRACT

Thomson, R., Rabinovich, A., Lupton, L., Mundschutz, S., and Hastings, N., 2023. Effect of global sea level rise over the near, intermediate and long-term on tsunami waves at the Seal Cove Coast Guard Station in northwestern British Columbia. Can. Tech. Rep. Hydrogr. Ocean Sci. 361: v + 75 p.

The coast of British Columbia is susceptible to flooding and strong currents from trans-oceanic tsunamis. Global sea level rise and vertical tectonic land motions further compound the effects of future tsunamigenic events. The present study centres on the Seal Cove Coast Guard Station and environ located in Prince Rupert Harbour. We examine historical tsunamis observed at this location and the results of numerical modelling of the two potentially most dangerous Seal Cove tsunamis – a 1964-type Alaska and a 1700-type Cascadia Subduction Zone (CSZ) tsunami – and estimate the risk for the region taking into account vertical tectonic motion and climatic sea level change.

Of the seven major tsunamis recorded between 1909 and 2021, only the 1964 event caused hazardous conditions in the Prince Rupert area. Centuries earlier, the magnitude M_w = 9.0 CSZ earthquake of 26 January 1700 generated a trans-oceanic tsunami that also strongly affected the British Columbia coast. Such an event is likely to occur again sometime in the next 500 to 700 years.

Based on reports by the United Nations Intergovernmental Panel on Climate Change (IPCC), *James et al.* [2015; 2021] and *Lemmen et al.* [2016] examined sea level rise in western Canada that takes into account both climatic effects and vertical tectonic motions for *low, moderate* and *high* global sea level rise scenarios. These findings enabled us to estimate the effect that sea-level changes will have on future tsunamis impacting the entire British Columbia coast. Detailed results focus on the Seal Cove Coast Guard Station in the northwest corner of the province.

RÉSUMÉ

Thomson, R., Rabinovich, A., Lupton, L., Mundschutz, S., and Hastings, N., 2023. Effect of global sea level rise over the near, intermediate and long-term on tsunami waves at the Seal Cove Coast Guard Station in northwestern British Columbia. Can. Tech. Rep. Hydrogr. Ocean Sci. 361: v + 75 p.

La côte de la Colombie-Britannique est vulnérable aux inondations et aux forts courants provoqués par les tsunamis transocéaniques. L'élévation du niveau de la mer à l'échelle mondiale et les mouvements tectoniques verticaux des terres aggravent encore les effets des futurs événements tsunamigènes. La présente étude porte sur la station de la Garde côtière de Seal Cove et ses environs situés dans le port de Prince Rupert. Nous examinons les tsunamis historiques observés à cet endroit et les résultats de la modélisation numérique des deux tsunamis de Seal Cove potentiellement les plus dangereux – un tsunami de type 1964 en Alaska et un tsunami de type 1700 dans la zone de subduction de Cascadia (CSZ) – et estimons le risque pour la région en prenant en compte le mouvement tectonique vertical et le changement climatique du niveau de la mer.

Parmi les sept tsunamis majeurs enregistrés entre 1909 et 2021, seul celui de 1964 a provoqué des conditions dangereuses dans la région de Prince Rupert. Des siècles plus tôt, le séisme de magnitude M_w = 9,0 CSZ du 26 janvier 1700 avait généré un tsunami transocéanique qui avait également fortement touché la côte de la Colombie-Britannique. Un tel événement est susceptible de se reproduire dans les 500 à 700 prochaines années.

Sur la base des rapports du Groupe d'experts intergouvernemental sur l'évolution du climat (GIEC) des Nations Unies, *James et al.* [2015; 2021] et *Lemmen et al.* [2016] ont examiné l'élévation du niveau de la mer dans l'ouest du Canada en tenant compte à la fois des effets climatiques et des mouvements tectoniques verticaux pour des scénarios d'élévation mondiale du niveau de la mer faibles, modérés et élevés. Ces résultats nous ont permis d'estimer l'effet qu'auront les changements du niveau de la mer sur les futurs tsunamis touchant l'ensemble de la côte de la Colombie-Britannique. Les résultats détaillés se concentrent sur la station de la Garde côtière de Seal Cove, dans le nord-ouest de la province.

1. INTRODUCTION

Large segments of the British Columbia coast are susceptible to tsunamis generated by major earthquakes within the Pacific Ocean and by local underwater earthquakes. The catastrophic tsunamis of the last two decades, including the 2004 Sumatra, 2010 Chile and 2011 Tohoku events, as well as two recent 2018 tsunamis in Indonesia (Sulawesi and Anak-Krakatau), demonstrate the serious threat of major seismically generated tsunamis to various regions of the world's oceans, including coastal communities in northern British Columbia, in particular the area of Seal Cove and Prince Rupert Harbour [cf. *Leonard et al.*, 2014]. The northern part of Hecate Strait is partially sheltered from tsunami waves incoming from the open ocean; nevertheless, tsunamis from major events (e.g., the 1964 Alaska and 2011 Tohoku tsunamis) have penetrated into the region where they have been recorded by CHS and NOAA tide gauges. The 1964 Alaska ("Good Friday") earthquake (M_w 9.2)

produced the strongest tsunami response ever observed on the coast of British Columbia and caused significant damage in Prince Rupert Harbour [cf. *Rabinovich et al.*, 2019a, 2019b].

Rabinovich et al. [2019a] accumulated all available archive and mareographic information and data to define the tsunami threat to the Seal Cove Coast Guard Station. In particular, they found that at Prince Rupert only eight tsunamis, mainly associated with earthquakes of magnitude 8.6 or greater, have been recorded over the entire observational period. Observations suggest that, prior to reaching Prince Rupert, high frequency waves are dampened or filtered out by the shallow water topography as they propagate through Dixon Entrance and across the shelf. On the other hand, paleotsunami evidence suggests that Seal Cove is at risk from CSZ-generated tsunamis.

A major tsunami generated in the Cascadia Subduction Zone (CSZ) deserves specific attention. The Great CSZ earthquake of 26 January 1700, with an estimated magnitude M_w 9.0, formed a massive trans-oceanic tsunami that caused significant destruction in Japan on the opposite side of the Pacific Ocean [cf. *Atwater et al.,* 2005], and strongly affected the outer coast of British Columbia. Paleotsunami findings in the coastal zone of Vancouver Island [cf. *Clague et al*., 2000, 2003] show that tsunami waves of ~15 m likely struck this coast at the time of the 1700 CSZ event.

Vertical tectonic motions and changing climate are crucial factors that contribute to significant regional and global sea level variations and, in this way, can substantially increase the risk of marine sea level hazards impacting the coastal regions of British Columbia. The global climatic effects include changes in air and water temperature, precipitation patterns, wave climate, sea ice, hydrology (including glacier melting) and ocean-water properties (e.g., salinity and density). These changes exacerbate existing risks and bring new challenges to coastal engineers and emergency response managers.

Several observational and numerical modelling studies have been conducted recently on various types of natural hazards for the coast of northern British Columbia, including the area of Seal Cove and Prince Rupert Harbour. *Fine et al.* [2018a, 2018b] numerically simulated the 1964 Great Alaska and the 1700 Cascadia Subduction Zone (CSZ) tsunamis, focussing on the region of Seal Cove. *Rabinovich et al.* [2019] collected all available observations, modelling results and other information to estimate the main statistical

parameters of five major trans-oceanic tsunamis during the “recent” observational period (1946, 1952, 1957, 1960 and 1964) along the coast of British Columbia, including Prince Rupert and other tide gauge stations located nearby.

In recent years, the United Nations Intergovernmental Panel on Climate Change (IPCC) published several reports, in particular the 2019 ICPC Special Report on the Ocean and Cryosphere in a Changing Climate (SROCC) with a specific Chapter 4 on sea level rise [*Oppenheimer and Glavovic*, 2019]. Also, *James et al.* [2015, 2021] and *Lemmen et al.* [2016] prepared special reports considering sea level rise in western Canada that takes into account both global climatic sea level rise and vertical tectonic motions on the coast of British Columbia. *Rabinovich and Thomson* [2020] evaluated vertical tectonic motions and changing sea levels along the southeastern coast of Vancouver Island for *low, moderate* and *high* global sea level rise scenarios; the corresponding findings were used to estimate expected coastal flooding due to major trans-oceanic tsunamis and other marine hazards for that coast, focussing on the Canadian Coast Guard Station in Victoria.

The purpose of the present report is to summarize previous findings and to examine changes to the existing estimates of coastal flooding to the Canadian Coast Guard Station in Seal Cove due to major trans-oceanic tsunamis and sea level rise. In Section 2, we estimate the tsunami risk for Prince Rupert and Seal Cove based on all available observational data for the period of 1910-2020. Section 3 examines the main modelling results of *Fine et al.* [2018a, 2018b] for the 1964 Alaska and the 1700 CSZ tsunamis for the Seal Cove area. In Section 4, we consider sea level rise for Sea Cove caused by the combined effect of climate change and vertical tectonic motions. The results of Sections 3 and 4 are merged in Section 5, while the general conclusions are given in Section 6.

2. SEAL COVE AND PRINCE RUPERT: HISTORICAL AND RECENT TSUNAMIS

Seal Cove is located adjacent to Prince Rupert, British Columbia, Canada, close to southeastern Alaska, i.e., to the USA/Canada border (Figure 1). The Seal Cove Water Airport is actively used by Inland Air, Vancouver Island Helicopters and White River Helicopters. It is classified as an airport of entry by Nav. Canada and is controlled by the Canada Border Services Agency.

Prince Rupert has a population of roughly 12,500 and this port is the land, air, and water transportation hub for British Columbia's North Coast. Situated on Kaien Island, the city lies just north of the mouth of the Skeena River and is linked by a short bridge to the mainland. The city is located along the island's northwestern shore, fronting on Prince Rupert Harbour.

Although detailed tsunami zoning for Seal Cove and Prince Rupert areas is only possible through numerical modelling of the entire region (which is the topic of a separate project [Fine et al., 2018a,b]), some preliminary estimates can be obtained based on historical data and the information on tsunamis and earthquakes observed in this region [cf. *Rabinovich et al.*, 2019a]. There are three main sources of information on historical tsunamis in this region: (1) Paleotsunami studies; (2) Archived material, local newspapers, magazines, and existing tsunami catalogues; and (3) Tide gauge records and other instrumental data.

Paleo-examination of tsunami waves is an effective method for identifying historical tsunamis and for estimating actual onshore run-up heights [cf. *Clague et al.,* 2000, 2003; *Wang et al*., 2013]. Unfortunately, detailed paleotsunami studies in the vicinity of Prince Rupert and in northern British Columbia began only recently [*Peter Bobrovsky*, 2017; Pers. Comm.], and no results are yet available.

Tsunami catalogues give crucial information about historical tsunamis. In this study, we have used catalogues by Lander [1996] and *Stephenson et al.* [2007] and also recent papers on tsunami occurrences along the coast of British Columbia [*Stephenson and Rabinovich*, 2009; *Rabinovich et al.*, 2013, 2019b; *Fine et al.,* 2015]. We have also examined local newspapers for major tsunami events that occurred in the Pacific Ocean, in particular for information on the 1946 Aleutian, 1952 Kamchatka, 1957 Andreanof Islands, 1960 Chile and 1964 Alaska tsunamis. The only information in newspapers for these events in the Prince Rupert region is for the 1964 tsunami, the strongest tsunami recorded at Prince Rupert [*Prince Rupert Daily News*, 1964].

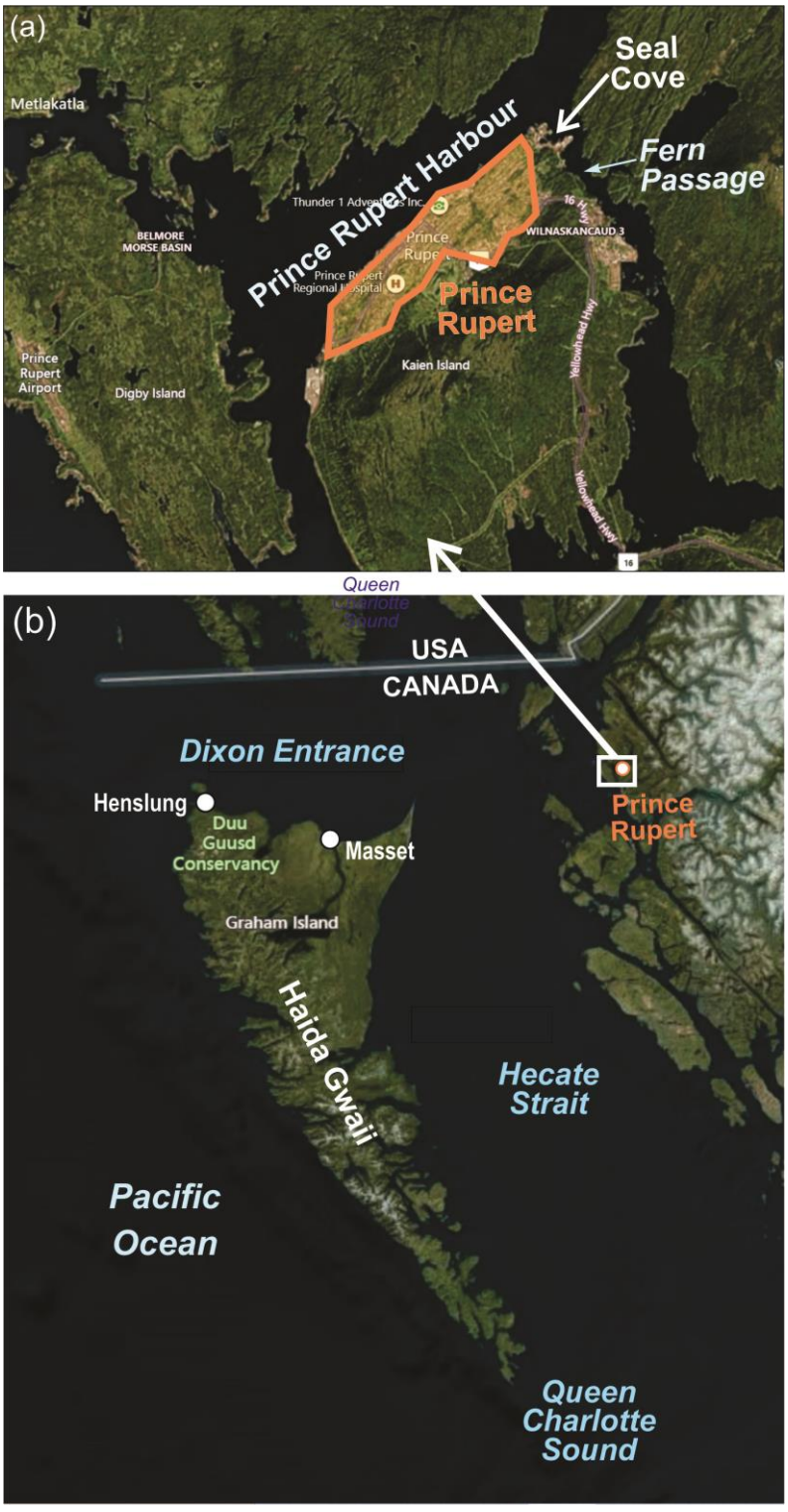

Figure 1. Maps showing the areas of (a) Seal Cove/Prince Rupert Harbour and (b) Haida Gwaii, Dixon Entrance and Hecate Strait; white circles indicate locations of Canadian Hydrographic Service (CHS) tide gauge stations at Henslung and Masset.

The most useful information on historical tsunamis is obtained from the analysis of tide gauge records. Although there is no tide gauge at Seal Cove, there is an instrument at Prince Rupert, located only a few kilometres to the southwest (Figure 1). This gauge can be used effectively to obtain preliminary estimates of tsunami occurrence in this region.

2.1. TIDE GAUGE OBSERVATIONS

The Prince Rupert tide gauge has been operational since 1909 and has one of the longest records for the Pacific coast of Canada. Tsunami observations at this station for the period of 1909-2006 were examined by *Stephenson et al.* [2007]. For this report, we re-examined several analogue tsunami records for major historical events of 1909-1998 measured at Prince Rupert, digitizing record segments containing these events and also analyzed the last twenty years of digital records at this site [*Rabinovich et al.*, 2019a, 2019b].

In 1998, the Canadian Hydrographic Service (CHS) initiated a major upgrade of the existing Tsunami Warning Stations (TWS) and Permanent Water Level Network (PWLN) on the British Columbia (BC) coast. The new digital instruments were designed to continuously measure sea level variations with much higher precision than the earlier analogue gauges and to store sea level data at one-minute sampling increments [*Rabinovich and Stephenson*, 2004]. Altogether these new instruments have recorded more than 35 tsunamis since 1998 along this coast. This includes waves from the Great Sumatra tsunami of 26 December 2004 in the Indian Ocean [*Rabinovich et al.*, 2006], a number of trans-Pacific tsunamis and local tsunamis generated off the west coast of Canada [*Stephenson et al.,* 2007; *Stephenson and Rabinovich*, 2009; *Thomson et al.,* 2011; *Rabinovich et al.*, 2013; *Fine et al.*, 2015; *Wang et al.*, 2020].

Although the total length of the Prince Rupert tide gauge record is >100 years, only six tsunamis were measured at this site during the pre-digital period (Figure 2; Table 1). Four of them were associated with the most powerful earthquakes of the 20th century, with momentum magnitude $M_w \geq 8.6$: specifically, the 1952 Kamchatka (M_w = 9.0), 1957 Andreanof Islands (M_w = 8.6), 1960 Chile (M_w = 9.5), and 1964 Alaska (M_w = 9.2) earthquakes. One other tsunami listed by *Stephenson et al.* [2007] was the 1938 Shumagin Islands event (M_w = 8.3; M_s = 8.7) and one more for this site was an “event of unknown

origin" (1963) but was likely due to atmospheric processes. It is noteworthy that the 1946 Aleutian tsunami, generated by a M_w = 8.6 earthquake (one of the strongest in the Pacific Ocean), which was clearly recorded at Tofino and Victoria, was not detected at Prince Rupert (despite very accurate digitizing and examination of the corresponding paper record) [cf. *Rabinovich et al.,* 2019b]. Neither was there recorded a tsunami caused by the 1949 Queen Charlotte Islands earthquake (M_w = 8.1; the largest earthquake near the coast of BC since 1700 [*Stephenson et al.*, 2007]) with the source located very close to Prince Rupert (Figure 3).

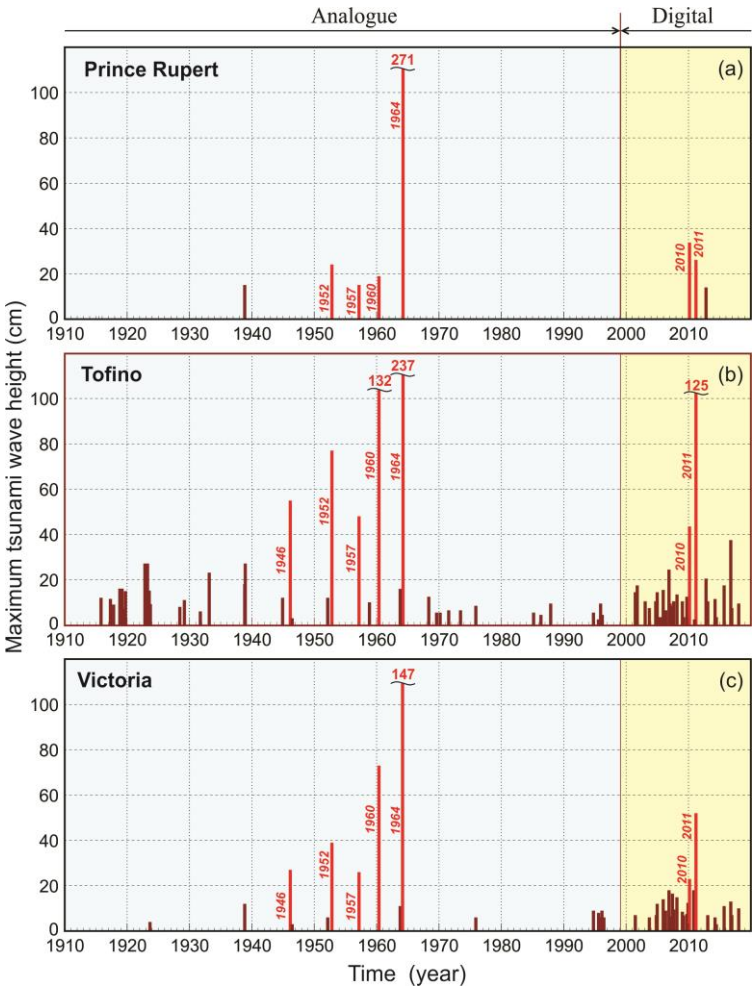

Figure 2. Maximum trough-to-crest wave heights of tsunamis recorded at (a) Prince Rupert, (b) Tofino and (c) Victoria during the period 1910–2019. Up to 1997, measurements were made by analogue tide gauges; since July 1997, digital tide gauges have been used. Red bars indicate tsunami wave heights for the five great tsunamis of the 20th century (1946, 1952, 1957, 1960 and 1964) and two of the 21st century (2010 and 2011); all the others are indicated by magenta bars.

Table 1. Parameters of the earthquake-generated tsunamis recorded at Prince Rupert, British Columbia and statistical parameters of the tsunamis derived from the tide gauge observations at Prince Rupert*. Travel time is measured relative from the start of the earthquake.

Region	Year	Date (dd-mm)	Momentum magnitude (M_w)	Type of record	Travel time (hh:min)	Maximum amplitude (cm)	Maximum wave height (cm)	Wave period (min)
Shumagin Is.	1938	10-11	8.3	Analogue	3:51	8	15	100
Kamchatka	1952	04-11	9.0	Analogue	7:45	12	24	110
Andreanof Is.	1957	09-03	8.6	Analogue	4:44	7	15	110
Chile	1960	22-05	9.5	Analogue	19:10	26	40	100
Graham Island	1963	28-03	-	Analogue	-	?	52?	?
Alaska	1964	28-03	9.2	Analogue	2:54	132	271	100
Chile	2010	28-02	8.8	Digital	18:44	17.0	33.6	110
Tohoku	2011	11-03	9.0	Digital	9:45	13.0	26.0	120
Haida Gwaii	2012	28-10	7.7	Digital	1:57	8.6	13.9	105

* Parameters of the 1952, 1957, 1960 and 1964 tsunamis at Prince Rupert were estimated from digitized paper records (*Rabinovich et al.* [2019b]); parameters of the 1938 tsunami were approximately estimated directly from the analogue record.

It is important to note that the tides at Prince Rupert are quite large (>6 m) [*Thomson*, 1981], making the detection of relatively weak tsunamis from analogue records almost impossible. Moreover, this makes difficult the reliable direct estimation of tsunami parameters even for the greatest tsunamis as, for example, the 1952 Kamchatka, 1957 Andreanof Islands, 1960 Chile and 1964 Alaska tsunamis. For this reason, *Rabinovich et al.* [2019b] used digitized records for these events to subtract the tides, enabling accurate estimation of the wave heights, periods and other parameters of the observed tsunami waves (Table 1).

The ability to measure tsunami waves changed markedly in 1998 after CHS upgraded the existing tide gauge network for the coast of British Columbia (BC) [*Rabinovich and*

Stephenson, 2004]. The new high-resolution water level data enabled investigators to identify and examine not only major events, but also many weak tsunamis and to significantly improve the general statistics of tsunamis for the BC coast. However, from numerous tsunamis, clearly measured at Henslung, Tofino, Winter Harbour and Victoria since 1998, only three tsunamis have been identified in the Prince Rupert tide gauge records. Two of these tsunamis, the 2010 Chile tsunami and 2011 Tohoku tsunami, were generated by the two strongest Pacific Ocean earthquakes in the 21st century, with magnitudes M_w = 8.8 and M_w = 9.0, respectively. The one additional tsunami in this list was generated by the M_w = 7.7 Haida Gwaii earthquake of 28 October 2012. This corresponds to the second strongest, instrumentally recorded, local earthquake in Canadian history (after 1949) and the largest thrust fault earthquake ever recorded along a predominantly strike-slip margin associated with the Queen Charlotte Fault [*Cassidy et al*., 2013; *Leonard and Bednarski*, 2014]. The epicenter of this earthquake was located westward from Moresby Island, Haida Gwaii (former Queen Charlotte Islands, see *Thomson* [1981]), relatively close to Prince Rupert (Figure 3).

All nine events observed at Prince Rupert are listed in Table 1, together with their major characteristics: wave amplitude, wave height and period (except for the 1963 event, which remains mysterious and poorly known). The maximum wave height of 271 cm was measured during the 1964 Alaska event; tsunami wave heights for all other events were significantly smaller: ≤40 cm. The epicenters of eight earthquakes that generated tsunamis measured at Prince Rupert are shown in Figure 3. Also, in this figure are shown the epicenters of two strong earthquakes (1946 and 1949), which did not produce tsunamis at Prince Rupert, and the epicenter of the potentially destructive 1700 CSZ earthquake.

An important feature of all tsunami waves recorded at Prince Rupert was their long ’ringing” (duration of substantial oscillations). This feature is consistent among all observed tsunamis at this location. A visual inspection of the wave forms for all eight seismically generated events yields periods of 100-120 minutes, which is much longer than at other sites on the British Columbia coast [cf. *Stephenson et al*., 2007; *Stephenson and Rabinovich*, 2009]. Specific information on the individual events is given below.

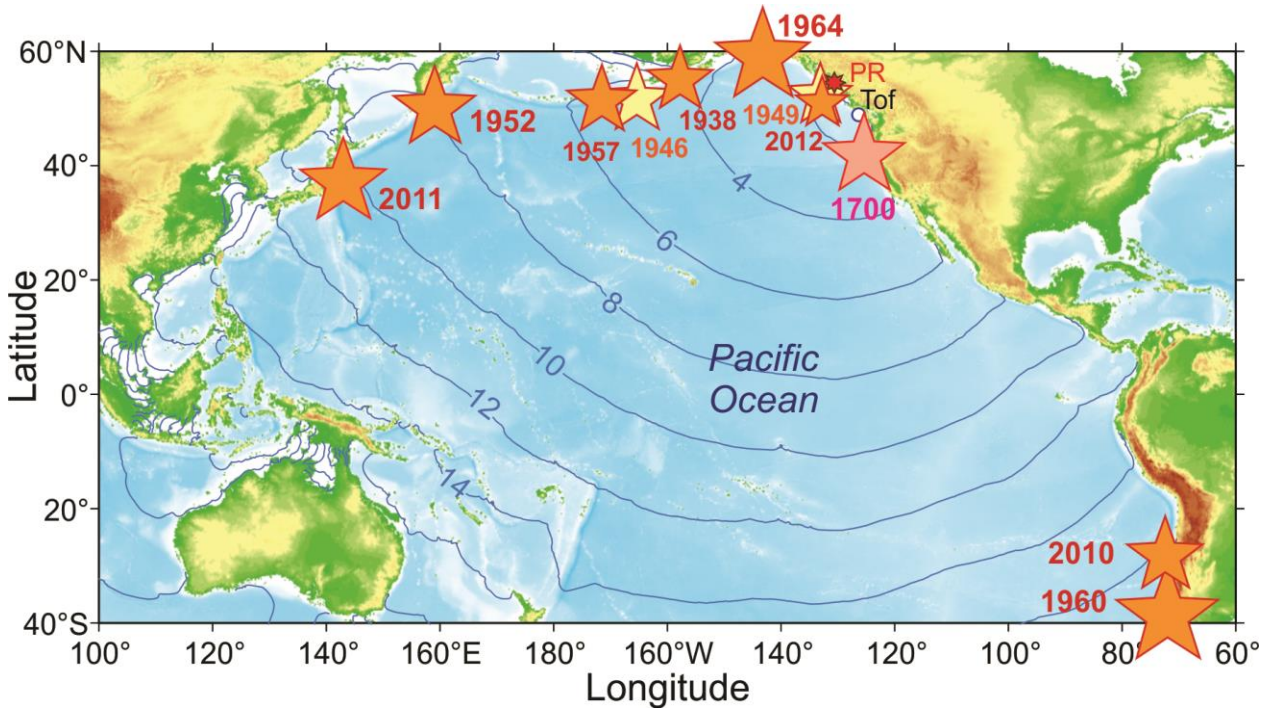

Figure 3. Epicenters (orange stars) of eight earthquakes (1938 Alaska, 1952 Kamchatka, 1957 Andreanof Islands., 1960 Chile, 1964 Alaska, 2010 Chile, 2011 Tohoku and 2012 Haida Gwaii) in the Pacific Ocean that produced tsunamis recorded at Prince Rupert. Also are shown epicenters (ivory stars) of two strong earthquakes in this region (1946 Aleutian and 1949 Queen Charlotte) that have not produced tsunamis at Prince Rupert. The size of the star is proportional to the earthquake magnitude (M_w). The solid blue lines are inverted isochrones of the tsunami travel time (in hours) from various parts in the Pacific Ocean to Tofino ("Tof"), British Columbia (denoted by the *white circle*). The epicenter of the 1700 Cascadia Subduction Zone earthquake is denoted by the pink star. The multibeam red star indicates the location of Prince Rupert ("PR").

2.2. TSUNAMIS RECORDED AT PRINCE RUPERT

most of pre-digital historical tsunamis, which were recorded at Prince Rupert, were also recorded at Tofino, Alert Bay and Victoria (locations of the stations is shown in Figure 4). Tofino is the "beacon station" for the west coast of Canada and one of the most important "tsunami warning stations" for the entire Pacific coast of North America [*Wigen*, 1983; *Rabinovich and Stephenson*, 2004]. Almost all seismically generated tsunamis observed since 1910 along the coast of British Columbia were instrumentally recorded at this station (Figure 3b). For this reason, we use Tofino as the *reference station* in our study of tsunamis

at Prince Rupert. The digitized tsunami records from these stations are shown in Figures 5, 6a and 7 together with the Prince Rupert records.

After upgrading the CHS tide gauge network in 1998, many additional permanent stations were installed. Three stations, Tofino, Winter Harbour and Langara, began to work as *Tsunami Warning Stations* in the general frame of the Pacific Tsunami Warning System. Later, station Langara was replaced by station Henslung Cove, situated at the same island (Langara Island) but in a safer place. This station (indicated in the following text as "Henslung" for brevity) is located at the entrance to *Dixon Entrance* – the main "gate" of tsunami waves arriving at Prince Rupert and Seal Cove (Figures 1b and 4). Another important station is a temporary CHS station Masset located on the northern coast of Graham Island, the southern coast of Dixon Entrance (Figure 1b); this station was in operation during the 2010 Chile tsunami [cf. *Rabinovich et al.*, 2013]. These two stations, Henslung and Masset, enable us to examine the evolution of trans-oceanic tsunami waves propagating from the open ocean to Prince Rupert. In general, tsunami records from the stations shown in Figure 4 were used to illustrate the corresponding events and compare recorded oscillations with those at Prince Rupert.

Figures 5-8 present tsunami records for the seven major events listed in Table 1 (except the 1938 and 1963 events). The displayed records are for Prince Rupert and other available stations shown in Figure 4. To construct these plots, all original paper records for 1952, 1957, 1960 and 1964 events were carefully hand-digitized. All records, including the digital records of the 2010, 2011 and 2012 events, were then de-tided (i.e., the predicted tides were subtracted from the initial records). The de-tiding procedure is crucial for the correct estimation of the tsunami parameters (in particular, the trough-to-crest tsunami wave heights). This procedure is illustrated by Figure 7 for the 1964 Alaska tsunami. Figure 7a shows the original records at Prince Rupert, Alert Bay, Tofino and Victoria (with tides), while Figure 7b presents the same records with the tides subtracted. Figure 7a indicates the importance of the tide height at the time of the event, with high tide at Prince Rupert adding about 4 m to the tsunami height compared to low water.

For 1952. 1957 and 1960 events tsunami waves at Tofino (i.e., on the outer open-ocean coast of Vancouver Island) are substantially higher than at Prince Rupert or at any other stations (Figure 5 and 6a). For the 2010, 2011 and 2012 events, the tsunami records

at Winter Harbour (another TWS station, Figure 4) were even larger than at Tofino and significantly larger than at Prince Rupert (Figures 6b and 8). It appears that tsunami waves arriving from the open ocean strongly attenuate in Dixon Entrance and further weaken when they arrive in northern Hecate Strait.

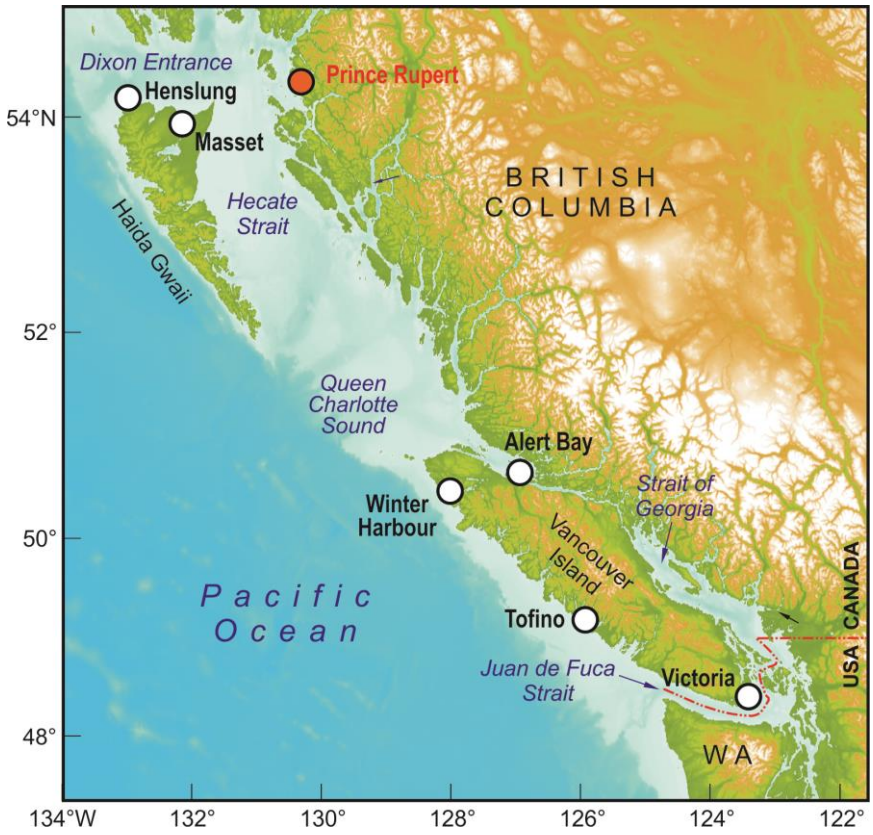

Figure 4. Locations of CHS permanent and temporary tide gauges operating on the coast of British Columbia (*white circles*); records of these gauges are used in the present study to compare with the records from Prince Rupert (indicated in the map by the *red circle*).

On 28 March 1963, an anomalous “tidal wave” occurred on the northern and eastern coasts of Graham Island. Because the wave coincided with unusually high tide, an extraordinary high sea level of 7.5 m occurred at Prince Rupert. This sea level was 0.52 m above the predicted high tide. At Wiah Point (north coast of Graham Island), the wave, or waves, washed over a high-water rock and dislodged two big oil tanks and washed them onto the shore. A wave on the western coast of the island reached 10.7 m high, tore oil tanks from a concrete base and apparently took the life of one man. The wave caused extensive damage at Wiah Point and at the village of Masset [*Stephenson et al*., 2007]. An oceanic

disturbance was reported from the Dixon Entrance region to the Queen Charlotte Islands (Haida Gwaii) during the night of 30-31 March 1963. Wave heights reached 3.7 to 5.5 m above high tide and caused minor damage at Langara Island, Wiah Point and Port Simpson. The disturbance was probably due to atmospheric activity and wind-generated storm waves, but was not recorded by any tide gauge and was not reported in any other area [*Stephenson et al.,* 2007]. No correlation between this event and any seismic or atmospheric activity was found [*Cloud*, 1963]. Nevertheless, some features, in particular very low pressure in Hecate Strait, are evidence of a meteorological origin for this "tsunami". It is likely that the event was caused by the superposition of several correlated factors, including low atmospheric pressure, strong winds, and wind-wave set-up.

The Alaska earthquake of 28 March 1964 with magnitude M_w 9.2 was the second strongest in the 20th century (after the 1960 Chilean earthquake) and the strongest ever instrumentally recorded earthquake in the North Pacific Ocean. This earthquake produced a catastrophic tsunami with the maximum water rise of 20 m at the source. The earthquake also initiated a great number of landslides and submarine landslides that generated local tsunamis with a runup up to 70 m [*Lander*, 1996]. The earthquake occurred in the region of Prince William Sound, leading to widely used name of the "Prince William Sound Earthquake" [*Spaeth and Berkman*, 1967; *Johnson et al*., 1996]. Because of the date (28 March 1964), this earthquake and associated tsunami are also called the "Good Friday Earthquake and Tsunami". Of 132 fatalities associated with the 1964 event, 122 were caused by tsunamis [*Lander*, 1996]. The tsunami spread over the entire Pacific Ocean and was recorded by a great number of coastal tide gauges. The tsunami swept southward from the source area in Prince William Sound along the British Columbia coast, causing about $10 million in damage (1964-dollar values). The highest wave reported in Canada was at Shields Bay on the west coast of Graham Island where the crest wave was reported to be ~5.5 m above the spring high water; the wave damaged a logging camp located in this region. The main damage occurred at the twin towns of Alberni and Port Alberni, with the maximum tsunami run-up at Port Alberni reaching more than 8 m [*Stephenson et al*., 2007; *Rabinovich et al.,* 2019a,b]. **This event generated the strongest tsunami response ever recorded at Prince Rupert.**

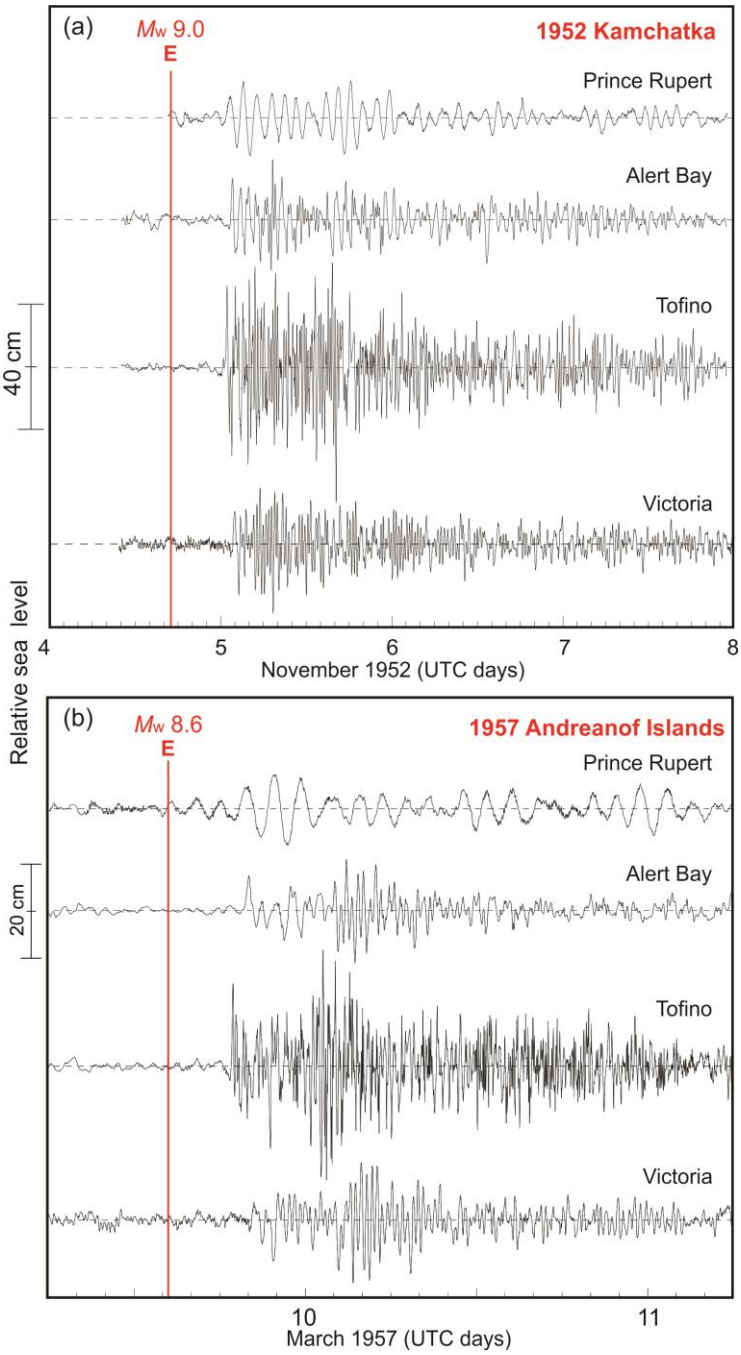

Figure 5. (a) The 4 November 1952 Kamchatka and (b) March 1957 Andreanof Islands tsunamis recorded at Prince Rupert, Alert Bay, Tofino and Victoria. The solid vertical red line labelled “E” denotes the times of the earthquake (modified from *Rabinovich et al.* [2019b]).

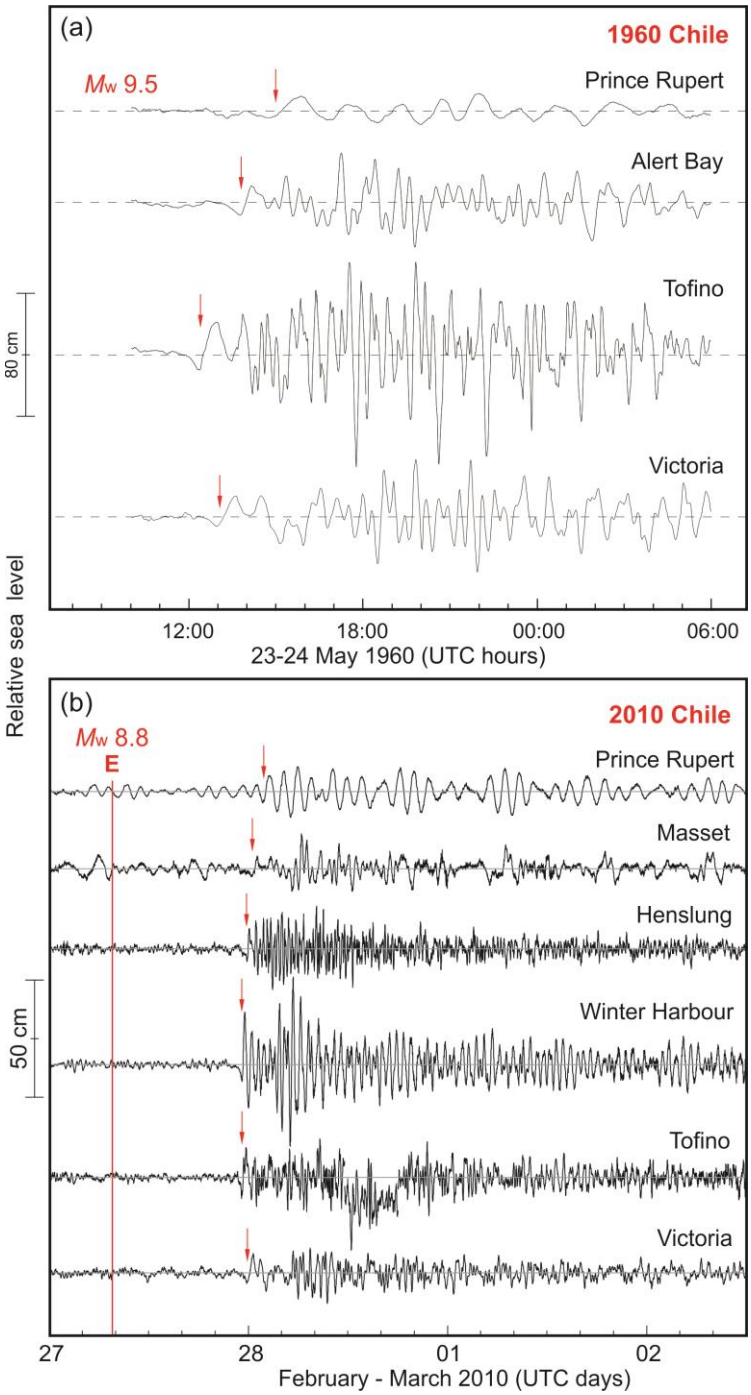

Figure 6. (a) The 22 May 1960 Great Chile tsunami recorded at Prince Rupert, Alert Bay, Tofino and Victoria. (b) The 27 February 2010 Chile (Maule) tsunami recorded at Prince Rupert, Masset, Henslung, Winter Harbour, Tofino and Victoria. The solid vertical red line labelled "E" denotes the times of the earthquake (modified from *Rabinovich et al.* [2013, 2019b]).

Tsunami waves created severe damage at Prince Rupert. The details of the tsunami effects in Prince Rupert are described by local newspapers [cf. *Prince Rupert Daily News*, 1964]. Specifically:

• The vessel Yaloa sank at her Digby Island moorings;

• Eight to nine million feet of logs in Metlakatla Pass and Casey Cove were cut loose;

• The float and pierhead at Metlakatla were torn out;

• There was extensive breakwater damage at Fairview Bay;

• The submarine cable providing telephone service and main power supply to Digby Island was put out of action, causing Digby Island airport and homes to go on emergency power.

Because the 1964 Alaska tsunami was the highest and the most important tsunami to impact the coast of British Columbia, all available paper records of the event (see *Wigen and White* [1964]; *Spaeth and Berkman* [1967]; *Stephenson et al.* [2007]) were carefully digitized and examined [*Rabinovich et al.*, 2019b]. The initial records of this event at Prince Rupert, Alert Bay, Tofino and Victoria are shown in Figure 7a; the de-tided (but unfiltered) tsunami records from these four tide gauges are shown in Figure 7b

According to our estimates, the first wave arrived at Prince Rupert at 06:30 UTC, 2 h and 54 min after the main shock and had an amplitude of 62 cm. The second wave was the highest (Figure 7b), with a trough-to-crest wave height of 271 cm. These estimates are in good agreement with the results of numerical modelling by *Fine et al.* [2018a]. The specific results of numerical modelling of this tsunami are discussed in Section 3.1.

During the 46 years after the 1964 Alaska earthquake, the Pacific region was relatively quiet (Figure 2a). However, on 27 February 2010, a magnitude M_w 8.8 thrust-fault earthquake occurred near the coast of Central Chile, offshore of the Maule region. The source area of the 2010 Chilean earthquake, which was about 550 km long and more than 100 km wide, was located immediately to the north of the rupture zone of the M_w 9.5 Great Chilean Earthquake of 22 May 1960. The 2010 Chilean earthquake generated a trans-oceanic tsunami that caused major damage and loss of life along 800 km of the Central Chilean coastline. The 2010 tsunami was recorded by more than 200 high-precision digital coastal tide gauges and by a large number of Deep-ocean Assessment and Reporting of Tsunamis (DART) bottom pressure stations operated by NOAA.

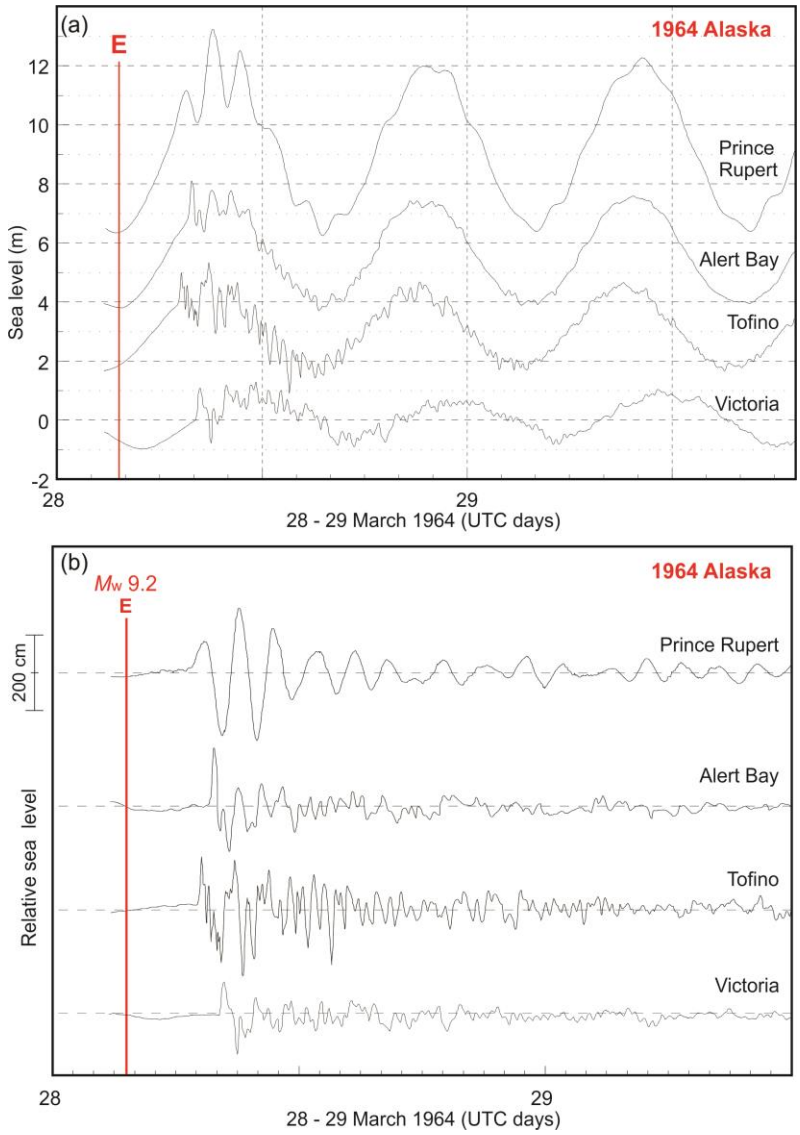

Figure 7. (a) The 28 March 1964 Alaska tsunami, including tides, as recorded at stations Prince Rupert, Alert Bay, Tofino and Victoria. For display purposes, the records have been vertically shifted relative to each other, and (b) the same records but de-tided (residual). The solid vertical red line labelled "E" denotes the time of the earthquake. (Modified from *Rabinovich et al.* [2019b]).

The 2010 Chilean tsunami was clearly recorded by the Ocean Network Canada's (ONC) cabled bottom geophysical observatory array deployed to the west of Vancouver Island, and by many tide gauges along the British Columbia coast. Detailed analysis of these data is provided by *Rabinovich et al.,* [2013]. Tsunami waves recorded at Prince Rupert had

a maximum trough-to-crest wave height of 33.6 cm. The tsunami waves arrived at this station at 01:18 UTC on 28 February 2010, 18 hours and 44 minutes after the earthquake. As with other tsunami events, the waves at Prince Rupert had a dominant period of around 100 minutes. Figure 6b shows the tsunami record at this station; for comparison we also include the records of this tsunami for Henslung, Masset, Winter Harbour, Tofino and Victoria (locations of the stations are shown in Figure 4). The tsunami waves at Prince Rupert had much longer observed periods than at the other stations. Comparison of the Prince Rupert and Winter Harbour records shows that the main trains of tsunami waves at these stations were similar but that wave heights at the latter station were much higher, probably because of high-frequency components.

Almost one year after the 2010 Chile earthquake, on 11 March 2011, a giant thrust fault earthquake of magnitude M_w 9.0 occurred off the coast of Tohoku District, northeastern Honshu, Japan. The earthquake was the strongest in Japan's history and one of the strongest ever instrumentally recorded. Waves from the tsunami reached run-up heights of up to 41 m along the coast of Japan. The tsunami was responsible for almost 20,000 deaths and caused enormous structural damage, including the serious accident at the Fukushima Dai-ichi nuclear power station. The 2011 tsunami was recorded by approximately 250 coastal tide gauges throughout the Pacific Ocean and by numerous bottom pressure gauges at autonomous and cabled observatories. The 2011 Tohoku tsunami waves were recorded by 20 CHS permanent and temporary tide gauges along the coast of British Columbia by NEPTUNE-Canada and VENUS bottom observatories. Tsunami waves that reached Prince Rupert were strongly attenuated and only attained a maximum trough-to-crest wave height at this station of 26 cm. Tsunami waves recorded at these stations, together with the waves recorded at Henslung, Winter Harbour, Tofino and Victoria, are shown in Figure 8a. Similar to the 2010 Chilean tsunami observations, the waves at Prince Rupert had much lower frequencies (longer periods) than at other stations. At the same time, there is visual similarity between the tsunami records for Henslung and Prince Rupert (the entire group structure of these two records is similar; see Figure 8a). The Henslung station is located near the entrance to Dixon Entrance, while Prince Rupert is deep inside the channel (Figure 4). Comparison of these two records suggests that low frequency motions penetrate along Dixon Entrance to Prince Rupert, whereas high frequency tsunami waves are effectively

suppressed. Tsunami waves reached Prince Rupert at 15:31 UTC on 11 March 2011, exactly 9 hours and 45 minutes after the main shock.

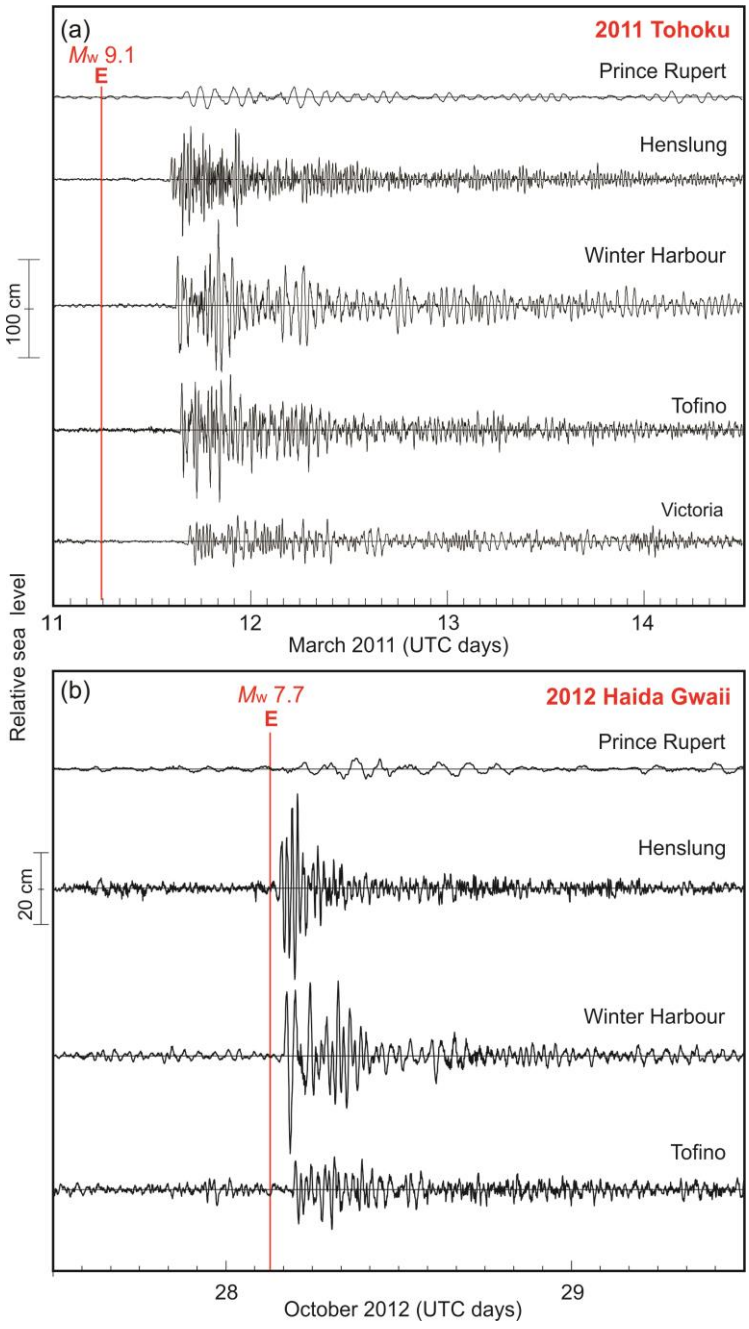

Figure 8. (a) The 11 March 2011 Tohoku tsunami recorded at Prince Rupert, Henslung, Winter Harbour, Tofino and Victoria. (b) The 28 October 2012 Haida Gwaii tsunami recorded at Prince Rupert, Henslung, Winter Harbour and Tofino (Victoria tide gauge was not in operation during this event). The solid vertical red line labelled “E” denotes the times of the earthquake.

At 03:04 UTC on 28 October 2012, a major M_w 7.7 earthquake occurred off the west coast of Moresby Island, the southern part of Haida Gwaii. The earthquake caused several local landslides on Moresby Island and minor damage in and near Queen Charlotte City on the eastern side of the island. The 2012 Haida Gwaii earthquake was the second strongest instrumentally recorded earthquake in Canadian history (after 1949, see Figure 3) and the largest thrust earthquake ever recorded along this predominantly strike-slip margin [*Cassidy et al.,* 2013]. The 2012 Haida Gwaii earthquake generated a tsunami that propagated throughout the Pacific Ocean where it was recorded by many tide gauges on the coasts of the USA, Canada, Japan, New Zealand and at various Pacific islands by a large number of open-ocean DART stations off Alaska, the US West Coast and in other regions of the Pacific Ocean. The West Coast/Alaska Tsunami Warning Center issued a warning for the area extending from the north coast of Vancouver Island to the Alaska-British Columbia border. The warning was cancelled three hours after the earthquake when it became clear that there was no threat to local settlements in the area.

The 2012 Haida Gwaii tsunami strongly affected the nearby coast of Moresby Island [cf. *Leonard and Bednarski*, 2013] and was measured along the British Columbia coast by a number of CHS digital coastal tide gauges and by offshore ONC (NEPTUNE) bottom pressure recorders. Altogether, the 2012 Haida Gwaii tsunami was recorded by 11 CHS coastal tide gauges, including two temporary stations at Hartley Bay and Kitimat. The tsunami was observed at Prince Rupert but the maximum wave height at this station was only 13.9 cm. The tsunami record at Prince Rupert along with the records for Henslung, Winter Harbour and Tofino are shown in Figure 8b. The tsunami signal at Prince Rupert was much weaker than in the two latter stations and, once again, had much longer periods. As with previous events, the observational data suggest that low frequency wave motions propagated along Dixon Entrance to Prince Rupert, whereas high frequency tsunami waves were effectively filtered out. The tsunami arrived at Prince Rupert at 05:01 UTC on 28 October, 1 hour and 57 minutes after the main earthquake.

2.3. SUMMARY OF OBSERVATIONS

Table 1 presents a summary of the nine tsunami-events observed at Prince Rupert. At nearby Seal Cove likely occurred very similar events, with similar maximum tsunami wave heights. The 1963 event observed off Graham Island appears to have had an atmospheric origin. The extensive region of shallow water along the northern part of Hecate Strait creates favourable conditions for storm surge, meteorological tsunamis and other types of sea level oscillations related to atmospheric activity. However, during the entire observational period of 1909-2021 at Prince Rupert, no non-seismic event with a wave height greater than 1 m above the tidal level has been observed. This height is much smaller than the tsunami wave heights at this site from the 1964 Alaska earthquake. Consequently, the threat of atmospherically generated waves at Seal Cove may be ignored relative to the tsunami threat.

All recorded seismic tsunamis, except the 1964 Alaska tsunami, had relatively small maximum trough-to-crest wave heights of $h_{tsu} \leq 50$ cm; these events had not produced any noticeable damage at this site and did not attract any public or media attention. The 1964 Alaska “Good Friday” tsunami was exceptional. This was the strongest tsunami observed on the coast of British Columbia. This specific tsunami initiated the severest damage along the BC coast (mostly at Port Alberni and Prince Rupert [*Rabinovich et al.*, 2019b]). The maximum recorded wave height from this event at Prince Rupert was 271 cm and the tsunami caused significant damage in and around the vicinity of the city [*Prince Rupert Daily News*, 1964]. It is evident that 1964-type tsunamis potentially present the greatest danger for the Prince Rupert area, including the Seal Cove Coast Guard Station. Therefore, based on modelling results of *Fine et al.* [2018a], we consider the corresponding threat, taking into account the climatic and tectonic sea level changes in this region.

The other region of attention is the Cascadia Subduction Zone (CSZ), which is a convergent plate boundary that stretches from central Vancouver Island (Canada) to Northern California (USA). The Great CSZ earthquake of 26 January 1700, with an estimated magnitude M_w 9.0, generated a major trans-oceanic tsunami that caused significant destruction in Japan, on the opposite side of the Pacific Ocean [cf. *Atwater et al.,* 2005], and strongly affected the outer coast of British Columbia. In Figure 2, the epicenter of the 1700 CSZ earthquake is indicated by a pink star. There is no reliable information on

historical heights on the coast of British Columbia associated with this tsunami, however, paleotsunami findings on the coast of Vancouver Island [cf. *Clague et al*., 2000, 2003] show that tsunami waves of ~15 m likely struck the outer coast of the island at the time of the 1700 earthquake and that the waves also penetrated into Juan de Fuca Strait and the Strait of Georgia. We do not know the tsunami wave heights produced by this event on the coasts of northern British Columbia, including the area of Prince Rupert/Seal Cove: paleotsunami studies in this region are only planned. However, we should take the threat of such tsunami into consideration. Therefore, the modelling results of *Fine et al*. [2018b] for the 1700 CSZ-type tsunami for the Seal Cove area is especially important and in Section 3.3 briefly consider these results.

2.4. FREQUENCY PROPERTIES OF THE PRINCE RUPERT AREA

The modern CHS network of digital high-precision coastal tide gauges established in 1999 enabled to detect a large number of tsunamis from source areas located all around the Pacific Ocean, [cf. *Rabinovich et al*., 2006, 2013; *Stephenson and Rabinovich*, 2009; *Fine et al.*, 2015; *Wang et al.*, 2020]. However, despite more than 30 detected events, only three tsunamis (the 2010 Chile, 2011 Tohoku and 2012 Haida Gwaii tsunamis) were digitally recorded at Prince Rupert (Table 1). The question: "*Why all other tsunamis have not recorded at Prince Rupert*?" is important scientifically and from the applied point of view. Certainly, one of the principal reasons is that all non-recorded tsunamis were relatively weak. Nevertheless, they were measured and identified at other British Columbia stations. A possible explanation is that occurrences of tsunami waves at Prince Rupert are related not only to the strength of the earthquake event, but also to the geographical and bathymetric properties of the regions surrounding Prince Rupert which filter out high-frequency tsunami waves.

Figures 9a and 9b shows frequency-time (*f-t*) diagrams for four records of the 2011 Tohoku tsunami (Henslung, Prince Rupert, Tofino and Victora; see Figure 8a.) and for six records of the 2010 Chile tsunami (the same stations plus Masset and Winter Harbour, see Figure 6b), respectively. These diagrams, which show the temporal variation in the tsunami signal as a function of frequency (wave period), clearly demonstrate the difference in

spectral properties of these stations. For both events and all records except Prince Rupert, tsunami waves occupy a broad frequency band, with the main spectral energy at periods from 15 to 80 minutes. In contrast, Prince Rupert shows no tsunami energy in this particular frequency band, but considerable energy at the dominant tsunami wave periods of 100-120 minutes. Thus, tsunami wave energy at Prince Rupert is negligible at high frequencies (frequencies > 0.01 cpm; periods less than 100 minutes) but relatively high at low frequencies (with peak frequencies at 0.008-0.010 cpm; periods of 100 to 125 minutes). In contrast, the main spectral energy of tsunami waves at other British Columbia stations (e.g. at Henslung, Winter Harbour, Tofino, Bamfield and Bella Bella) is mainly concentrated at much higher frequencies.

The 2010 Chile *f-t* diagrams for Henslung, Masset and Prince Rupert (Figure 9b) allows us to examine modification of the frequency content <composition> of tsunami waves propagating through Dixon Entrance. At the entrance to Dixon Entrance (i.e., at Henslung) the tsunami arrival is very clear; the incoming tsunami waves are a broad-band process including frequencies from 0.4 to 10 cph (periods from 2.5 hours to 6 min) with a peak frequency 2.4 cph (25 min). At Masset this “tsunami band” becomes much narrower: 0.4-2.0 cph (periods from 2.5 hours to 30 min), while at Prince Rupert only low-frequency waves – 0.4-0.8 cph (2.5 hours – 75 min) – are observed. It appears that Dixon Entrance plays the role of a low-frequency filter that pass low frequencies but suppress high frequencies.

This filtering effect of Dixon Entrance explains why only eight tsunamis (Table 1) have been detected at Prince Rupert, while many others (recorded at other stations; see Figure 2a,b) have not. The reason is not only that the recorded tsunamis were considerably stronger in this region than the others, but also because seven of the eight were related to major earthquakes with $M_w \geq 8.3$ that had huge extension source areas and, consequently, produced tsunami waves with much lower frequencies (i.e., longer wavelengths) than those with $M_w \leq 8.3$.

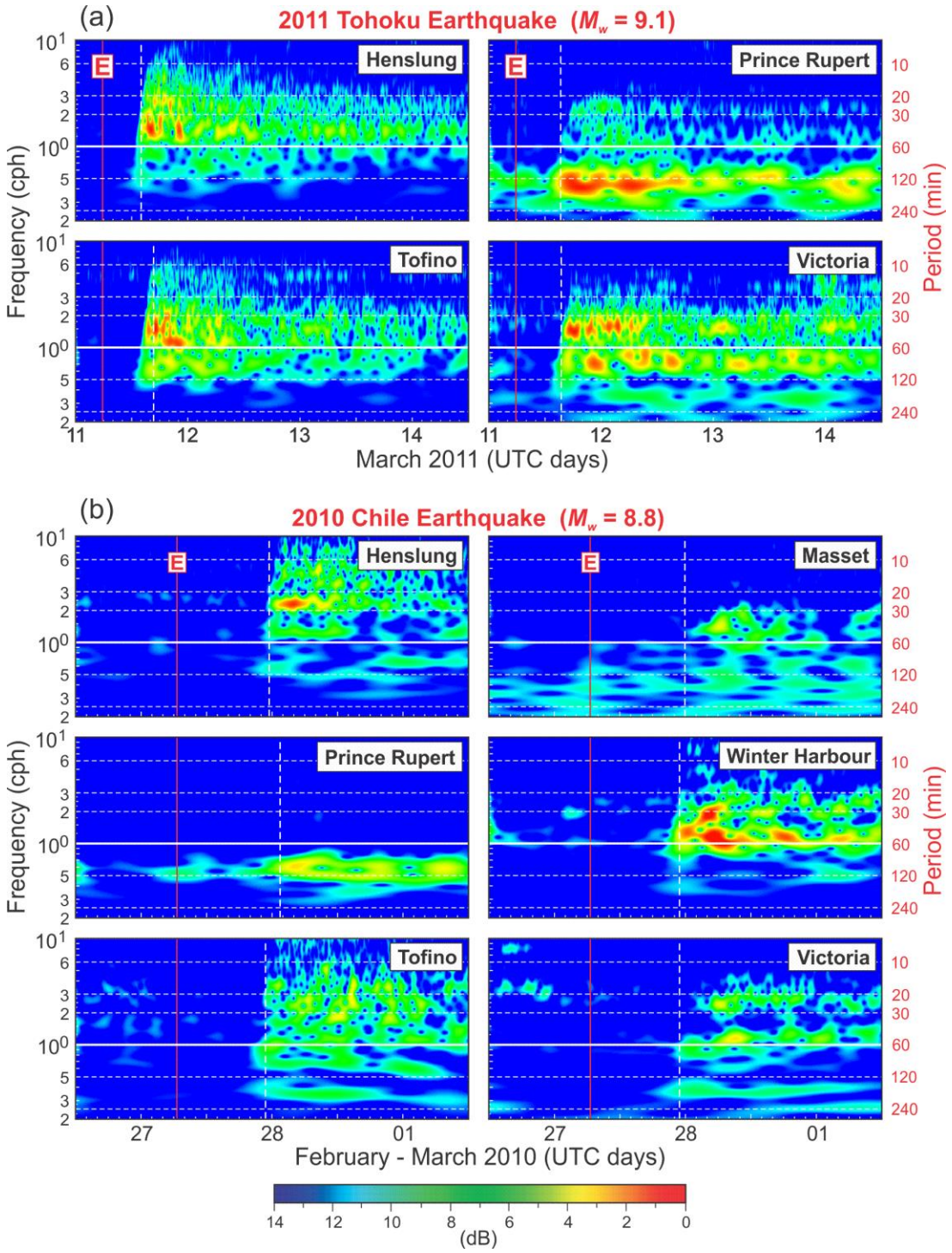

Figure 9. (a) Frequency-time plots (*f-t* diagrams) for (a) the 11 March 2011 Tohoku and (b) the 27 February 2010 Chile tsunami records at stations located along the coast of British Columbia. The solid vertical red line labelled "E" denotes the time of the earthquakes; the dashed white line indicates the tsunami arrival.

This high-frequency filtering feature is not specifically related to tsunami waves but reflects the general frequency properties of this region. *Rabinovich and Stephenson* [2004] used long records of background oscillations to estimate the topographic response properties for CHS tide gauge sites along the coast of British Columbia. These plots (Figure 10) show that, while at most coastal stations long waves resonantly amplify at certain high frequencies, the waves arriving at Prince Rupert from the open ocean are strongly attenuated at high frequencies. As a result, Dixon Entrance and the shelf adjacent to Prince Rupert strongly shelter the area of Seal Cove from high-frequency (small-source) tsunamis. This aspect of the Prince Rupert region indicates that only tsunamis with very long wavelengths associated with the largest earthquakes, like 1964 Alaska or 1700-type CSZ earthquakes, can present a major threat to this region.

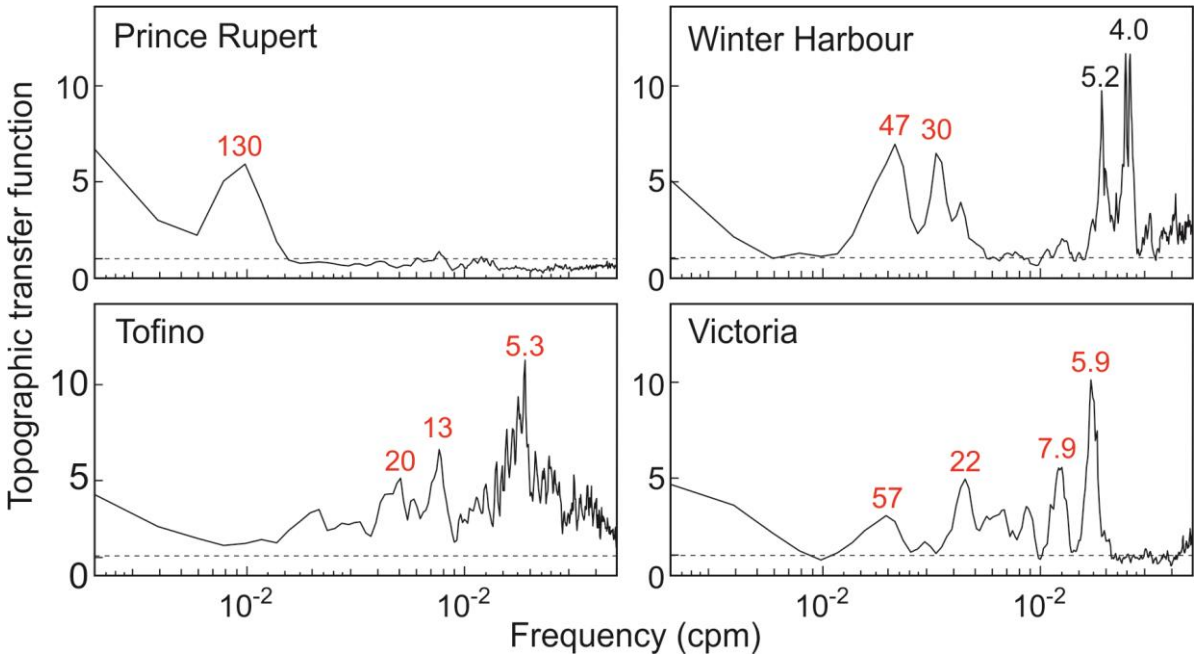

Figure 10. Topographic transfer (frequency admittance) functions for Prince Rupert, Winter Harbour, Tofino and Victoria estimated based on long-term measurements of longwave oscillation at these sea stations. Red numbers indicate the periods of the corresponding peaks (in minutes).

3. MODELLING MAJOR TSUNAMIS FOR THE AREA OF SEAL COVE

Based on all findings and on preliminary numerical modeling results, *Fine et al.* [2018a,b] concluded that the major threat for the area of Seal Cove is associated with great tsunamis generated in two specific source regions that actually are the closest to the coast of British Columbia: (1) Alaska (a 1964-type event) and (2) the Cascadia Subduction Zone (a 1700-type event), while other tsunami-source regions may be ignored. Their numerical studies provide estimates of the expected maximum tsunami wave amplitudes arising from these two types of events.

A high-resolution, nested-grid tsunami model was used by *Fine et al.* [2018a,b] to simulate the distribution of tsunami waves and wave-induced currents. The model is based on a finite-difference formulation of the linear shallow-water equations and is similar to that of *Imamura* [1996] and to the one by *Fine et al.* [2013, 2015] for numerical modelling of the 2011 Tohoku and 2012 Haida Gwaii tsunamis.

3.1. NESTED GRIDS

Accurate numerical simulation of tsunami waves in the rapidly shoaling regions of the west coast of British Columbia requires setting up the model domain as a series of nested grids of ever finer spatial and temporal resolution. The use of nested grids of smaller cell dimensions and time steps makes it possible to resolve tsunami wave configurations as they propagate into the shallow coastal regions. A good interface between the inner and outer domains is required to avoid errors and model instability associated with point matching between the different grids. High resolution bathymetry, external forcing and observations are needed for model domain setup, initialization and validation at each domain level. In their numerical simulations of the 1964-type Alaska and 1700-type CSZ tsunamis, *Fine et al*. [2018a, b] fulfilled all these requirements and used the nested-grid formulation similar to that one in well-known tsunami models, TUNAMI and COMCOT [*Imamura,* 1996; *Liu et al.*, 1998; *Imamura et al.*, 2006].

For both projects (1964 Alaska and 1700 CSZ), *Fine et al*. [2018a, b] used a series of four nested grids; Grid 2, Grid 3 and Grid 4 were the same for both projects, while Grid 1A for the 1964 Alaska project was different from Grid 1B for the 1700 CSZ project (Table 2). The choice of model grids took into account the need for high spatial resolution to accurately resolve the reflection and transformation of the tsunami waves.

Table 2: Parameters of the numerical grids used in the tsunami generation and propagation models. Grid extent is along the *x* (eastward) and *y* (northward) coordinate directions and is presented in latitude and longitude degrees (°). Numerical grid cell sizes for Grids 2, 3 and 4 are roughly 275, 55 and 10 m, respectively.

Grid No.	Extent (*x, y*; degrees)	Array (number of grid points)	Cell size (*x, y*; degrees)	Source of data	Processing type
1A	35.0, 17.0 (1964, Alaska)	1401, 1361	0.025, 0.0125	GEBCO 2014 30 arc-seconds gridded data	Filtering and bilinear interpolation
1B	28.0, 24.0 (1700, CSZ)	1121, 1921	0.025, 0.0125	GEBCO 2014 30 arc- seconds gridded data	Filtering and bilinear interpolation
2	5.0, 6.2	1201, 2480	0.00416667, 0.0025	BC Coastal Relief, 3 sec; US Coastal Relief, 8 sec	Filtering and bilinear interpolation
2B	2.45, 1.95 (1700, CSZ)	589,780	0.00416667, 0.0025	BC 3 arc-sec bathymetric DEM	Filtering and bilinear interpolation
3	1.0086, 0.526	1339, 1503	0.0008333, 0.0005	CHS 3 sec bathymetry data	Filtering and bilinear interpolation
4	0.13, 0.06	781, 701	0.00016666 7, 0.0000833	CHS bathymetry data; coast line chart	Kriging, smoothing, bilinear interpolation

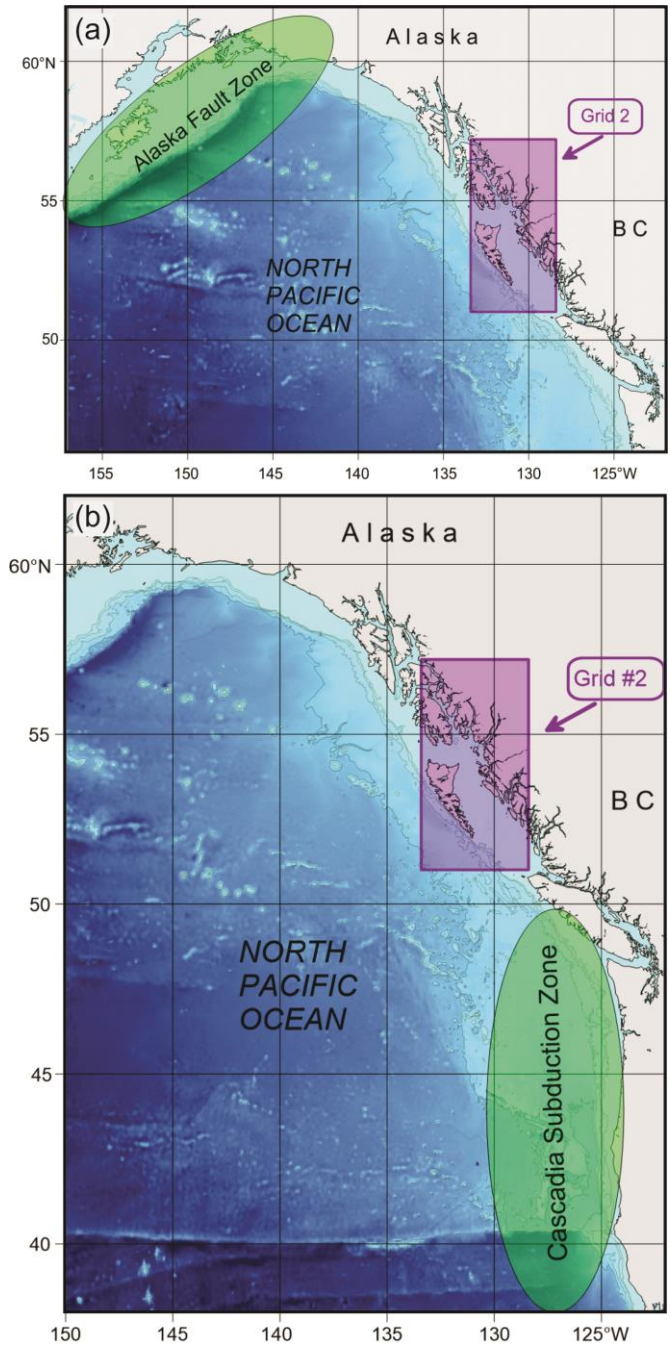

Figure 11. The regions of the northeast Pacific covered by the large-scale coarse grid numerical models. (a) Grid 1A for numerical modelling of an Alaska 1964-type tsunami; also shown is the Alaska Fault Zone that could generate tsunamis that impact the Coast Guard facility. (b) Grid 1B for numerical modelling of a CSZ 1700-type tsunami; also shown is the Cascadia Subduction Zone where a tsunami could be generated that would impact the Seal Cove Coast Guard facility. The location of the first nested grid (Grid 2), which is the same for (a) and (b), is shown covering the area of Seal Cove/Prince Rupert Harbour. (Modified from *Fine et al.* [2018a,b]).

Grid 1A is the outer domain covers the northeast Pacific, encompassing the major source region - the Alaska Fault or failure Zone – that was used by *Fine et al.* [2018a] in the simulation of the 1964-type Alaska tsunami (Figure 11a). The spatial resolution of the coarse grid was 90 arc-seconds in the east-west direction (spatial scales in the *x*-range from 1.4 km to 2.2 km, depending on latitude) and 45 arc-seconds in the north-south direction (1.4 km grid size in the *y*-direction). The grid is bounded by 45– 62° N, 157 – 122° W and was created using the 30 arc-second global bathymetry dataset GEBCO2014. Grid 1B, which was used to simulate the 1700-type CSZ tsunami, is similar to Grid 1A but bounded by 38– 62° N, 150 – 122° W (Figure 11b) and was created using the 30 arc-second GEBCO dataset [*Becker et al*., 2009].

Grid 2 was used both for the 1964-type Alaska and 1700-type CSZ tsunami models; it covers northern British Columbia and the southern part of Alaska (Figure 12). The location and coverage of the grid was chosen so that it extends equally north and south of the Prince Rupert region. This intermediate grid enables simulation of wave shoaling and wave transformation as the tsunami propagates from the deep ocean to the shelf and into coastal areas. The grid is also important for energy exchange between different parts of the coast and shelf areas. The southern part of the grid was created using the British Columbia 3 arc-second Digital Elevation Model [*NOAA*, 2017]; the northern part was constructed based on the 8 arc-second Southern Alaska Coastal Relief [*Caldwell et al.*, 2012]. The grid was corrected and completed by *Fine et al.* [2018a,b] based on CHS data. Thus, the northern boundary between the datasets was at around 54.5° N in the northern part of Dixon Entrance. Grid 2 had a resolution of 15 arc-seconds in the east-west direction and 9 arc-seconds in the north-south direction, corresponding to spatial scales of approximately 270 m by 280 m, respectively (Table 2

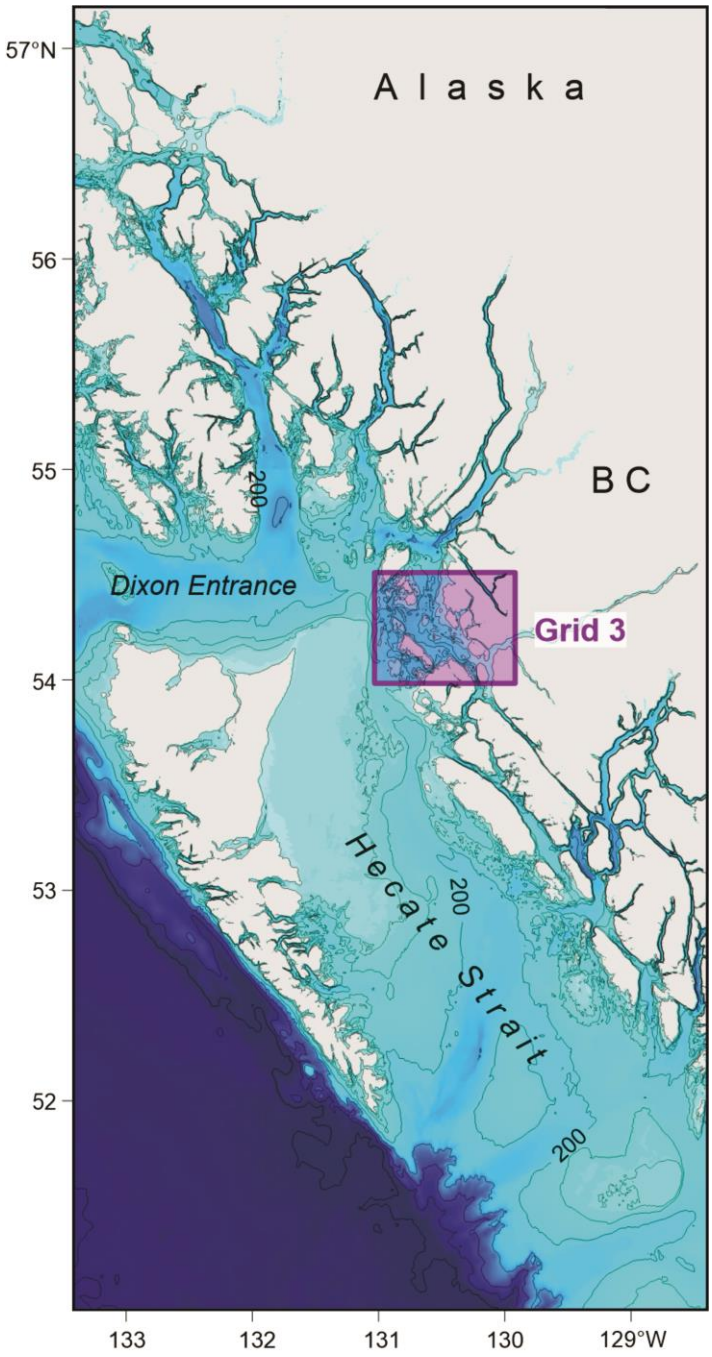

Figure 12. The region covered by the medium-scale bathymetric grid (Grid 2) for the northwest coast of British Columbia|. The horizontal (*x, y*) grid cell scales for this region are approximately 270 m and 280 m, respectively. (b) The Salish Sea region covered by the medium-scale bathymetric grid (Grid 2) for the southwest coast of British Columbia. The horizontal grid cell scales (*x, y*) for this region are approximately 270 m by 280 m, respectively. The inset shows the boundaries and location of the second nested grid (Grid 3) covering the region of Prince Rupert/Seal Cove. Depths, *H*, are in metres (m). (Modified from *Fine et al.* [2018a,b]).

The third nested grid (Grid 3) covers Chatham Sound, the Prince Rupert Harbour waterway and surrounding passes and inlets (Figure 13); it was used both for the 1964-type Alaska and 1700-type CSZ models. This grid is of considerable importance since it determines the periods, *Q*-factor (attenuation rate) and other parameters of the eigen oscillations set up in the harbour by incoming tsunami waves. Model grid cells were created using the 50-m pre-gridded CHS data provided to *Fine et al.* [2018a,b]. The gridded data were subsequently re-interpolated from the original local UTM projection to a geographical coordinate system (NAD83 standard) with a rectangular grid cell size of 3 arc-seconds by 1.8 arc-seconds (approximately 54 m by 56 m) in the east-west and north-south directions, respectively.

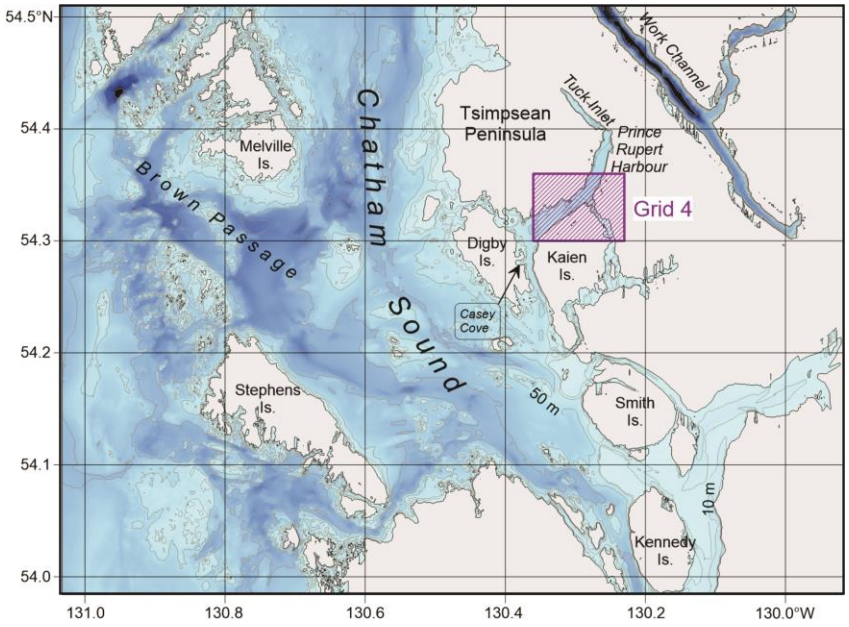

Figure 13. Coastal region covered by Grid 3, including Chatham Sound, Brown Passage and Prince Rupert Harbour. The grid scale for this region is approximately 54 m by 56 m. The insert shows the boundaries and location of the third nested grid (Grid 4) covering Seal Cove. Depths are in metres (m). (From *Fine et al.* [2018a,b]).

The final (fourth) numerical Grid 4 was also used both for the 1964-type Alaska and 1700-type CSZ models Final Grid (Grid 4). This grid had the highest spatial resolution and covered coastal areas near the DFO Coast Guard facilities (Figure 14). A Kriging algorithm

[*Matheron*, 1963] was used to create the grid from the original, irregularly spaced CHS bathymetric data, coast line and data from analogue chart, used in the study. The grid (*x*, *y*) scale is approximately 11 m by 9 m.

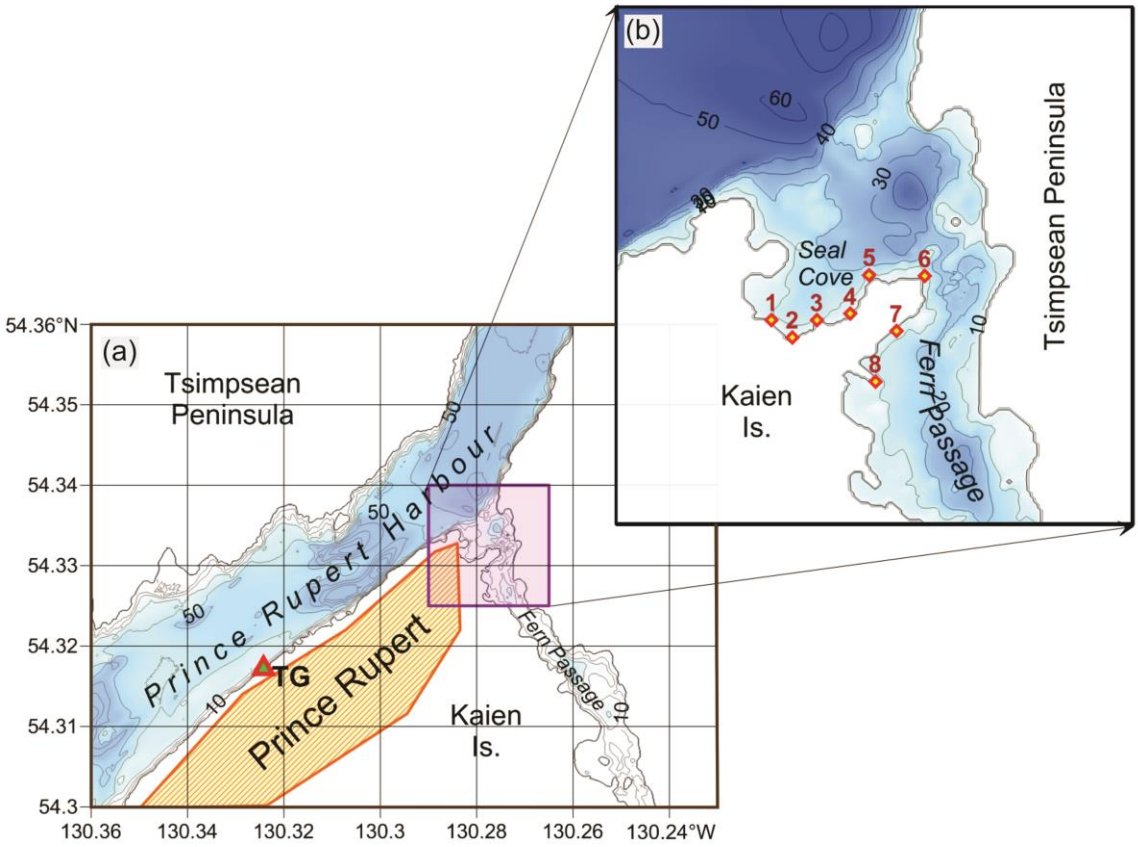

Figure 14. (a) The region covered by Grid 4; the fine-scale bathymetric grid has adjusted topography for the region of Seal Cove Harbour, and has a grid (*x, y*) scale of approximately 12 m by 9 m. (b) The location of the Prince Rupert tide gauge (TG) and the sites (1-8) within the Seal Cove harbour for which tsunami waveforms were simulated. Depths are in metres (m). (Modified from *Fine et al.* [2018a,b]).

3.2. MODELLING A 1964-TYPE ALASKA TSUNAMI

The momentum magnitude (M_w) 9.2 Alaska earthquake of 28 March 1964 occurred within the Alaska-Aleutian megathrust zone, where the Pacific Plate subducts under the North American Plate (Figure 15). This zone has the greatest potential to generate destructive tsunamis and is one of the most seismically active fault zones in the North Pacific. The 1964 megathrust Alaska earthquake caused the most destructive tsunami in

Alaskan history and, further south, strongly impacted the west coasts of the USA and Canada [cf. *Johnson et al*., 1996; *Lander*, 1996].

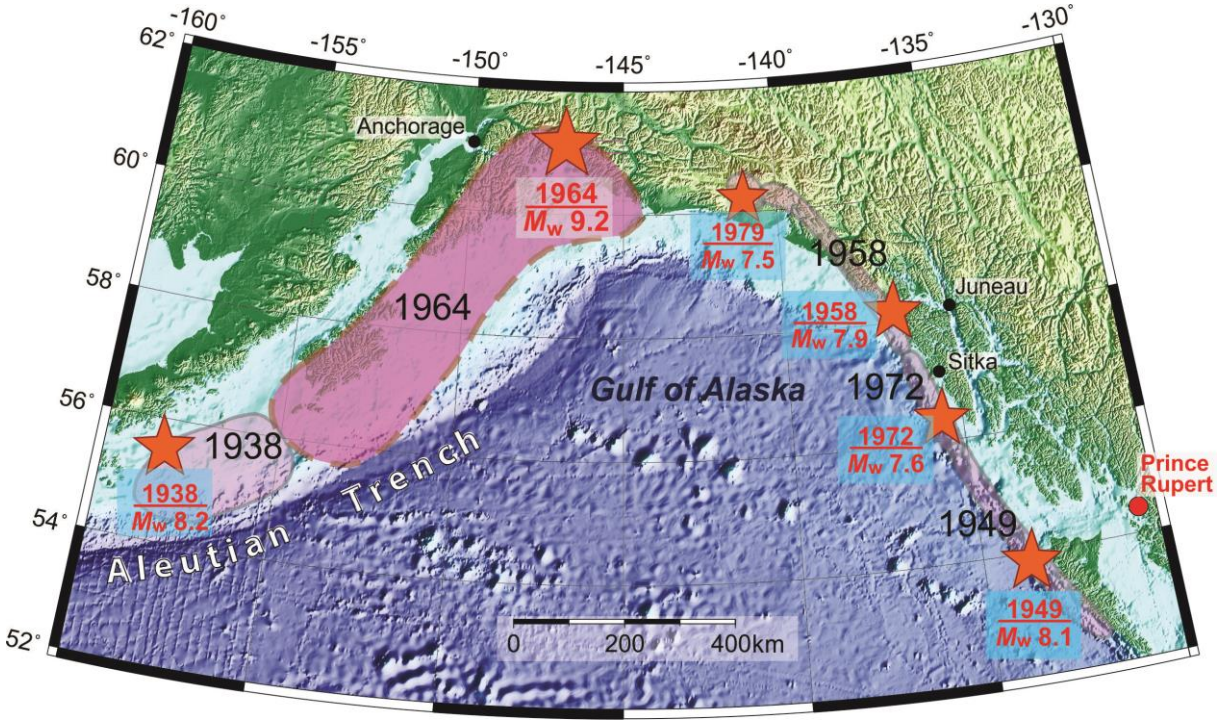

Figure 15. Map of south-central and south-eastern Alaska with the rupture zones of six major historical earthquakes (shaded); the rupture zone of the 1964 Alaska earthquake is contoured by a thick brown dashed line. Red stars indicate epicenters of the earthquakes; the sizes of the stars are proportional to the earthquake magnitudes. Tide gauges at Sitka, Juneau and Anchorage are indicated by solid black circles; the red circle denotes the tide gauge at Prince Rupert. (Modified from *Rabinovich et al.* [2019b]).

The 1964 tsunami spread over the entire Pacific Ocean and was recorded by 18 instruments on the coast of British Columbia, including Prince Rupert [*Rabinovich et al.*, 2019b]. The tsunami caused about $10 million in damage (1964-dollar values), mainly at the twin towns of Alberni and Port Alberni and at Prince Rupert [cf. *Rabinovich et al.*, 2019b]. Several numerical models were constructed to simulate tsunami wave propagation from the 1964 source, including the coast of British Columbia [cf. *LeBlond et al.*, 1989; *Dunbar et al.*, 1991; *Myers and Baptista*, 2001]. However, the models were based on preliminary source estimates and very coarse grids with 1.0-5.0-km spatial resolution. To estimate maximum possible tsunami amplitudes and tsunami-generated currents in the area of Seal Cove and

Prince Rupert, more detailed high-resolution bathymetry, which became available recently, and a more refined source region, are needed. The 1964 Alaska tsunami is typically considered as a proxy for a major future tsunami along the Pacific coast of North America [*Suleimani et al*., 2013]. Therefore, to compute the expected tsunami waves for the Prince Rupert area and, specifically, for the Seal Cove Coast Guard Station, *Fine et al.* [2018a] applied an Alaska 1964-type (M_w 9.2) earthquake as the tsunami source.

The numerical simulation of the 1964 tsunami was based on the newly revised [*Suleimani et al.*, 2013] coseismic slip distribution for the 1964 rupture derived from the model of *Suito and Freymueller* [2009]. *Fine et al.* [2018a] applied the inversion-based model by *Johnson et al.* [1996] as the basis for their coseismic slip model, adjusting it to the new geometry and critically reinterpreting the coseismic data. *Suleimani* [2011] and *Suleimani et al.* [2013] used results of the near-field modelling of the 1964 tsunami to constrain the amount of slip placed on intraplate splay faults, and to evaluate the extent of the Patton Bay fault. The resulting coseismic vertical deformation is shown in Figure 16. The tsunami simulations revealed that including deformation due to horizontal displacements in the source function resulted in an increase in the far-field tsunami amplitudes.

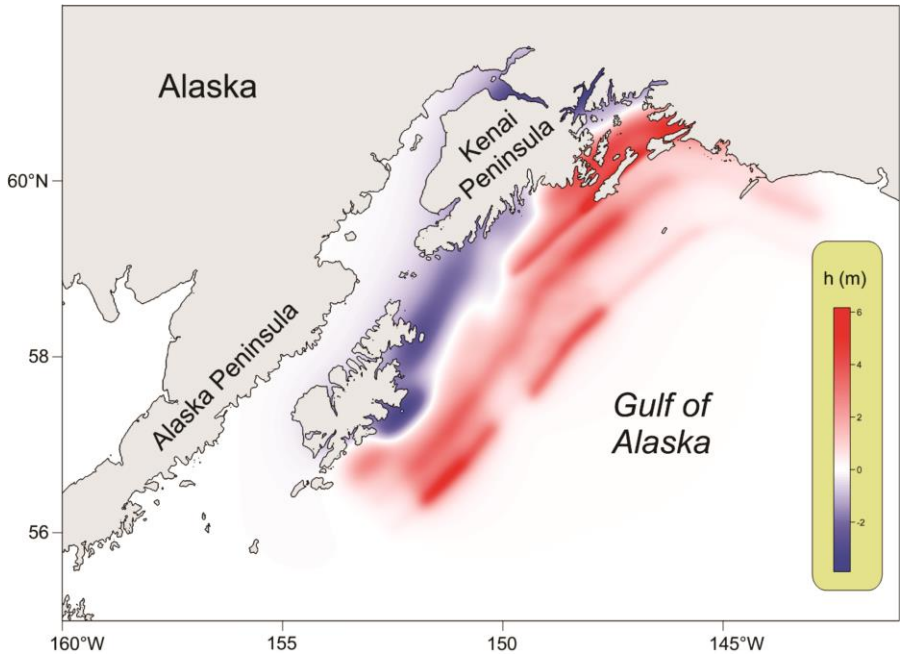

Figure 16. Seafloor vertical displacements (m) at the source region for the March 1964 Alaska tsunami. The displacements range from roughly -3 m (blue) to +6 m (red). (Modified from *Suleimani et al*. [2013]).

To verify their model, *Fine et al.* [2018a] numerically simulated a tsunami waveform of the 1964 Alaska tsunami for the Prince Rupert tide gauge site and compared the modelled results with the actual record of the tsunami (Figure 7b). Comparisons of the observed and modelled results are shown in Figure 17 and Table 3. It is evident that the modelled record fits the observed record quite well. For both the observed and simulated records, the first wave is a crest wave and is the largest wave in the records. The maximum tsunami travel times coincide within a few minutes, indicating that they are very similar, despite the observations being based on a digitized analogue record [cf. *Rabinovich et al*., 2019b].

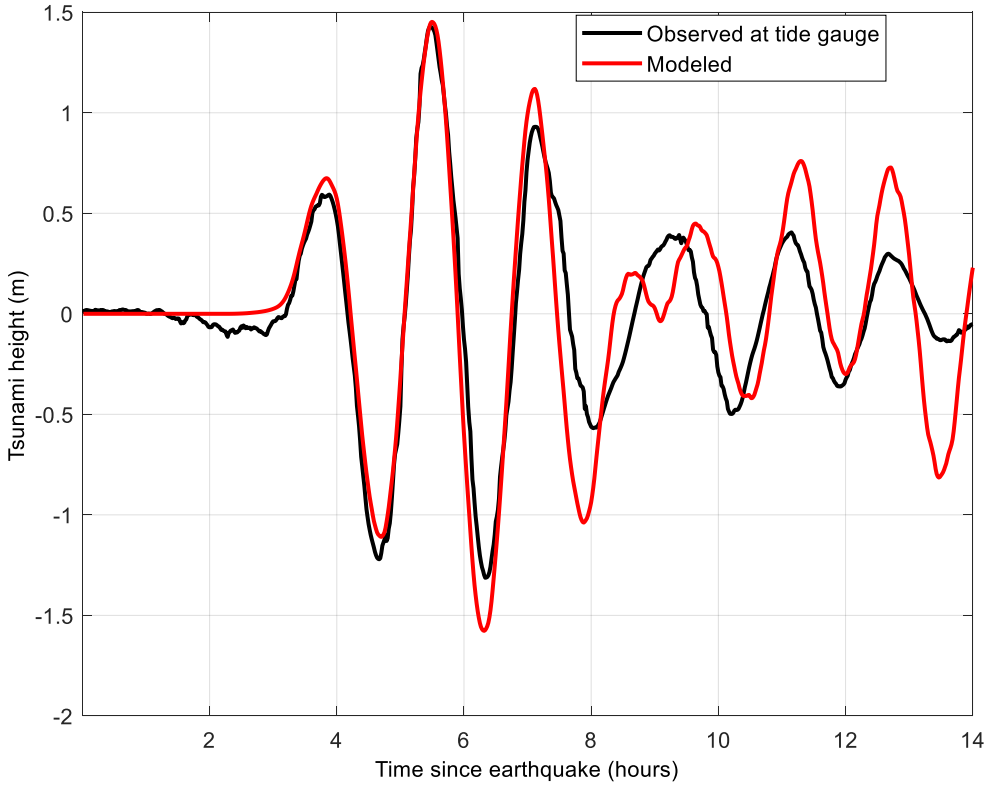

Figure 17. Observed versus modelled wave records for the March 1964 Alaska tsunami for the Prince Rupert tide gauge site. (From *Fine et al.* [2018a]).

Table 3. Statistical properties of modelled and observed tsunami waves at the Prince Rupert tide gauge location for the March 1964 Alaska tsunami source region. Wave amplitudes (zero-to-crest) are in metres and travel times are in hours (h) and minutes (min).

Type	First wave		Maximum crest		Maximum trough	
	Amplitude (m)	Travel time	Amplitude (m)	Travel time	Amplitude (m)	Travel time
Modelled	0.71	3h 51	1.48	5h 35 min	-1.55	6h 24 min
Observed	0.59	3h 46	1.43	5h 28 min	-1.31	6h 20 min

The wave maxima for the 1964-type tsunami for Grids 1 and 2 computed by *Fine et al.* [2018a] are presented in Figures 18 and 19, respectively. Figure 18 shows the "rays" of maximum tsunami wave heights for the entire northeast Pacific. The main 1964 tsunami energy flux radiated southeast toward the coast of British Columbia. In Southern Alaska and British Columbia, the most affected coastal zones are those exposed to the open ocean, such as the west coasts of Vancouver Island and Haida Gwaii. The highest wave reported in Canada was in Shields Bay on the west coast of Graham Island, where the crest wave was reported to be ~5.2 m above the spring high water (9.8 m above tidal datum) [*Rabinovich et al.*, 2019b]. The most severe damage from the event occurred at the twin towns of Alberni and Port Alberni, with maximum tsunami run-up at Port Alberni reaching almost 8 m [*Stephenson et al*., 2007]. In more protected areas such as Hecate Strait, the computed tsunami wave amplitudes are markedly smaller (Figure 19; Grid 2).

According to the numerical computations of *Fine et al.* [2018a], results for the finer resolution grids (Grids 3 and 4) demonstrate the considerable spatial variability in the incoming tsunami wave heights for the study region. Figure 20a shows the distribution of the tsunami wave heights in Chatham Sound and neighbouring areas for Grid 3. The wave amplitudes increase toward the shoreline, especially in Prince Rupert Harbour and Tuck Inlet, where the wave amplitudes are 4-5 times higher than in the eastern part of Chatham Sound and Brown Passage. The pronounced increase in tsunami wave heights in the Prince Rupert Harbour basin is related to resonance amplification of the tsunami waves whereby

the period (~ 2 hours) of the incoming waves is close to the period of the eigen-oscillations of the basin.

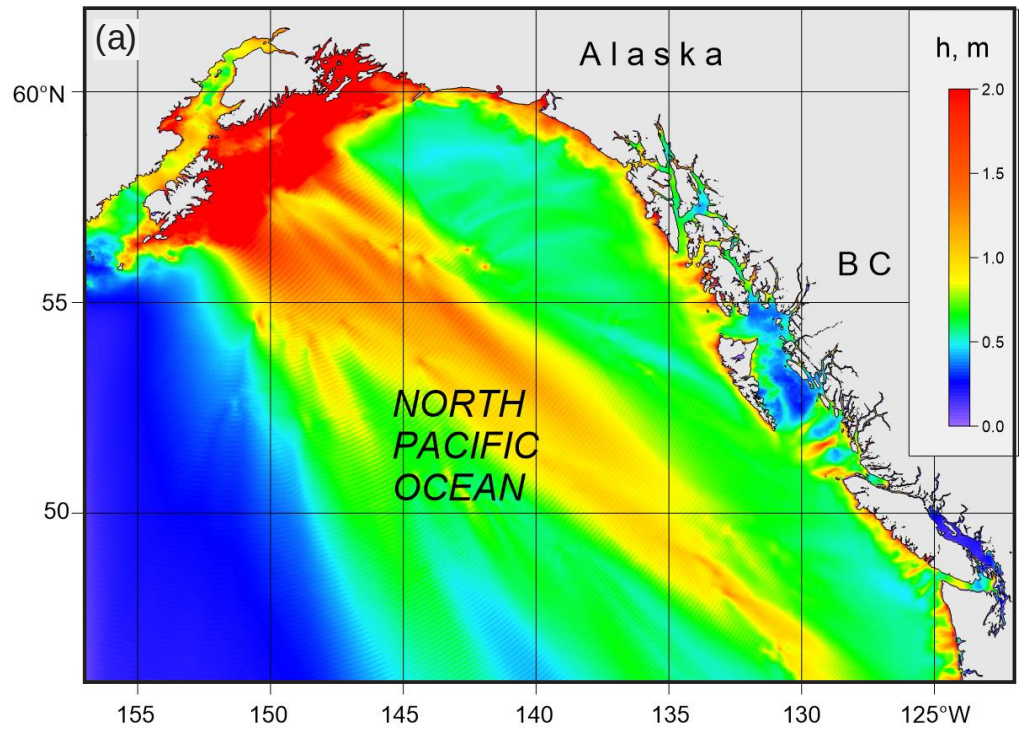

Figure 18. Distribution of maximum tsunami wave amplitudes (meters) for Grid 1 of the nested-grid model for waves generated by simulation of the 1964 tsunami. (From *Fine et al.* [2018a]).

Figures 20b and 20c present a high-resolution map of the maximum tsunami heights in Prince Rupert and vicinity for numerical Grid 4. As the figure indicates, amplitudes of the tsunami waves gradually increase along Prince Rupert Harbour, from 1.3 m in the south-west to 1.7 m at the northeast end of the grid. In Seal Cove, the tsunami wave maxima are distributed almost uniformly, with a mean value of around 1.55 m. In Fern Passage, just south of Seal Cove, the tsunami wave amplitudes decrease to 1.2 to 1.3 m. *Fine et al.* [2018a] also estimated maximum tsunami-induced currents for the study region and found that mostly they are weak and do not exceed 0.5 m/s (1 knot). The exceptional area is Fern Passage where these currents are much stronger and in the middle of Fern Passage can reach 2.5 m/s (5 knots).

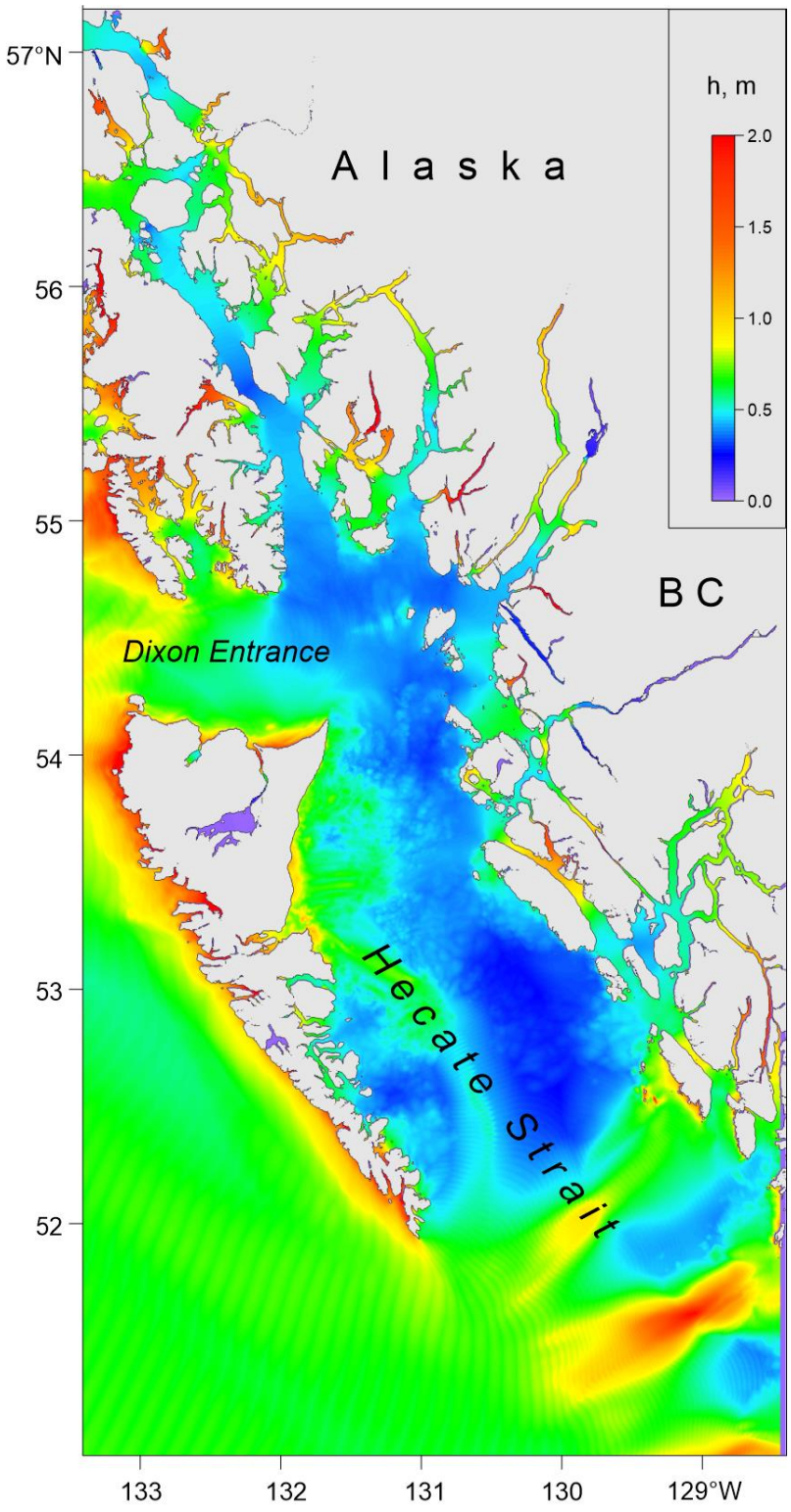

Figure 19. Distribution of maximum tsunami wave amplitudes (meters) for Grid 2 of the nested-grid model for waves generated by simulation of the 1964 tsunami. (From *Fine et al.* [2018a]).

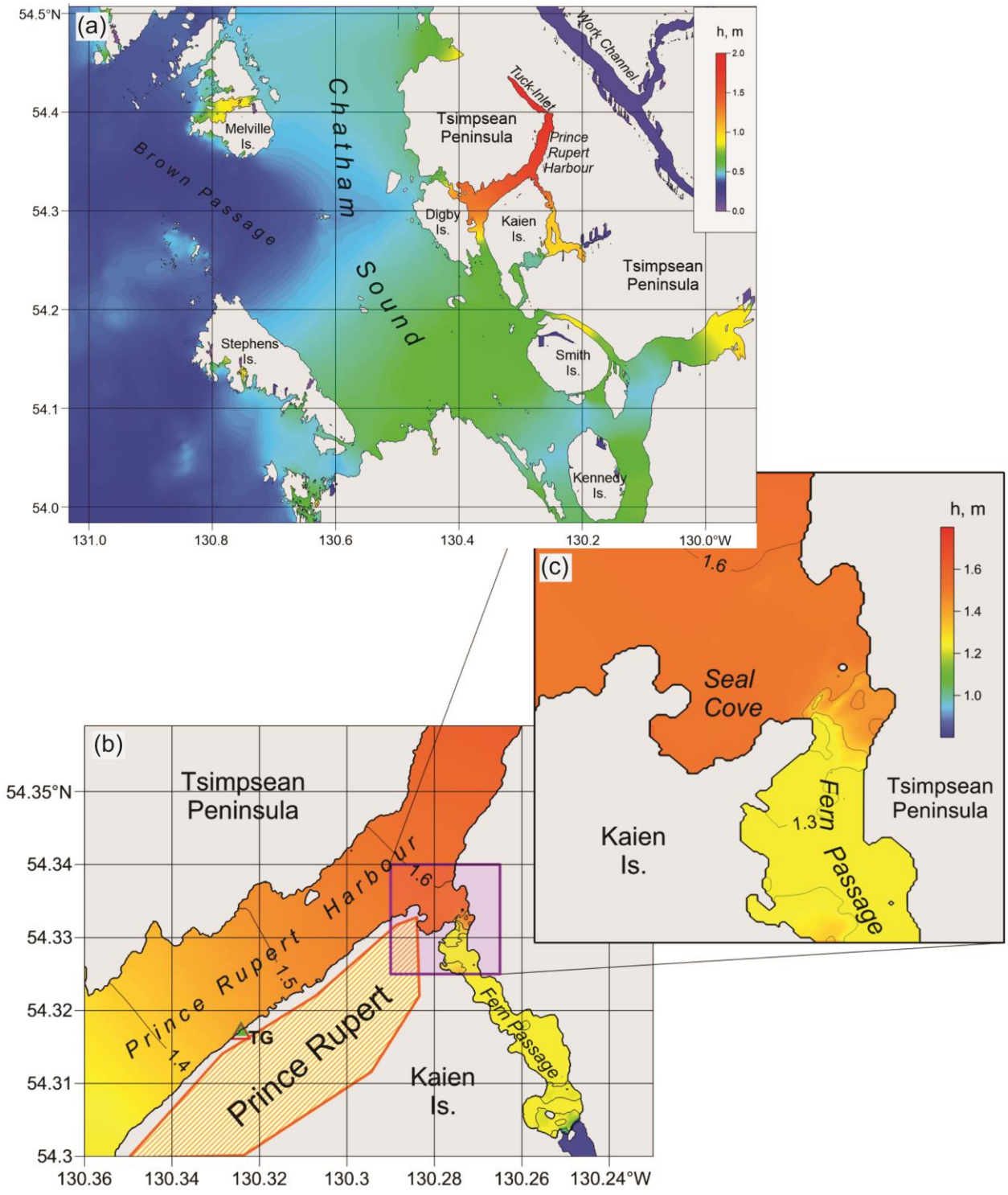

Figure 20. Distribution of maximum tsunami wave amplitudes (metres) for (a) Grid 3 and (b) Grid 4 of the nested-grid model for waves generated by simulation of the 1964 tsunami. (c) An enlarged map for Seal Cove Harbour with the Sites 1 to 8 marked. (Modified from *Fine et al.* [2018a]).

Simulated tsunami-generated sea level variability at specific sites on the north coast, around Seal Cove and the mouth of Fern Passage, is shown in Figure 21. Tsunami waves arriving at Seal Cove from this simulated event are 5-10% higher than those at the Prince Rupert tide gauge but generally alike those for Prince Rupert Harbour. The wave amplitudes at Sites 1, 2, 3 and 4 are very similar and hence only Site 4 results are shown (Figure 21a). The simulated wave heights for Site 5 (Figure 21b) are also similar to those for Sites 1-4, while tsunami wave simulations at Sites 6, 7, and 8 are a bit lower. In general, all records are very similar, indicating that the Seal Cove basin is too small to amplify the low frequency (period about 2 hours) of the incoming waves generated during a future 1964-type tsunami.

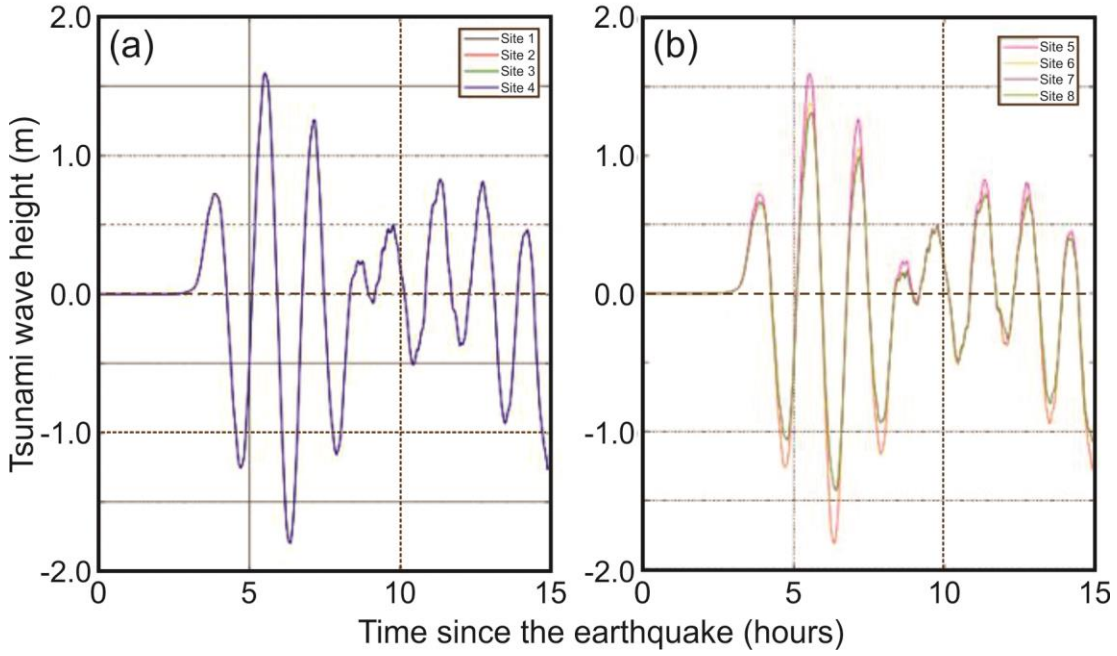

Figure 21. Simulated records of sea level variation for the Alaska 1964 tsunami at (a) Sites 1 - 4 and (b) Sites 5 – 8 within Seal Cove Harbour (See Figure 20c for the site locations). (Modified from *Fine et al.* [2018a]).

Detailed analysis of the sea level variability was carried out by *Fine et al.* [2018a] for 8 sites around Sea Cove Harbour (Figure 20c), ranging from the outer breakwater (Site 1) to the location of the tide gauge in the inner harbour (Site 8). Figures 16a and 16b show that

the simulated tsunami waves at the Coast Guard site are 5 to10% lower than those at the tide gauge site in the inner harbour (Figure 13).

In general, the high-resolution, nested-grid tsunami simulation by *Fine et al.* [2018a] yielded the following principal results:

1. Tsunami wave heights in Seal Cove will reach **1.55 m** above the tidal level at the time of the event; the second wave will be the highest wave;

2. The second wave crest will arrive approximately **100 min** after the first wave crest. Tsunami wave periods range from 70 to 105 min;

3. Tsunami wave amplitudes will be nearly uniform throughout Seal Cove;

4. Tsunami-induced currents in Seal Cove will be weak **(< 0.5 m/s**), but in neighbouring Fern Passage will be quite strong and reach speeds of approximately **2.5 m/s;**

5. Because the details of future possible tsunamis remain unknown in many aspects, we recommend use of a **safety factor of 50%** to be added to estimated tsunami amplitudes during a 1964 Alaska-type event. In this case, the safety water level for Seal Cove should be at least **2.28 m** above Mean Higher High Water (MHHW), or **4.6 m** above Mean Sea Level (MSL).

3.3. MODELING A 1700-TYPE CASCADIA TSUNAMI

The Cascadia Subduction Zone (CSZ) is a convergent plate boundary that stretches from central Vancouver Island (Canada) to Northern California (USA). It is here that the Explorer, Juan de Fuca, and Gorda plates slide eastward below the continental North American Plate (Figure 22). The Great CSZ earthquake of 26 January 1700, which had an estimated magnitude M_w 9.0, generated a major trans-oceanic tsunami that caused significant destruction in Japan on the opposite side of the Pacific Ocean [cf. *Satake et al.*, 1996; *Atwater et al.,* 2005], and strongly affected the outer coast of British Columbia. There is no reliable information or data concerning historical heights on the coast of British Columbia associated with this tsunami, however, paleotsunami findings on the coast of Vancouver Island and the west coast of the USA [cf. *Wang et al.*, 2003; *Clague et al*., 2000, 2003; *Wang et al.,* 2013] show that tsunami waves of ~15 m likely struck these coasts at the time of the 1700 CSZ earthquake.

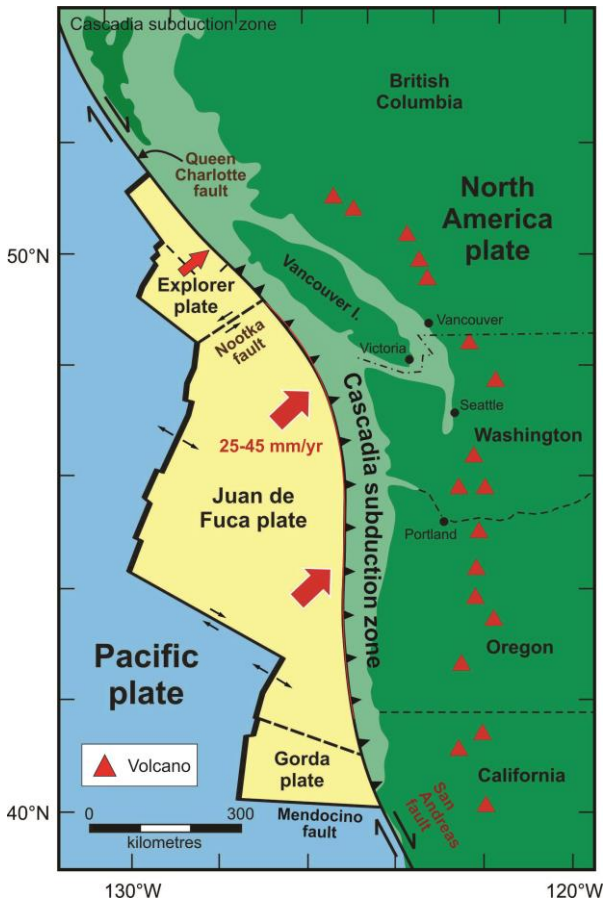

Figure 22. The Cascadia subduction zone, a convergent plate boundary stretching 1000 km from northern Vancouver Island (BC) to northern California. The Juan de Fuca Plate and two smaller plates are sliding beneath the North American Plate.

Cascadia Subduction Zone (CSZ) tsunamis are considered as the main tsunami threat for the west coast of British Columbia [*Clague et al.*, 2003; *Leonard et al.*, 2014]. Preliminary numerical modelling of CSZ tsunamis for coastal North America [cf. *Ng et al*., 1991; *Whitmore*, 1993; *Cherniawsky et al.*, 2007; *Fine et al.*, 2008; *Cheung et al*., 2011, *AECOM*, 2013] demonstrates the high threat of CSZ tsunamis for British Columbia. Numerous seismotectonic studies indicate that great megathrust earthquakes in the CSZ region have occurred on a regular basis in the past and can be expected to occur with an average return period of about 500 years in the foreseeable future [*Witter et al.*, 2013; *Wang and Tréhu*, 2016].

Based on recent advances in Cascadia tsunami source development [cf. *Wang and Tréhu*, 2016], *Fine et al.* [2018b] considered two different CSZ earthquake source models

for tsunamis impacting the coast of British Columbia: Model A, the "buried" model; and Model B, the "splay" model. The models correspond to the same seismic momentum magnitude (M_w 9.0) but to different cross-shore distributions of the associated seismic seafloor uplifts, h_0. The models have the northward extensions from the *Witter et al.* [2013] seismic sources off California to Washington, but also include source areas located to the west of Vancouver Island.

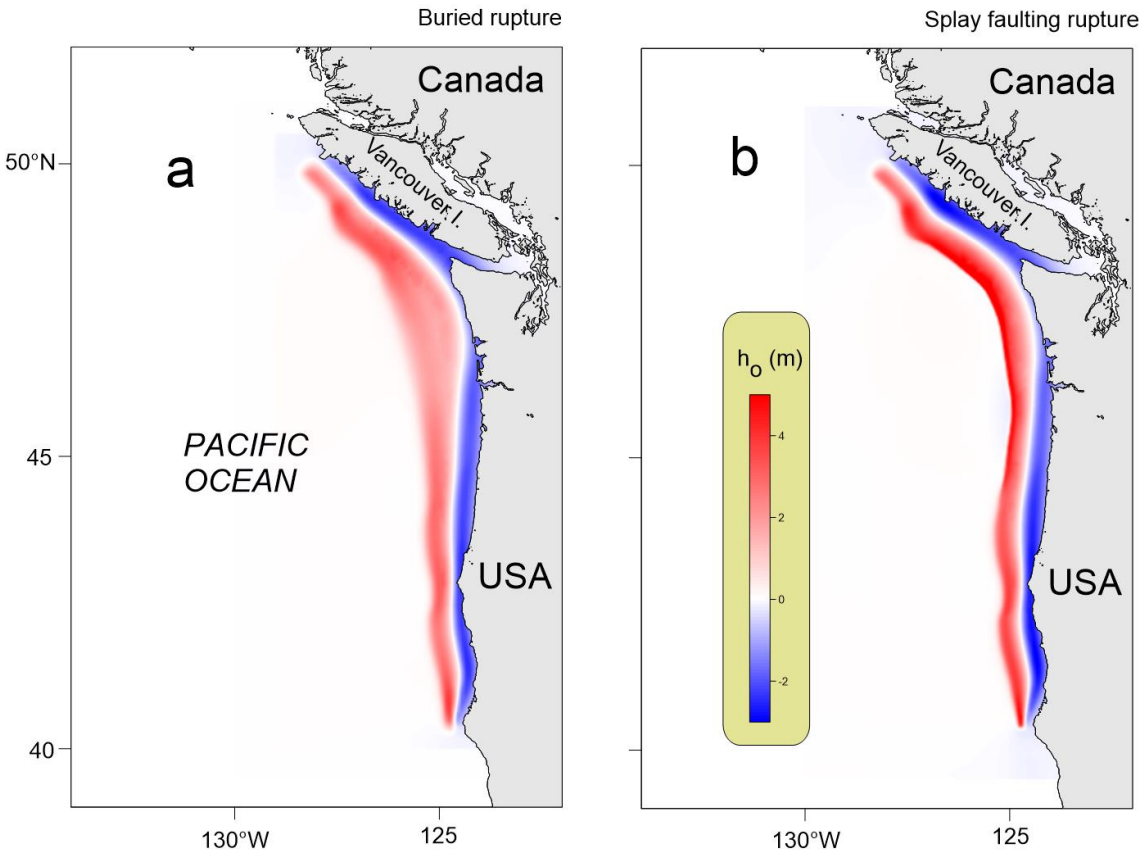

Figure 23. Maps of the Cascadia rupture zone tsunami sources according to *Gao* [2016]. Seafloor displacements, h_0, are in metres. (a) Whole margin buried rupture (Model A); and (b) Whole margin splay-faulting rupture (Model B). (From *Fine et al.* [2018b]).

The splay-fault rupture (“Model M1”) is of particular importance as it best represents a CSZ earthquake given present understanding of the faulting processes. For this model, *Witter et al.* [2013] used an extremely dense numerical mesh to allow accurate modelling of the surface-breaching rupture. The numerical study of *Fine et al.* [2018b] used a slightly modified version of the model according to the recommendations of *Wang and Tréhu* [2016]

to simulate the tsunami risk for the Seal Cove area. The splay-faulting rupture model includes a contribution from coseismic horizontal displacements to the initial tsunami wave field through a component of ocean surface uplift due to the horizontal motion of the steep ocean bottom slopes [*Gao*, 2016]. Numerical tsunami simulations reveal that including the deformation due to horizontal displacements in the source function results in an increase in the far-field tsunami amplitudes. The resulting coseismic vertical deformations (h_0) are shown in Figure 23.

Model A is the case when the source deformation slip is located well below the seabed, whereby the seafloor uplift has a smooth and gentle cross-shore profile, with maximum uplift of 4 m. Model B corresponds to the "splay" model, where the rapture edges are at the sea floor. This model is similar to the case "M1" in the *Witter et al.* [2013] classification and can be considered the most probable scenario. Maximum uplift is nearly 8 m. We note that the two previous models for Cascadia tsunami sources for the BC coast, *Cherniawsky et al*. [2007] and *AECOM* [2013], used tsunami sources that are somewhere between Models A and B.

Low-resolution results for CSZ tsunami simulations by *Fine et al.* [2018b] for Model A and Model B for Grid 1 (see Figure 11b) are presented in Figures 24a and 24b. The simulated maps of the tsunami height maxima for the open ocean are quite different. Model B produces much more intensive waves, with stronger interference of waves arriving from the northern and southern sectors of the CSZ. Waves generated by this model using the splay faulting rupture have a stronger impact on coastal areas of Vancouver Island and the US west coast than waves generated by Model A using the buried rupture source model. However, the effect on the area of interest, in Hecate Strait is much less intense in both models, with estimated wave heights of less than one metre.

Figure 25 shows the detail for the northern BC coast around Prince Rupert and Seal Cove (Grid 2). In this region the predicted tsunami wave heights are all between 0 to 1.0 m for both models, as noted for Grid 1. In general, Model B provides higher wave amplitudes than Model A, but not for all regions. In essence, northern British Columbia experiences only "side" effects from CSZ tsunamis.

The detailed results for Chatham Sound and surrounding inlets are shown in Figure 26 (Grid 3). It is apparent that for eastern Chatham Sound and Prince Rupert Inlet, tsunami

waves are slightly higher for the CSZ source Model A than for Model B, while for the southwestern part of the grid, the opposite is true: simulated tsunami waves are considerably higher for Model B than for Model A (Figure 26).

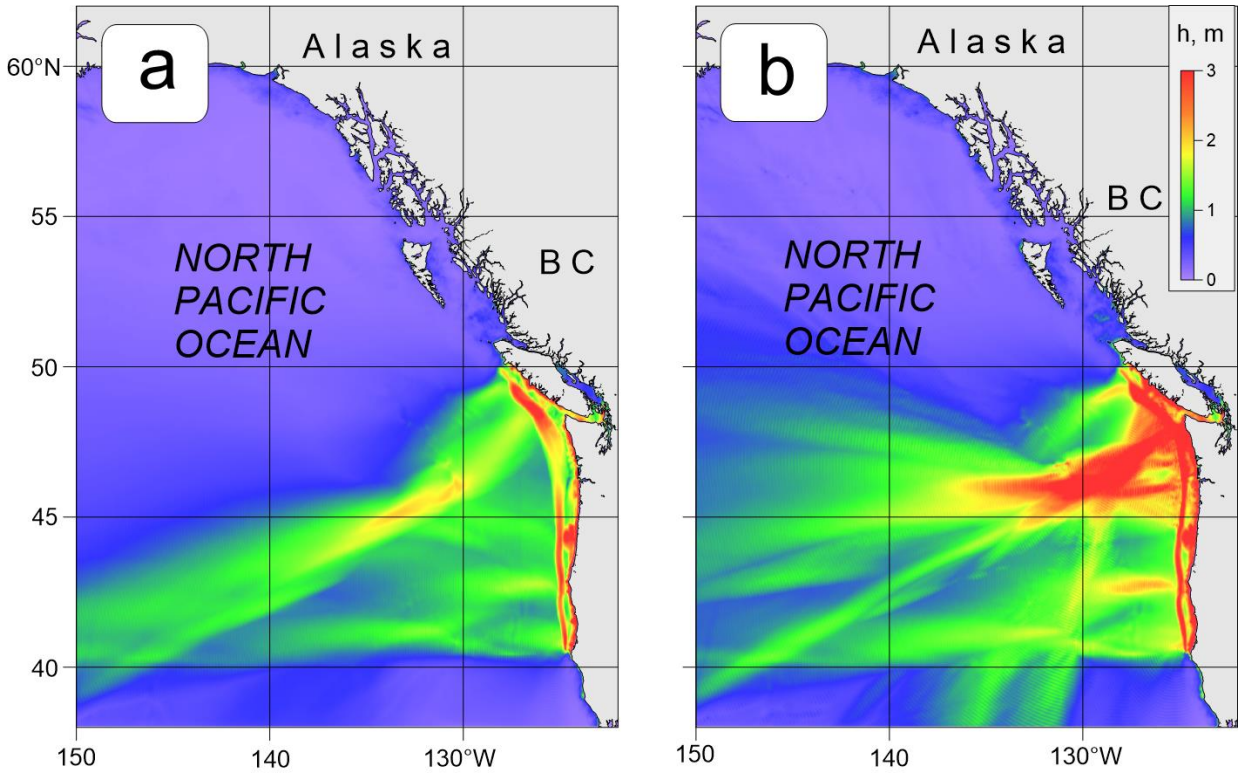

Figure 24. Spatial distribution of maximum tsunami wave amplitudes (*h*, in metres) for Grid 1 of the nested-grid model for waves generated by simulation of the CSZ tsunami for (a) Model A and (b) Model B. (From *Fine et al.* [2018b]).

The different tsunami generation responses for Model A and Model B are attributed to differences in the shapes of the tsunami sources: Model A has a smother shape, while Model B has a sharper shape and higher uplift (Figure 23). Accordingly, Model B produces more energy in the high frequency range and less energy in the low frequency range than Model A. In protected areas, such as Hecate Strait, the differences in wave heights between models is less pronounced, and in some places can be the opposite to that along the outer coast (see Figures 25-26).

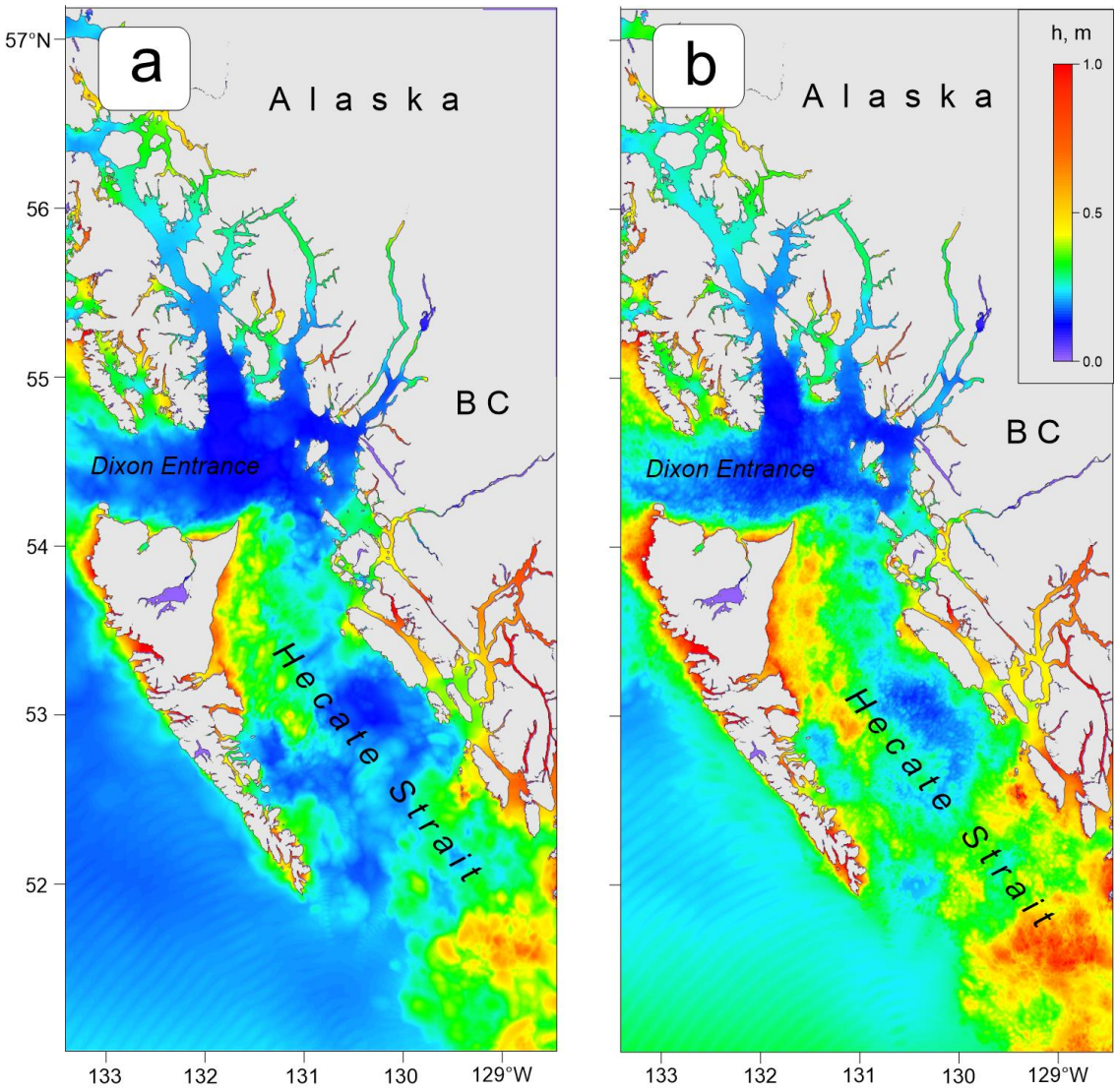

Figure 25. Spatial distribution of maximum tsunami wave heights (*h*, in metres) for Grid 2 of the nested-grid model for waves associated with the CSZ tsunami for (a) CSZ source Model A and (b) Model B. (From *Fine et al.* [2018b]).

Detailed distributions of the maximum wave heights in Seal Cove and surrounding areas are presented in Figures 27 and 28. According to the computational results by *Fine et al.* [2018b], the average maximum tsunami height in Seal Cove is about 0.75 m for Model A (Figure 27), and about 0.65 m for Model B (Figure 28). The height distributions are quite similar for both cases, but wave heights for Model B are 15% smaller than those for Model A. Inside Seal Cove, tsunami heights are nearly uniform and similar to the heights in neighbouring Prince Rupert Harbour. The waves become smaller inside Fern Passage, with wave amplitudes decreasing with passage through each narrow part of the channel.

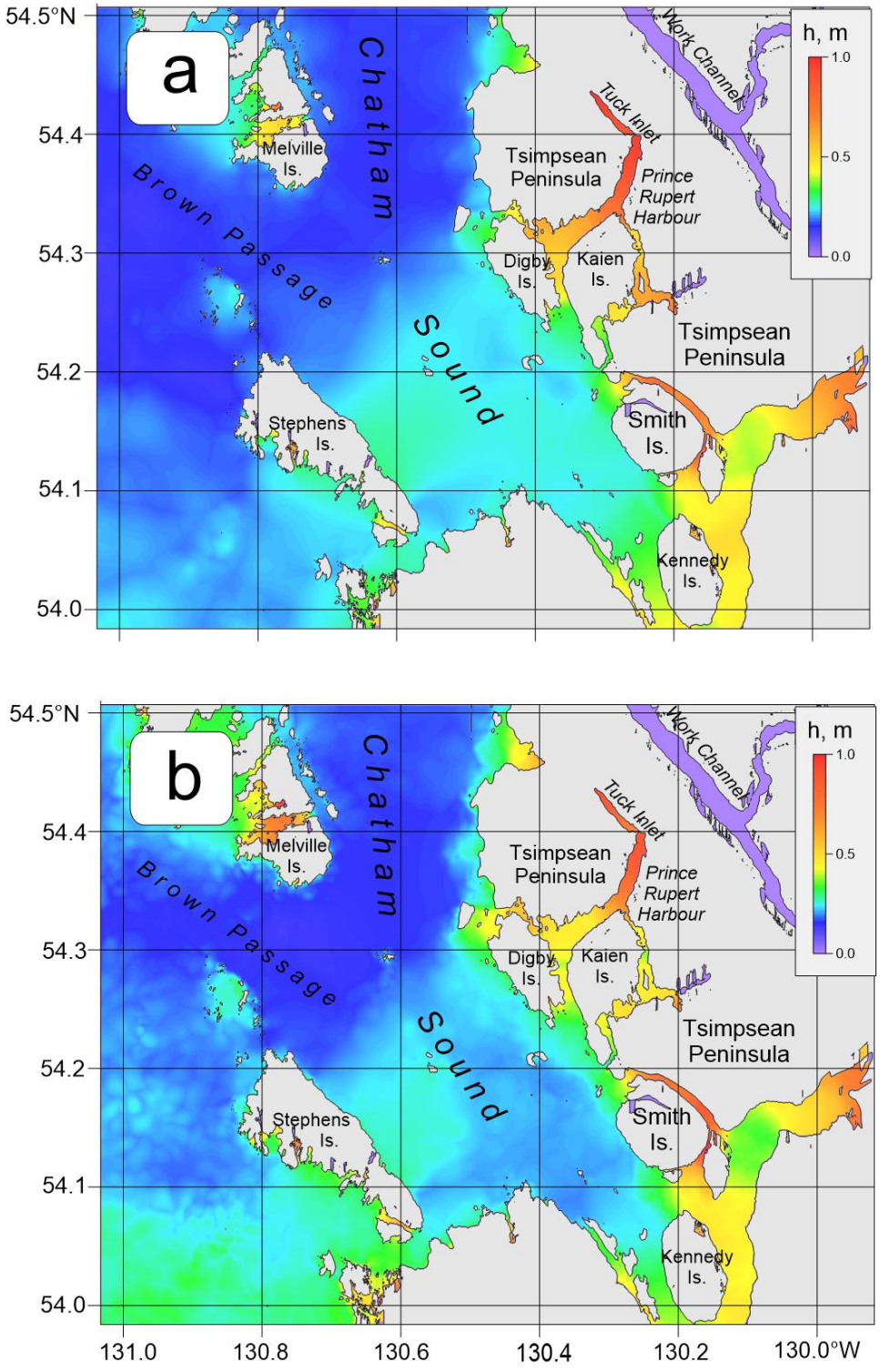

Figure 26. Spatial distribution of maximum tsunami wave heights (*h*, in metres) for Grid 3 of the nested-grid model for waves associated with the CSZ tsunami for (a) CSZ source Model A and (b) Model B. (From *Fine et al.* [2018b]).

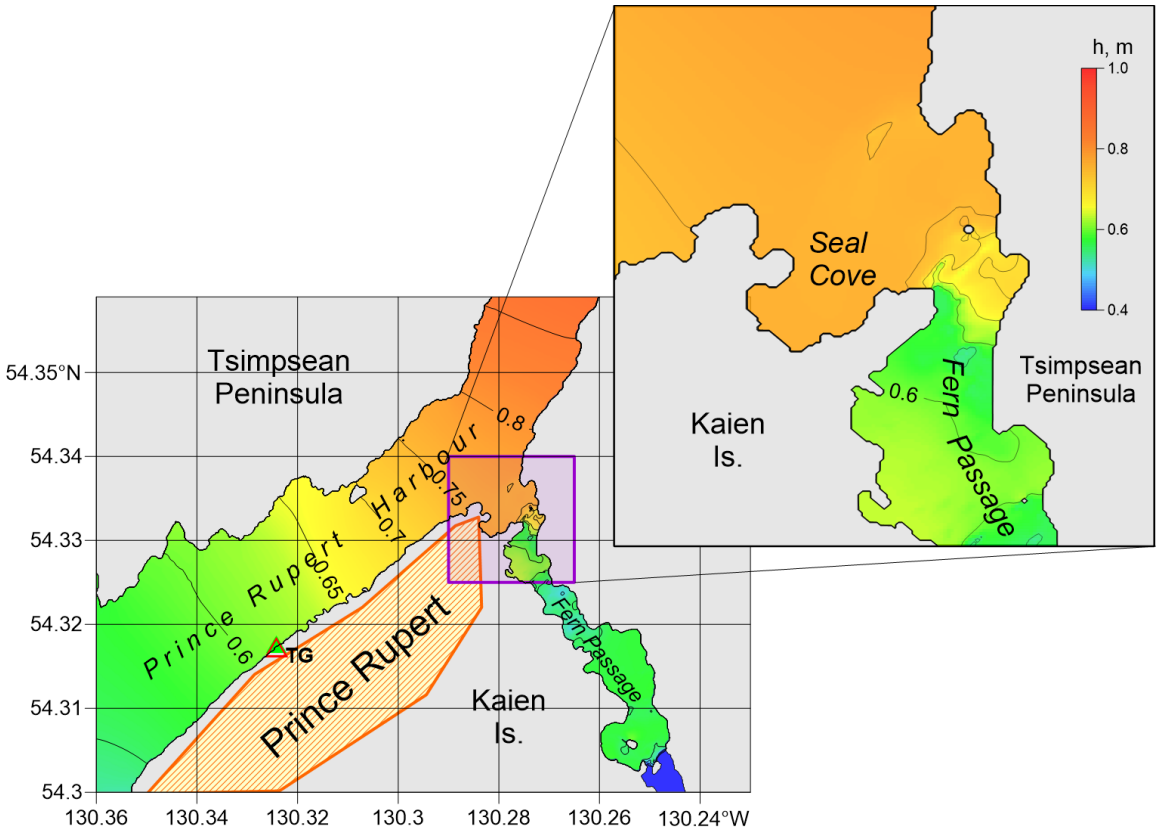

Figure 27. Model A: Spatial distribution of maximum tsunami wave heights (*h*, in metres) for Grid 4 of the nested-grid model for waves associated with the CSZ tsunami. The inset shows an enlarged segment of Seal Cove area. (From *Fine et al.* [2018b]).

The computed tsunami-induced currents are weak in Seal Cove both for Model A and Model B; much stronger currents are found to occur in Fern Passage. As with wave height, currents are stronger for Model A while the distributions of the currents for both models are similar.

Tsunami waveforms of the modelled waves at specific sites (see Figure 14b) are presented in Figures 29a and 29b; the statistical characteristics of these records are found in Tables 4 and 5. It is apparent that the wave heights are nearly identical for sites 1 to 4 with first crest heights of 0.26 m to 0.29 m and the largest wave heights reaching 0. 65 and 0.76 m for both A and B model simulations.

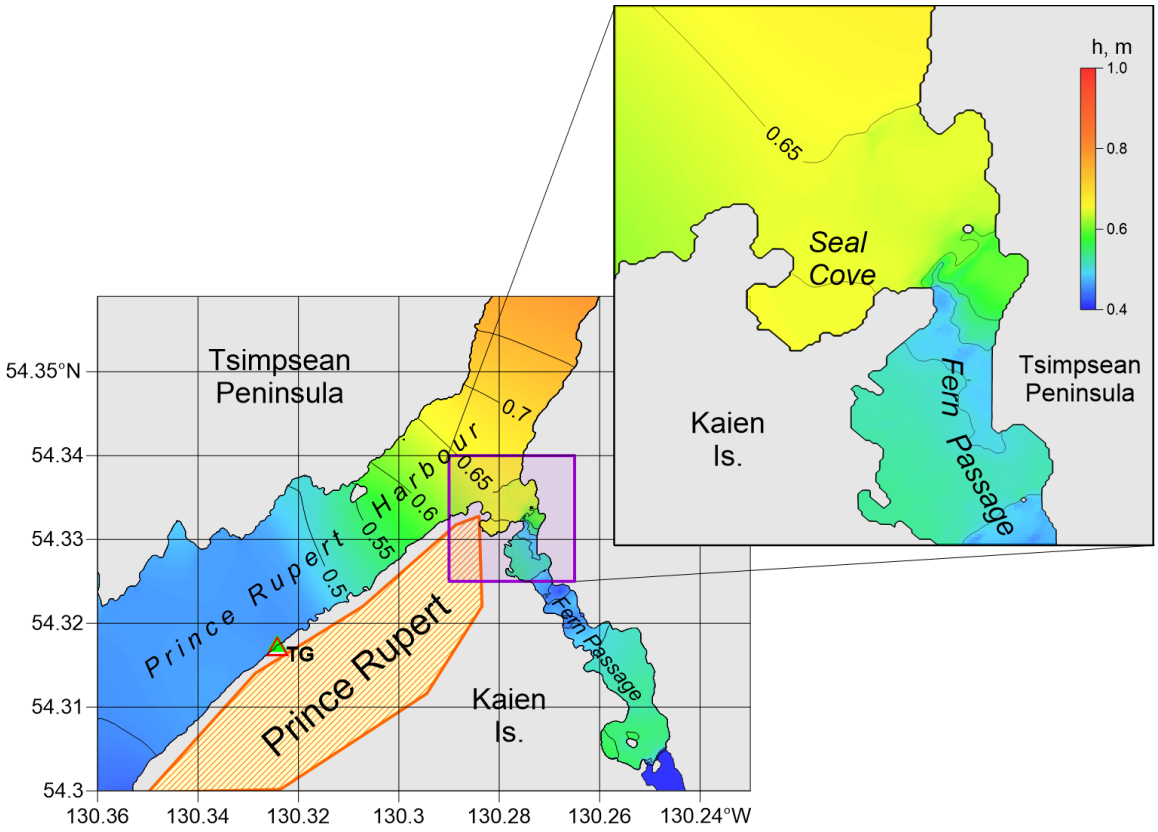

Figure 28. Model B: Spatial distribution of maximum tsunami wave heights (*h*, in metres) for Grid 4 of the nested-grid model for waves associated with the CSZ tsunami. The inset shows an enlarged segment of Seal Cove area. (From *Fine et al.* [2018b]).

At Sites 5 to 8 the first crest amplitude values are similar at Sites 1 to 4, with amplitudes of 0.26 m to 0.29 m at all sites. However, the maximum wave amplitude simulations from A and B are noticeably smaller at Sites 6 to 8, differing by up to 0.25 m (approximately 30 %). At Sites 6 to 8 Model A results range from 0.58 to 0.63 m and Model B results ranging from 0.5 to 0.53 m. The first wave reaches the Seal Cove region 3.5 hours after the earthquake and is expected to be quite small (less than 0.3 m). The highest wave (roughly 0.7-0.8 m), the sixth wave crest, arrives at Seal Cove 12 hours after the earthquake. Typical tsunami wave periods are about 100 min for both models.

Table 4. Model A simulated tsunami wave parameters for a Cascadia Subduction Zone tsunami at Seal Cove. See Figure 2.4 for the site locations. Travel times for the maximum waves are in hours and minutes after the start of the earthquake.

Site No	First crest		Highest crest		Deepest trough	
	Amplitude (m)	Travel time (hh:mm)	Amplitude (m)	Travel time (hh:mm)	Amplitude (m)	Travel time (hh:mm)
1	0.29	03:52	0.76	11:54	-0.73	12:12
2	0.29	03:52	0.76	11:54	-0.73	12:12
3	0.29	03:52	0.76	11:54	-0.73	12:12
4	0.29	03:52	0.76	11:54	-0.73	12:12
5	0.29	03:53	0.76	11:54	-0.74	12:12
6	0.29	03:53	0.63	11:55	-0.74	12:13
7	0.29	03:53	0.58	11:54	-0.60	12:15
8	0.29	03:53	0.61	11:55	-0.60	12:15

Table 5. Model B simulated tsunami wave parameters for a Cascadia Subduction Zone tsunami at Seal Cove. See Figure 2.4 for the site locations. Travel times for the maximum waves are in hours and minutes after the start of the earthquake.

Site No	First crest		Highest crest		Deepest trough	
	Amplitude (m)	Travel time (hh:mm)	Amplitude (m)	Travel time (hh:mm)	Amplitude (m)	Travel time (hh:mm)
1	0.26	03:53	0.65	11:58	-0.61	12:11
2	0.26	03:53	0.65	11:58	-0.61	12:11
3	0.26	03:53	0.65	11:58	-0.61	12:11
4	0.26	03:53	0.65	11:58	-0.61	12:11
5	0.26	03:53	0.65	11:58	-0.61	12:11
6	0.26	03:54	0.53	11:58	-0.63	12:12
7	0.26	03:54	0.50	11:58	-0.49	12:12
8	0.26	03:54	0.52	11:58	-0.49	12:12

According to numerical tsunami modeling results of *Fine et al.* [2018b], waves generated by a mega-thrust earthquake along the CSZ will be weak in the Seal Cove area. This result is not unexpected given that the area is not directly exposed to CSZ tsunamis and is affected only by side effects arising from the northern edge of the tsunami source region.

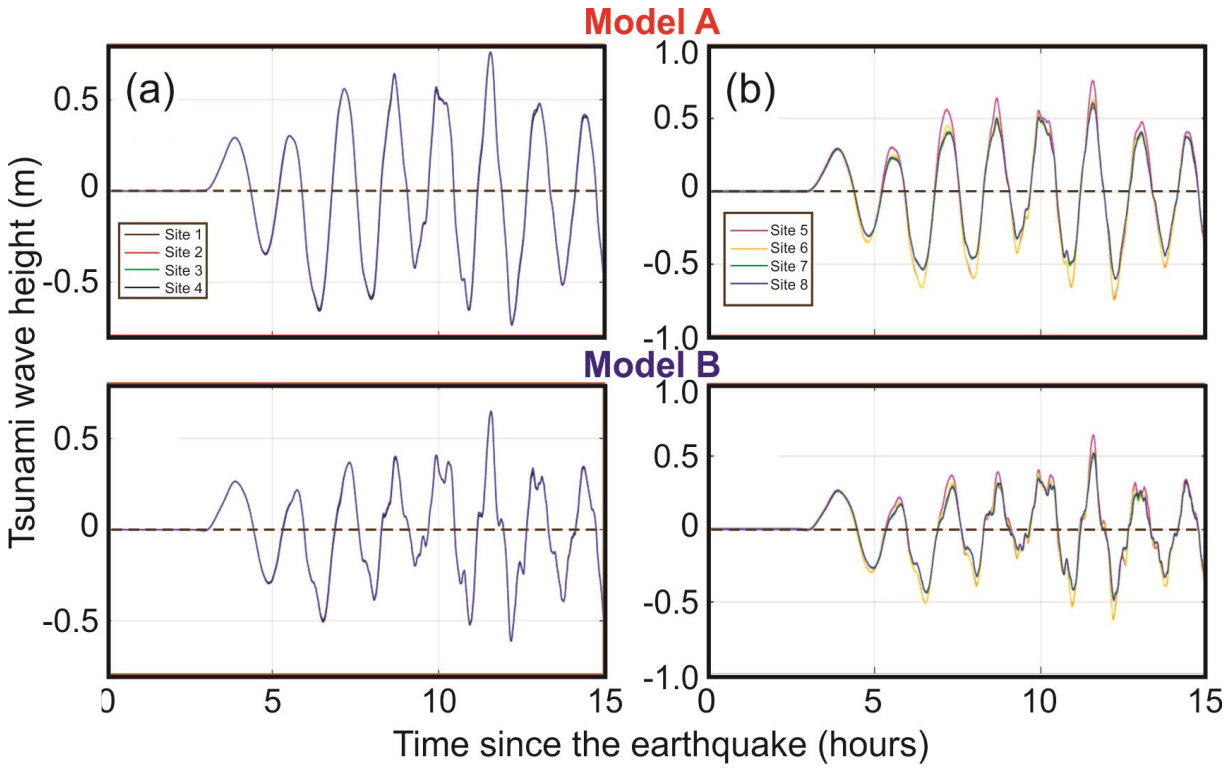

Figure 29. Simulated records of water level variations for a CSZ tsunami at Seal Cove Sites 1- 4 (a) Model A and (b) Model B and at Sites 5- 8 (c) Model A and (d) Model B. The site locations are shown in Figures 10b and 15c. (Modified from *Fine et al.* [2018b]).

Based on the modelling results, *Fine et al.* [2018b] provided the following summary and major conclusions:

• The whole margin buried rupture scenario (Model A) produced higher waves in the Seal Cover area than the whole margin splay-faulting rupture scenario (Model B);

• The maximum wave heights in Seal Cove will be **0.76 m** (Model A case) and **0.65 m** (Model B case) above the tidal level at the time of the event; the sixth wave is expected be the highest;

• Tsunami wave periods will range from **70 to 105** min;

• Tsunami wave amplitudes will be nearly uniform throughout Seal Cove;

• Tsunami-induced currents in Seal Cove will be weak, but in neighbouring Fern Passage they can be quite strong: up to **2 m/s** (**4 knots**).

Because many of the details of future possible tsunamis remain unknown, *Fine et al.* [2018b] recommend applying a safety factor of 50%, which should be added to the estimated tsunami amplitudes for a CSZ tsunami event. In particular, the safety level for Seal Cove should be **1.14 m** above MHHW, or **3.46 m** above MSL. This level, which specifically applies to a magnitude 9.0 CSZ tsunami, is below the recorded extreme high-water mark for the region.

4. GLOBAL AND REGIONAL SEA LEVEL RISE

The Intergovernmental Panel on Climate Change (IPCC) is a body of the United Nations that is dedicated to providing scientific information on climate change, its natural, political, and economic impacts and risks, and possible response options [*Weart,* 2011]. It was established in 1988 by the World Meteorological Organization (WMO) and the United Nations Environment Programme (UNEP) and endorsed by the UN General Assembly. The IPCC produces reports that contribute to the work of the United Nations Framework Convention on Climate Change (UNFCCC), the main international treaty on climate change. The IPCC's Fifth Assessment Report was a critical scientific input into the UNFCCC's *Paris Agreement* in 2015.

In 2019, the IPCC published Special Report on the Ocean and Cryosphere in a Changing Climate (SROCC) with a specific Chapter 4 on sea level rise [*Oppenheimer and Glavovic*, 2019], while *James et al.* [2015, 2021] and *Lemmen et al.* [2016] prepared special reports considering sea level rise in West Canada, in particular, on the coast of British Columbia that take into account both global climatic sea level rise and vertical tectonic motions. *Rabinovich and Thomson* [2020] used these findings to evaluate the sea level rise along the coast of Vancouver Island. The present chapter is based on this report, but focussing on the northwestern coast of British Columbia, specifically on the Prince Rupert area and Canadian Coast Guard Station in Seal Cove.

4.1. CLIMATE CHANGE AND GLOBAL SEA LEVEL RISE

A Representative Concentration Pathway (RCP) is a greenhouse gas concentration trajectory adopted by the IPCC. Four main pathways were used for climate modeling and research for the IPCC fifth Assessment Report (AR5) in 2014. The pathways describe different climate futures, all of which are considered possible depending on the volume of greenhouse gases (GHG) emitted in the years to come. The RCPs – originally **RCP2.6**, **RCP4.5**, **RCP6**, and **RCP8.5** – are labelled after a possible range of radiative forcing values in the year 2100 (Figure 23) [*Moss et al.,* 2008; *Weyant et al*., 2009].

The two most important RCPs are RCP4.5 and RCP8.5:

- **RCP 4.5** is described by the IPCC as an *intermediate scenario* (https://ar5-syr.ipcc.ch/topic_futurechanges.php). Emissions in RCP 4.5 peak around 2040-2050, then decline (Figure 29). Like all the other RCPs, RCP 4.5 requires negative CO_2 emissions (such as CO_2 absorption by trees) that would be 2 Gigatons of CO_2 per year (GtCO2/yr). RCP 4.5 is more likely than not to result in a global temperature rise of between 2°C and 3°C.

- In **RCP 8.5**, emissions continue to rise throughout the entire 21st century (Figure 30) [*Meinshausen et al.*, 2011]. RCP8.5 is generally taken as the basis for *critical climate change scenarios* since it is based on critical estimation of projected coal outputs. RCP8.5 remains useful for its aptness in both tracking historical total cumulative CO_2 emissions and predicting mid-century (and earlier) emissions based on current and stated policies.

During the last 30 years, global mean sea levels (GMSL) rose by 3.66 mm per year which is 2.5 times faster than the rate from 1900 to 1990 (SROCC, 2019). At this rate of acceleration, sea level rise could reach around 30 cm to 60 cm by 2100 even if greenhouse gas emissions are sharply reduced and global warming is limited to well below 2°C, but around 60 cm to 110 cm if emissions continue to increase strongly. In their summary SROCC indicated that "*…rate of rising sea levels is* ***unprecedented*** *over the past century*".

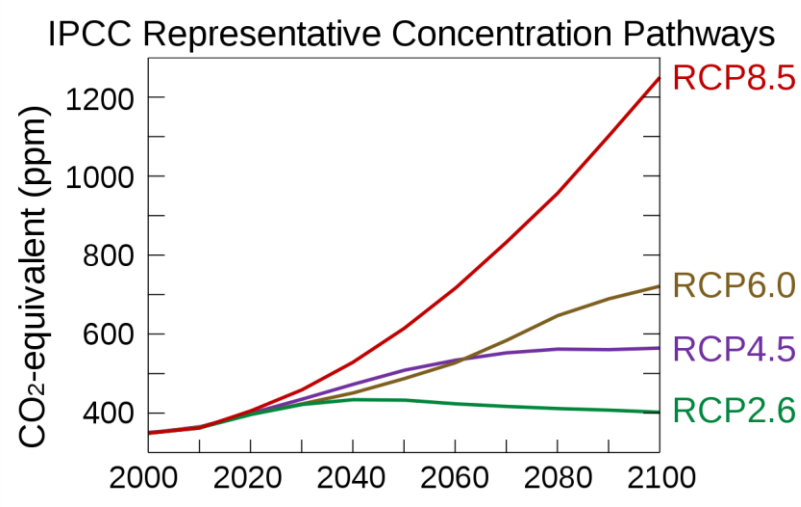

Figure 30. ICPC Representative Concentration Pathway (RCP) of CO_2-equivalent concentrations (in parts-per-million-by-volume) for 2000-2100. These four RCPs were used by the fifth IPCC Assessment Report to make predictions for sea level rise for the BC coast.

Future sea level changes are of particular importance for planning infrastructure maintenance and development in the coastal zone, for habitat management and for forecasting risk to populations. Sea-level rise leads to increased frequency and strength of coastal flooding and is an important factor responsible for coastal erosion. One of the most serious consequences of sea-level rise is its effect on extreme sea levels, which are typically associated with tsunamis, storm surges, meteotsunamis and other hazardous phenomena superposed on high tides. In the Pacific, large ENSO events can lead to significant sea-level changes (up to several tens of centimetres) [*Thomson et al.*, 2008].

Relative sea-level changes are observed or estimated relative to the solid surface of the Earth. Land uplift can offset global sea-level rise, leading to reduced rise or even a fall in relative sea level; on the other hand, land subsidence adds to absolute sea-level rise and increases relative sea-level rise. Relative sea-level rise leads to increased coastal flooding and erosion, depending on the physical nature of the coastline, while relative sea-level fall can lead to navigation hazards owing to reduced depth-under-keel [cf. *James et al*., 2014, 2021; *Lemmen et al*., 2016; *Bush and Lemmen*, 2019].

The global sea-level rise projections presented in the IPCC Fifth Assessment Report are based on the Representative Concentration Pathways (RCP) scenarios (Table 6). The

median projected sea-level rise of the highest emission RCP scenario (RCP8.5) is 1.7 times larger than that for the lowest emission RCP scenario RCP2.6 (Figure 31).

Table 6. Projections of changes in global mean temperature and sea level by 2100 under Representative Concentration Pathways scenarios (RCP) [*Rogelj et al.*, 2012].

RCP Scenario	Likely global surface temperature increase for 2081–2100* (°)	Likely global sea level rise for 2081–2100* (cm)
RCP2.6	0.3–1.7	26–55
RCP4.5	1.1–2.6	32–63
RCP6.0	1.4–3.1	33–63
RCP8.5	2.6–4.8	45–82

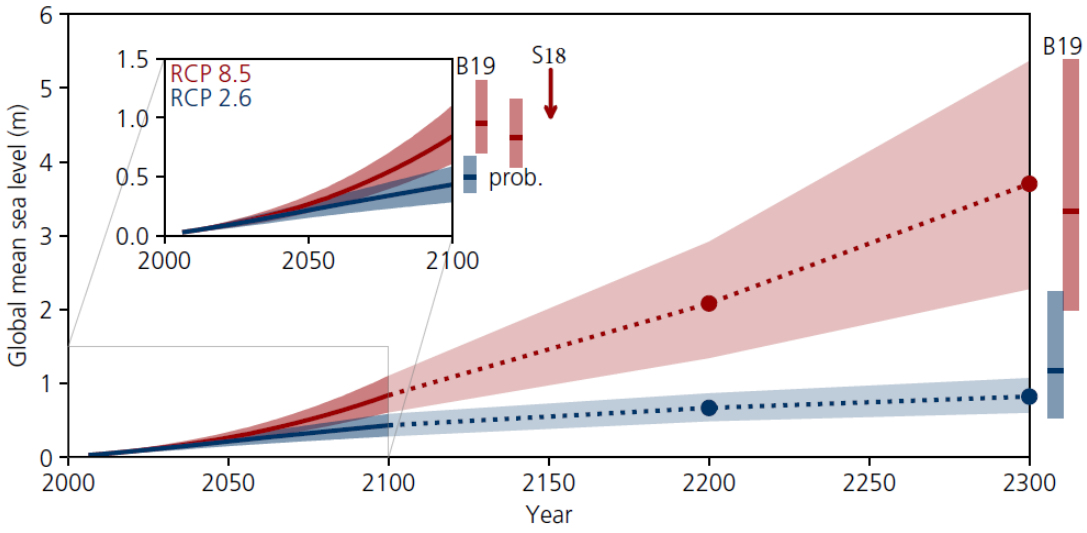

Figure 31. Projected sea-level rise until 2300. The inset shows an assessment of the likely range of the projections for RCP2.6 and RCP8.5 up to 2100 (*medium confidence*). Projections for longer time scales are highly uncertain but a range is provided. For context, results are shown from other estimation approaches in 2100. The two sets of two bars labelled B19 are from an expert elicitation for the Antarctic component and reflect the likely range for a 2 and 5° C temperature warming. The bar labelled “prob” indicates the likely range of a set of probabilistic projections. The arrow indicated by S18 shows the result of an extensive sensitivity experiment with a numerical model for the Antarctic ice sheet combined; as with the results for B19 and “prob. S18, the vertical bars show the *likely* range (from *Oppenheimer and Glavovic* [2019]).

Future rise in global mean sea level caused by thermal expansion, melting of glaciers and ice sheets, and land water storage changes, is strongly dependent on which RCP emission scenario is followed [*Oppenheimer and Glavovic*, 2019]. Sea level rise at the end of the century is projected to be faster under all scenarios, including those compatible with achieving the long-term temperature goal set out in the Paris Agreement. GMSL will rise between 0.43 m (0.29–0.59 m, likely range) for RCP2.6 and 0.84 m (0.61–1.10 m, likely range) for RCP8.5 by 2100 relative to 1986-2005 (Figure 31). Beyond 2100, sea level will continue to rise for centuries due to deep ocean heat uptake and mass loss of the Greenland and Antarctic ice sheets and with high confidence will remain elevated for thousands of years. Antarctica could contribute up to 28 cm of sea level rise (RCP8.5, upper end of likely range) by the end of the century (medium confidence) [*Oppenheimer and Glavovic*, 2019]. Under RCP8.5, the rate of sea level rise will be 15 mm/yr in 2100, and could exceed several cm/yr in the 22nd century. These high rates challenge the implementation of adaptation measures that involve a long lead-time but has not yet been studied in detail. *James et al.* [2014, 2021] and *Lemmen et al.* [2016] emphasize that the possibility of global sea-level rise exceeding 1 m by 2100 cannot be rejected and should be taken into account for estimation of possible extreme sea levels for the coast of British Columbia.

4.2. SEA LEVEL RISE FOR THE BRITISH COLUMBIA COAST

As indicated by *Oppenheimer and Glavovic* [2019], sea level does not and will not rise uniformly. Thermal expansion, ocean dynamics and land ice loss contributions will generate regional departures of about ±30% around the GMSL rise. Local anthropogenically-induced subsidence and change in wave height and period are important contributors to future changes in relative sea level (RSL) at the coast. Subsidence caused by human activities is currently the most important cause of RSL change in many delta regions. An important additional factor strongly influencing long-term sea level variations in specific regions are vertical land motions [*Lemmen et al.,* 2016]. They strongly influence changes in relative sea level. Land uplift will reduce the amount of sea-level rise experienced at a site; conversely, land subsidence will add to the amount of relative sea-level rise. Present-day land uplift or

subsidence is measured using Global Positioning System (GPS) technology and by Global Navigation Satellite Systems. This factor is especially important for seismically active zones such as the coast of British Columbia. Local processes are critical for projections of sea level impacts at local scales. Due to projected global mean sea level rise, extreme sea level events (ESLs), including those related to tsunamis and powerful storm surges, that are historically rare may become common by 2100 under all RCPs.

A dominant factor affecting relative sea-level change in British Columbia (as well as the rest of Canada) is vertical land motion. Vertical land movements in British Columbia arise from a combination of tectonic activity due to the interactions of the Juan de Fuca and Pacific oceanic plates with the North America plate, the land moving upward in response to the weight removed when the glaciers of the last ice age melted (glacial isostatic adjustment) and present-day ice-mass changes in the Coast Mountains and the Gulf of Alaska. On the Fraser River delta, sediment compaction contributes to land subsidence [*Thomson et al.*, 2008; *Bornhold and Thomson*, 2013]. Global Positioning System (GPS) observations show that the land is rising faster on the west coast of Vancouver Island than at Victoria and Vancouver, explaining why sea level has been falling at Tofino during the last 50 years but rising at Victoria and Vancouver.

Lemmen et al. [2016] in Chapter 7 of their report describe in detail the situation for the west coast of Canada. The authors emphasized that coastal British Columbia is geographically, ecologically and socially diverse. The climate changes anticipated for this region, and their impacts, are similarly varied. Nevertheless, several key findings are relevant to the region as a whole:

- Sea-level rise will not affect all areas of the British Columbia coast equally, largely due to differences in vertical land movement.
- The largest relative sea-level rise is projected to occur on the Fraser Lowland, southern Vancouver Island and on the north coast.
- Storm-surge flooding presents a greater threat to coastal communities than sea-level rise alone. Extreme water levels can be associated with climate variability (e.g., El Niño/La Niña Southern Oscillation) and storm-surge flooding. The risks associated with these events are expected to increase as sea level rises.

- Planning guidance for sea-level rise developed by the British Columbia government provides planning levels that slightly exceed the peak values (95%) of the sea-level projections at 2050. This could be considered a margin of safety that allows for possible additional sea-level rise arising from factors with significant uncertainty, such as contributions from the Antarctic Ice Sheet.

Using all previous findings, *James et al.* [2021], prepared maps of relative sea level changes on the coasts of British Columbia at 2050 and 2100 for the worst case (high-emissions) scenario, RCP8.5 (Figure 32) and moderate (median) scenario, RCP4.5 (Figure 33). According to the mapping results, the high-end predicted rise in relative sea level for the area of Prince Rupert and Seal Cove is 10-20 cm for 2050 (Figure 32), increasing to 60-80 cm for 2100 (Figure 33). Similar *median estimates* (RCP4.5) are 20-25 cm for 2050 are 40-60 cm for 2100 (Figure 33).

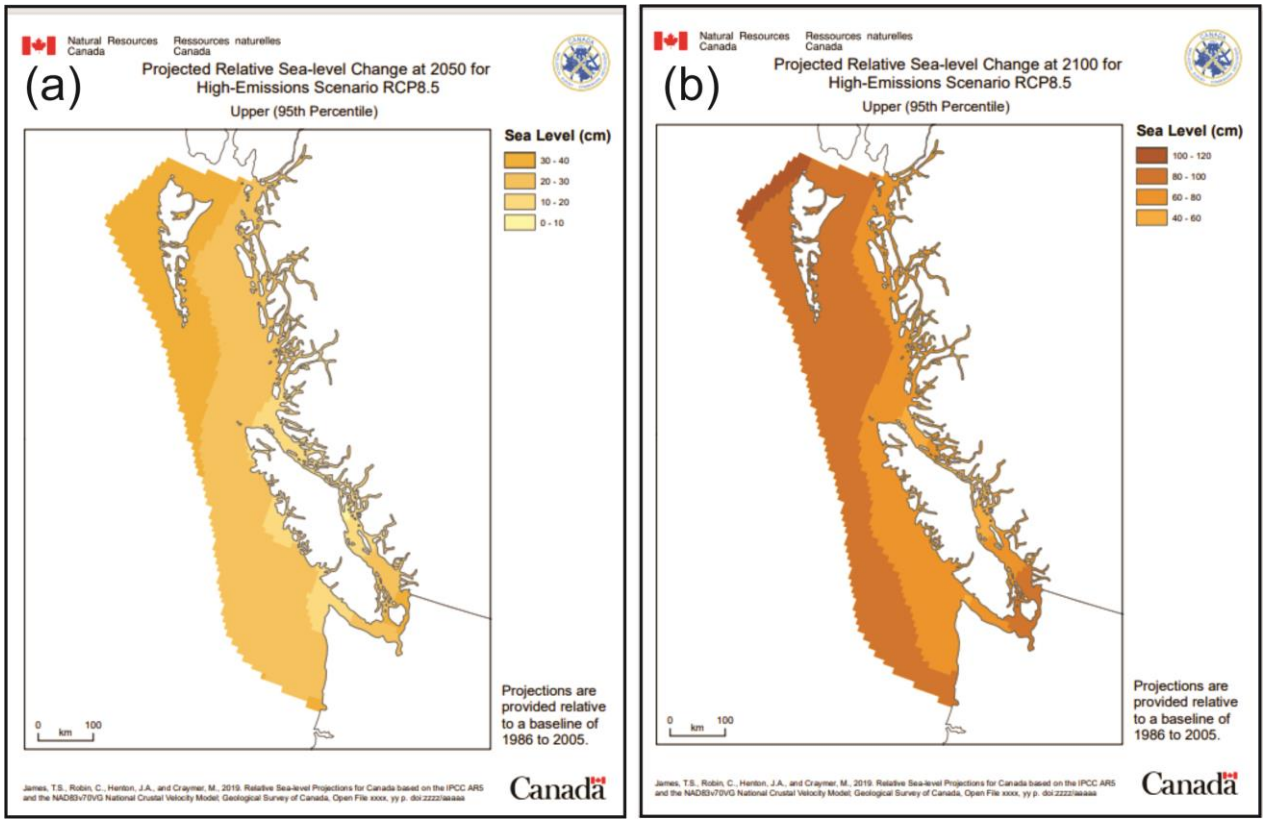

Figure 32. Projected relative sea-level changes at (a) 2050 and (b) 2100 for high-emissions scenario RCP8.5. Upper (95%). (From *James et al.* [2021]).

All final results of projected sea level changes at Victoria for 2050, 2100 and 2200 are presented in Table 7. These values were used to evaluate possible coastal flooding due to various marine sea level hazards for the area of Victoria under *low, moderate and high* global sea level rise scenarios. For comparison, based on results of *Rabinovich and Thomson* [2020], we have also included similar estimates for Patricia Bay (IOS) and Departure Bay, Nanaimo (PBS).

Hausfather and Peters [2020] indicate that, fortunately, by their opinion the world imagined in RCP8.5 is one that, in their view, becomes increasingly implausible with every passing year. Nevertheless, just RCP8.5 is typically used as the "**worst-case scenario**". Thus, *James et al.* [2021] indicate that, for comparative analyses of the costs of mitigation and adaptation, comparisons between a *high-emissions scenario* (RCP8.5) and *a low-emission scenario* (RCP2.6, strong mitigation), may be useful. Here, the impacts and costs of climate change for differing pathways of carbon emissions can be assessed and compared to the costs of mitigation.

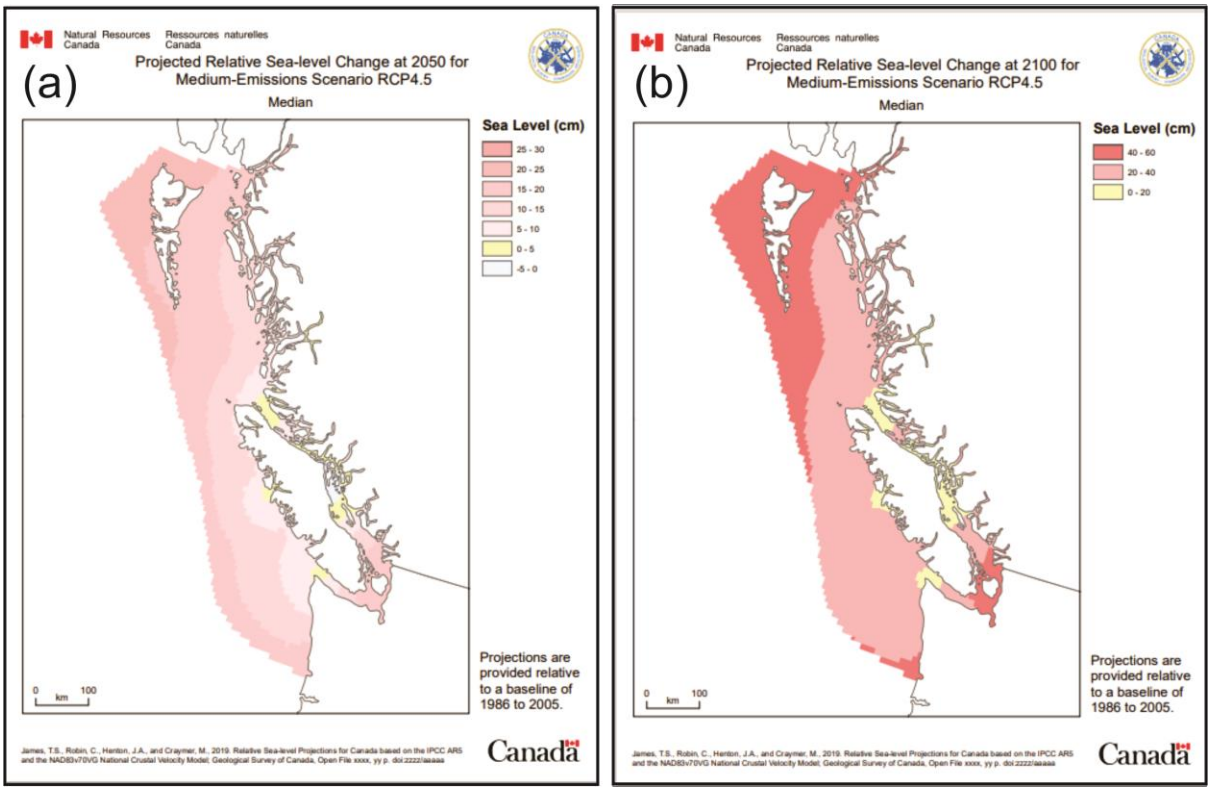

Figure 33. Projected relative sea-level changes at (a) 2050 and (b) 2100 for medium-emissions scenario RCP4.5. Median. (From *James et al.* [2021]).

Long-term Canadian Hydrographic Service (CHS) tide gauge measurements were used by *James et al.* [2015] to predict sea level rise at specific sites in British Columbia, taking into account both global sea level rise associated with climatic changes and vertical land motions. Based on the recommendations of *Hausfather and Peters* [2020] and *James et al.* [2021], we selected from the tables and results presented in Figures 25-27 of *James et al.* [2015, 2021] the *median values* of projected relative sea-level changes at Prince Rupert (Figure 34). The sea-level projections are based on a national model of vertical crustal motion derived from GPS measurements [*Robin et al*., 2020]. The relative projected sea level changes for various RCP values and years for this station are shown in Table 7. For comparison, similar estimates for Victoria are also included into this table. An important fact follows from these results: a substantial tectonic subsidence of the north coast of British Columbia. For this region the indicated subsidence significantly compensates the general Global Sea Level Rise. As a result, in the area of Prince Rupert the expected sea level changes for the period 2050-2100 (Table 7) are noticeably smaller than the climatic sea level changes (Table 6).

As indicated by Table 7, the relative projected sea level changes at Victoria and Prince Rupert are alike: approximately 36-43 cm for RCP2.6 and 55-58 cm for RCP8.5 (for 2100). In our study we used some very recent results presented to the authors by *Thomas James* (National Resources, Canada). The corresponding plots are shown in Figure 35. They enable us to estimate the general spatial structure of projected relative sea-level changes in Juan de Fuca Strait and in the Strait of Georgia and, in particular, for the Victoria region. They also give us some extrapolated values for 2200.

Prince Rupert, BC (BCPR)

Projected sea-level change is given in centimetres, relative to 1995.

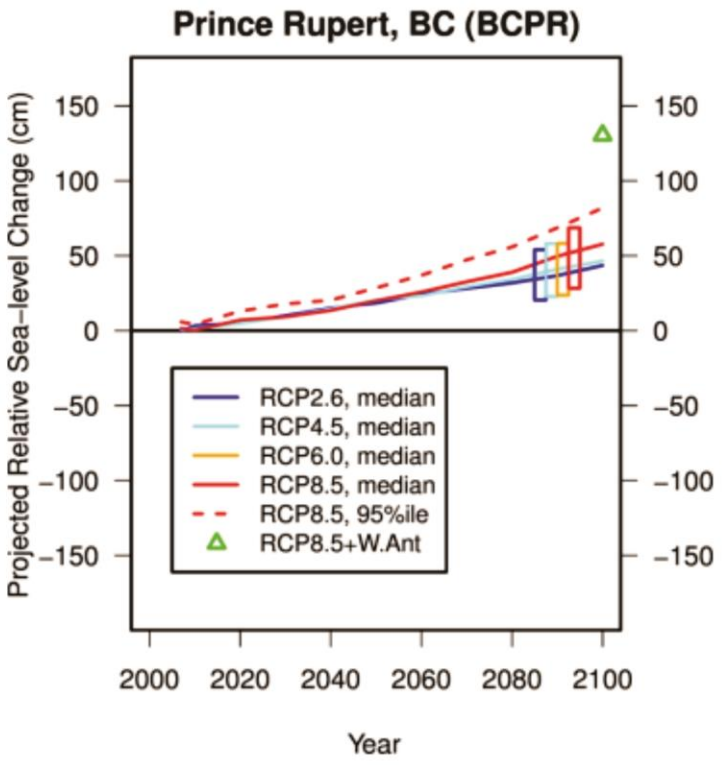

Figure 24. Projected relative sea-level change for RCP2.6, RCP4.6, and RCP8.5 (median values, solid lines; 95th percentile of RCP8.5, dashed line) (James et al., 2014). Rectangles also include RCP6.0 and give the 90% confidence range (5% to 95%) of the average for the time period 2081-2100. RCP8.5 +W.Ant is the median projection of RCP8.5 plus an additional 65 cm of global sea-level rise from West Antarctica(green triangle).

Average Projected Sea-level Change, 2081-2100

scenario	5%	median	95%
RCP2.6	20.4	37.2	54.0
RCP4.5	22.7	40.4	58.1
RCP6.0	23.6	40.9	58.2
RCP8.5	28.3	48.4	68.6

RCP8.5+W.Ant at 2100: 130.4 cm

RCP2.6

year	5%	median	95%
2007	-3.3	-0.4	2.6
2010	-1.8	3.2	8.3
2020	0.8	5.0	9.2
2030	4.5	10.0	15.4
2040	8.6	15.1	21.6
2050	10.6	18.4	26.3
2060	14.0	24.1	34.1
2070	15.5	28.1	40.7
2080	17.2	31.8	46.4
2090	19.8	36.7	53.6
2100	23.1	43.5	63.9

RCP4.5

year	5%	median	95%
2007	-2.5	0.5	3.5
2010	-2.7	1.5	5.8
2020	0.3	4.9	9.6
2030	4.3	9.2	14.1
2040	6.8	14.6	22.5
2050	12.8	20.5	28.2
2060	12.7	23.3	34.0
2070	15.7	29.1	42.6
2080	18.7	34.0	49.3
2090	22.5	41.0	59.5
2100	25.3	46.4	67.5

RCP8.5

year	5%	median	95%
2007	-3.1	1.4	5.8
2010	-3.5	0.3	4.1
2020	1.1	7.0	13.0
2030	0.6	9.2	17.8
2040	6.8	13.5	20.3
2050	11.2	19.9	28.5
2060	14.5	25.7	36.9
2070	18.1	32.6	47.2
2080	22.0	38.9	55.8
2090	30.7	49.6	68.6
2100	33.5	57.7	81.8

Figure 34. Projected relative sea-level changes at Patricia Bay for 2007-2100 for RCPs 2.6, 4.5 and 8.5 (From *James et al.* [2015])

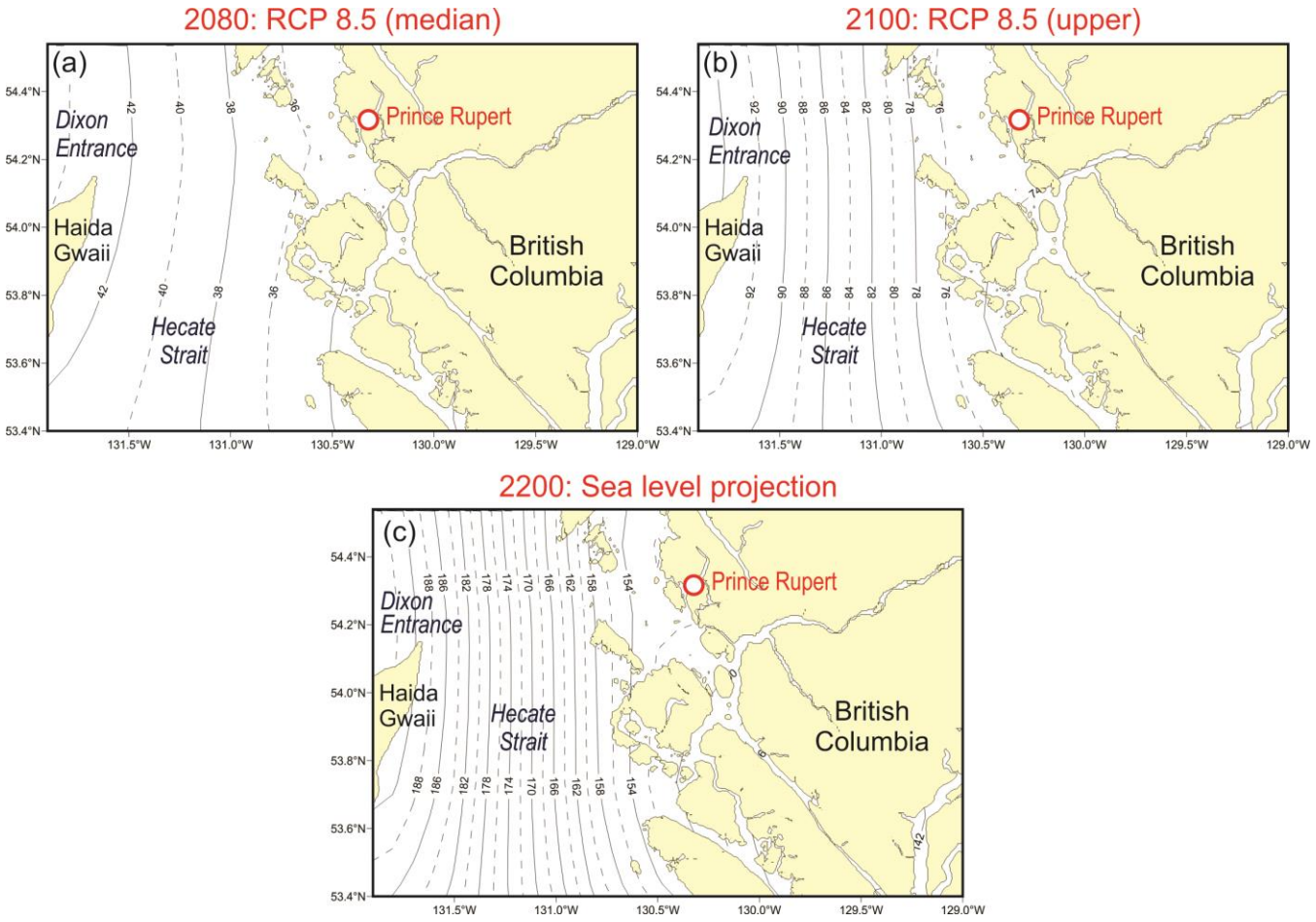

Figure 35. Projected relative sea-level changes for northern British Columbia for (a) 2080, scenario RCP8.5 (median), (b) 2100, RCP8.5 (upper) and (c) 2200 sea level projection (Constructed by Isaac Fine based on data provided by Thomas James, National Resources of Canada [*James et al*., 2021]). Location of Prince Rupert is indicated

Table 7. Relative projected sea level changes (median values) for Victoria and Prince Rupert (in cm) for 2050 and 2100 based on estimates by *James et al.* [2015, 2021]

RCP	Victoria		Prince Rupert	
	2050	2100	2050	2100
2.6	15.0	36.1	18.4	43.5
4.5	15.5	40.1	20.5	46.4
8.5	16.1	54.6	19.9	57.7

5. EFFECT OF SEA LEVEL RISE ON TSUNAMI HEIGHTS

In this section, we can combine the results of Sections 3 and 4 to estimate the tsunami risk for the Prince Rupert area and, specifically, for the Seal Cove Coast Guard Station, taking into account the expected long-term sea level changes caused by the global climatic sea level rise and vertical tectonic motions. The main results of this combination are shown in Figure 36. The maximum tsunami amplitudes in this figure were computed for (a) a 1964-type Alaska tsunami, and (b) for a 1700-type CSZ (Model A) tsunami. The total tsunami heights are shown in this figure relative to mean sea level (MSL) and relative to mean higher-high water, MHHW = 232 cm for Prince Rupert. All estimates are for 2100 for the three Representative Concentration Pathway (RCP) Scenarios: *Low* (RCP2.6), *moderate* (RCP4.5) and *high* (RCP8.5).

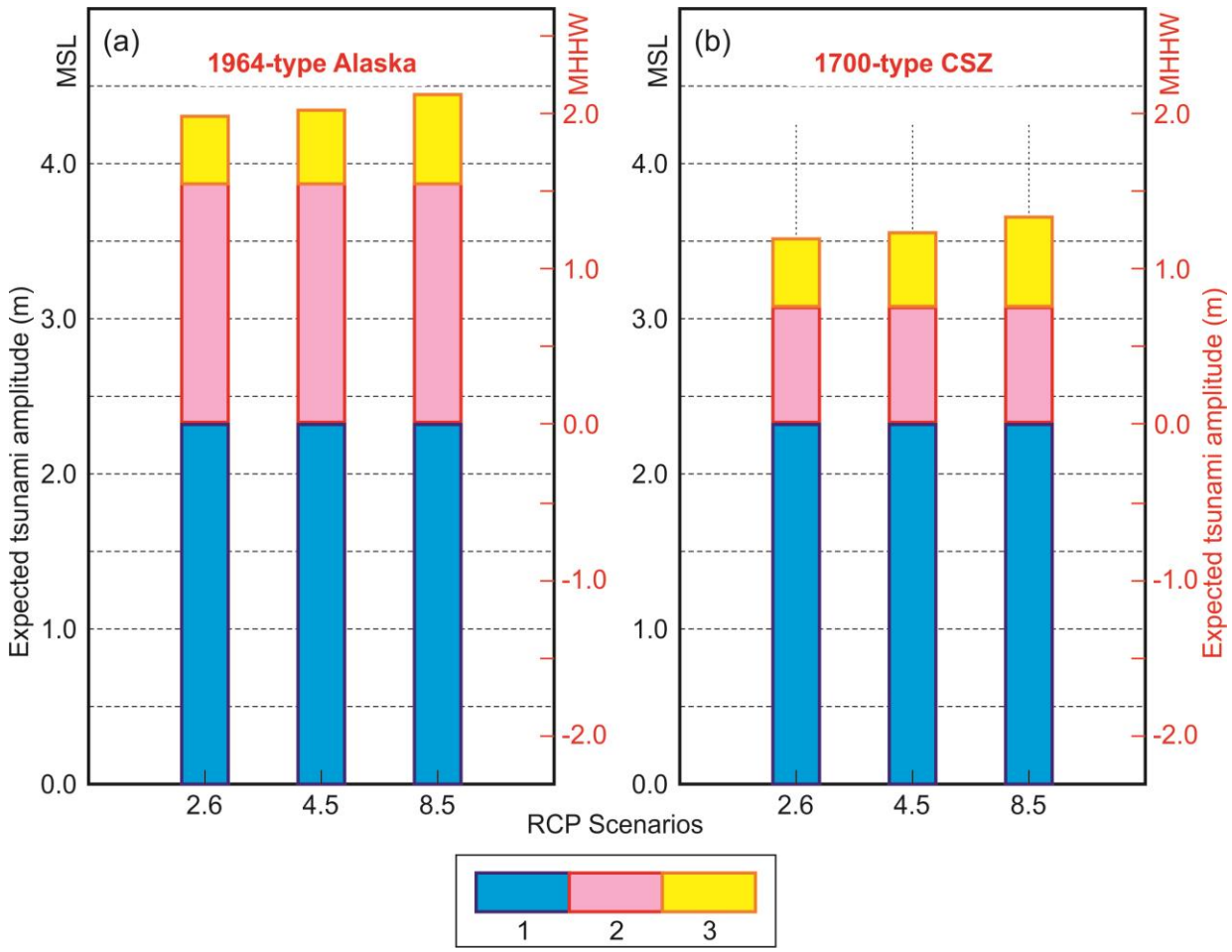

Figure 36. Expected effective tsunami heights numerically simulated by *Fine et al.* [2018a,b] for (a) a 1964-type Alaska earthquake and (b) a 1700-type CSZ (Model A) earthquake, taking into account possible sea level change for 2100 produced by the combined effect of global sea-level rise for Representative Concentration Pathway (RCP) Scenarios RCP2.6 (*low*), RCP4.5 (*moderate*) and RCP8.5 (*high*). Along the left Y-axis are the expected tsunami wave amplitudes relative to mean sea level (MSL); along the right Y-axis tsunami wave amplitudes are relative to mean higher-high water (MHHW = 232 cm for Prince Rupert). In the colour-coded legend: "1" is the MHHW level; "2" is the computed tsunami wave amplitude; and "3" is the expected sea level rise associated with the climate changes and vertical tectonic motions.

In summary, all components of the forecasted sea levels (in cm) for the two types of earthquakes can be presented as follows:

	Alaska	CSZ (A)
MHHW	232	232
Tsunami amplitude	155	76
RCP2.6	44	44
RCP4.5	46	46
RCP8.5	58	58
Total (RCP2.6)	**431**	**352**
Total (RCP4.5)	**433**	**354**
Total (RCP8.5)	**445**	**366**

Because many of the details of future possible tsunamis remain unknown, including the tidal and seasonal sea levels at the time of the event, uncertainties in the earthquake source distribution, possible storm surge or other oceanic events, we recommend that a safety factor of 50% be added, giving an estimated tsunami-generated sea level height: of **2.28 m** (=1.5×1.55) for a 1964-type Alaska tsunami and **1.14 m** (=1.5×0.76 m) for a Model A-type CSZ tsunami. The total effective wave heights in that case will be:

	Alaska	CSZ
Total (RCP2.6)	**5.04 m**	**3.90 m**
Total (RCP4.5)	**5.06 m**	**3.92 m**
Total (RCP8.5)	**5.18 m**	**4.04 m**

All predictions are for the year 2100; for 2200 we need to add ~**0.95 m** for RCP4.5 and **1.4 m** for RCP8.5.

6. DISCUSSION AND CONCLUSIONS

Large segments of the British Columbia coast are susceptible to floods produced by trans-oceanic tsunamis. Additional factors to consider for this area, as well as other coastal regions of British Columbia, are Global Sea Level Rise and vertical tectonic land motions. The main focus of the present study was the tsunami risk to the Seal Cove Coast Guard Station under projected sea level rise conditions. Seal Cove is located adjacent to Prince Rupert, British Columbia, Canada, close to southeastern Alaska. The study begins with an examination of the general historical information on tsunamis observed within Prince Rupert Harbour, the results of numerical modelling by *Fine et al.* [2018a,b] of two potentially most dangerous seismically generated tsunamis (a 1964-type Alaska and a 1700-type Cascadia Subduction Zone tsunami), and their risk for the study region, specified by taking into account the vertical motion of the west coast and climatic-induced sea level rise.

Prince Rupert has one of the world-longest tsunami measurement periods: from 1909 to 2021. However, during this period, only nine tsunamis were observed at this station. One of them (1963 Graham Island), is a “tsunami of unknown origin” (probably atmospherically-induced), while all others are seismically generated, mostly related to the major trans-oceanic tsunamis occurred in the Pacific Ocean. Five of these tsunamis are associated with great historical events: the 1938 Shumagin Islands (M_w 8.3); 1952 Kamchatka (M_w 9.0); 1957 Aleutian Islands (M_w 8.6); 1960 Chile (M_w 9.5) and 1964 Alaska (M_w 9.2) earthquakes. These tsunamis were recorded by “pen-and-paper” tide gauges; to estimate the tsunami parameters the corresponding records were carefully digitized. Three more tsunamis; 2010

Chile (M_w 8.8); 2011 Tohoku (M_w 9.1) and 2012 Haida Gwaii (M_w 7.7) were recorded by precise digital instruments.

Of the eight recorded events, only the 1964 Alaska "Good Friday" event generated tsunami waves that were hazardous to Prince Rupert: the maximum recorded trough-to-crest wave height at this site was h_{tsu} = 271 cm (maximum amplitude above tidal level was 132 cm); the tsunami caused significant damage in and around the vicinity of the city [*Rabinovich et al.*, 2019]. All other recorded seismic tsunamis, including those generated by 1952, 1960 and 2011 earthquakes with M_w = 9.0-9.5, produced tsunami with $h_{tsu} \leq 40$ cm. It is evident that only great Alaska earthquakes, with M_w = 9.0-9.3, is a major threat to the Prince Rupert/Seal Cove area.

Another, important tsunami threat for the coast of northern British Columbia is Cascadia Subduction Zone (CSZ) earthquakes [cf. *Leonard et al.*, 2014]. The Great CSZ earthquake of 26 January 1700, which had an estimated magnitude M_w = 9.0, generated a major trans-oceanic tsunami that, according to paleotsunami studies, strongly affected the outer coast of Vancouver Island [cf. *Clague et al.*, 2000, 2003]. No paleotsunami studies have yet been made in the area of Prince Rupert; therefore, numerical modeling is the only source of information on possible tsunami wave heights in this area produce by the 1700-type CSZ tsunami.

These two types of tsunami, the 1964-type Alaska and the 1700-type CSZ, were numerically simulated by *Fine et al.* [2018a,b] to estimate the tsunami risk for the vicinity of the Seal Cove Coast Guard Station. Their model was based on a finite-difference nested-grid formulation of the linear shallow-water equations and is similar to well-known tsunami models, TUNAMI and COMCOT [*Imamura*, 1996; *Liu et al.*, 1998; *Imamura et al.*, 2006]. For both the 1964 Alaska and 1700 CSZ events, *Fine et al*. [2018a, b] used a series of four nested grids; Grids 2-4 were the same for both projects, while Grid 1A for the 1964 Alaska project was different from Grid 1B for the 1700 CSZ project. These grids made it possible to achieve high spatial resolution and to accurately resolve the reflection and transformation of the tsunami waves in Dixon Entrance and on the northern shelf of Hecate Strait adjacent to the Prince Rupert/Seal Cove area.

The modelling results for the 1964-type Alaska tsunami gave the following main results: (1) The tsunami at the Seal Cove Coast Guard Facility will reach **1.55 m** above the tidal level

or (1.55 m + 2.32 m) = **3.87 m** above mean sea level at the time of the wave arrivals, with the third wave being the highest wave; (2) tsunami wave periods will range from 70 to 105 min; and (3) the distribution of tsunami wave amplitudes in Prince Rupert and Seal Cove harbour and the vicinity of the Seal Cove Coast Guard Facility will be nearly spatially uniform [*Fine et al.*, 2018a].

For a 1700-type CSZ tsunami, *Fine et al.* [2018b] used two models of the earthquake rupture type and tsunami source region: Model A is a buried rupture and Model B a splay-faulting rupture. Model A generates higher waves in the Seal Cove area than Model B and, therefore, can be considered as the "worst case scenario" for the region. The main findings of *Fine et al.* [2018b] are the following: (1) The maximum wave amplitudes at the Coast Guard Base will be **0.76 m** (Model A) and **0.65 m** (Model B) above the tidal level at the time of the event, or (0.76+2.32) m = **2.08 m** for Model A and (0.65+2.32) m = **1.97m** for Model B above the mean sea level at the time of the event; (2) the sixth-crest wave will be the highest wave; (3) tsunami wave periods will be approximately the same as for the 1964-type Alaska tsunami: 70 - 105 min; and (4) tsunami wave amplitudes will be nearly spatially uniform throughout Prince Rupert Harbour and Seal Cove Harbour.

Because many of the details of future possible tsunamis remain unknown, including the tidal level at the time of the event, seasonal variations, uncertainties in the earthquake source distribution, possible storm surge or other oceanic events, *Fine et al.* [2018a,b] recommend that a safety factor of 50% be added giving an estimated tsunami-generated sea level height of **2.28 m** =1.5×1.55 m for a 1964-type Alaska tsunami and **1.14 m** =1.5×0.76 m for a Model A-type CSZ tsunami (the worst-case scenario). The MHHW = **2.32 m** should be added to these values to estimate possible tsunami wave height relative to mean sea level.

Global sea level rise is an important additional factor influencing the tsunami risk for the British Columbia coast, including the Prince Rupert/Seal Cove area. Recently, the United Nations' Intergovernmental Panel on Climate Change (IPCC) published several reports and adopted Representative Concentration Pathway (RCP) scenarios for greenhouse gas concentration trajectories: **RCP2.6**, **RCP4.5**, **RCP6**, and **RCP8.5**. Based on these scenarios, *James et al.* [2015; 2021] and *Lemmen et al.* [2016] prepared special reports considering sea level rise in western Canada, focussing on the coast of British Columbia, which take into

account both global climatic sea level rise and vertical tectonic motions for *low, moderate* and *high* global sea level rise scenarios. All these findings allowed us to estimate the general spatial structure of projected relative sea-level changes on the coast of northern British Columbia and, specifically, in the Seal Cove region.

The following RCP-dependent apply to sea level rises at the Seal Cove Coast Guard Station:

- *Low* (RCP2.6): 0.184 m (2050), 0.44 m (2100) and 0.80 m (2200);
- *Moderate* (RCP4.5): 0.205 m (2050), 0.46 m (2100) and 0.95 m (2200);
- *High* (RCP8.5): 0.199 m (2050), 0.58 m (2100) and 1.40 m (2200).

Lastly, we combine the results of the numerical modelling of the 1964-type Alaska tsunami and the 1700-type CSZ tsunami with the expected sea level changes in Seal Cove for 2100 to obtain the following tsunami wave heights relative to the tide at the time of the event:

	Alaska	CSZ
Low (RCP2.6)	(1.55 m + 0.44 m) = **1.99 m**	(0.76 m + 0.44 m) = **1.20 m**
Moderate (RCP4.5)	(1.55 m + 0.46 m) = **2.01 m**	(0.76 m + 0.46 m) = **1.22 m**
High (RCP8.5)	(1.55 m + 0.58 m) = **2.13m**	(0.76 m + 0.58 m) = **1.34 m**

Because many of the details of future possible tsunamis remain unknown, both in local background oscillations and the earthquake source parameters, *Fine et al.* [2018a,b] recommend addition of a safety factor of 50% to the estimated tsunami-generated sea level heights. The total effective wave heights in that case will be:

	Alaska	CSZ
Total (RCP2.6)	**5.04 m**	**3.90 m**
Total (RCP4.5)	**5.06 m**	**3.92 m**
Total (RCP8.5)	**5.18 m**	**4.04 m**

All these predictions are for 2100; for 2200 we need to add ~**0.85 m** for RCP4.5 and **1.2 m** for RCP8.5.

Finally, *James et al*. [2021] specify an *enhanced RCP8.5 scenario* for the projected sea level at 2100 that provides an additional **65 cm** of global sea-level rise relative to the median projection of RCP8.5 arising from possible melting of the West Antarctic Ice Sheet.

REFERENCES

AECOM (2013), *Modelling of Potential Tsunami Inundation Limits and Run-Up*, Capital Regional District, Project No. 6024 2933, 36 p.

Atwater, B.F., Musumi-Rokkaku, S., Satake, K., Tsuji, Y., Ueda, K., and Yamaguchi, D.K., (2005), *The Orphan Tsunami of 1700—Japanese Clues to a Parent Earthquake in North America*, U.S. Geological Survey Professional Paper No. 1707, 133 p.

Becker, J.J., Sandwell, D.T. Smith, W.H.F. et al. (2009), Global Bathymetry and Elevation Data at 30 Arc Seconds Resolution: SRTM30_PLUS, *Marine Geodesy*, 32(4), 355-371, doi: 10.1080/01490410903297766

Bornhold, B.D. and Thomson, R.E. (2013), Trends in sea level; In *Climate Trends and Projections for the Pacific Large Aquatic Basin*, (ed.) J.R. Christian and M.G.G. Foreman; Canadian Tech. Rep. Fish. Aquatic Sci. No. 3032, 113 p.

Bush, E. and Lemmen, D.S., editors (2019), *Canada's Changing Climate Report*; Government of Canada, Ottawa, ON. 444 p. Available online at: https://changingclimate.ca/CCCR2019/.

Caldwell, R.J., Taylor, L.A., Eakins, B.W., Carignan, K.S., and Collins, S.V. (2012), *Digital elevation models of Juneau and Southeast Alaska—Procedures, data sources and analysis*, National Geophysical Data Center, NOAA Tech. Mem. NESDIS NGDC-53, 66 p.

Cassidy, J.F., Rogers, G.C., and Hyndman, R.D., (2013), An overview of the October 28, 2012 M_w 7.7 earthquake in Haida Gwaii, Canada: a tsunamigenic thrust event along a predominantly strike-slip margin, *Pure and Applied Geophysics*, 171; doi: 10.1007/s00024-014-0775-1.

Cherniawsky, J.Y., Titov, V.V., Wang, K., and Li, J.-Y. (2007), Numerical simulations of tsunami waves and currents for southern Vancouver Island from a Cascadia megathrust

earthquake, *Pure and Applied Geophysics,* 164 (2-3), 465-492, doi:10.1007/s00024-006-0169-0.

Cheung, K.F., Wei, Y., Yamazaki, Y., and Yim, S.C.S. (2011), Modeling of 500-year tsunamis for probabilistic design of coastal infrastructure in the Pacific Northwest, *Coastal Engineering*, 58, 970–985.

Clague, J.J., Bobrowsky, P.T., and Hutchinson, I., (2000), A review of geological records of large tsunamis at Vancouver Island, British Columbia, and implications for hazard, *Quaternary Science Reviews*, 19, 849-863.

Clague, J.J., Munro, A., and Murty, T.S. (2003), Tsunami hazard and risk in Canada, *Natural Hazards,* 28(2-3), 407-434.

Cloud, H., (1963), *Part of U.S. Earthquakes*. Coastal and Geodetic Survey, p.46.

Dunbar, D., LeBlond, P., and Murty, T.S. (1991), Evaluation of tsunami amplitudes for the Pacific coast of Canada. *Progress in Oceanography,* 26, 115-177.

Fine, I.V., Cherniawsky, J.Y., Rabinovich, A.B., and Stephenson, F.E. (2008), Numerical modeling and observations of tsunami waves in Alberni Inlet and Barkley Sound, British Columbia, *Pure and Applied Geophysics*, 165, (11/12), 2019-2044.

Fine, I.V., Kulikov, E.A., and Cherniawsky, J.Y. (2013), Japan's 2011 tsunami: Characteristics of wave propagation from observations and numerical modelling. *Pure and Applied Geophysics*, 170, 1295-1307.

Fine, I.V., Cherniawsky, J.Y., Thomson, R.E., Rabinovich, A.B., Krassovski, M.V. (2015), Observations and numerical modeling of the 2012 Haida Gwaii tsunami off the coast of British Columbia, *Pure and Applied Geophysics*, 172 (3-4), 699-718; doi: 10.1007/s00024-014-1012-7.

Fine, I.V., Thomson, R.E., Lupton, L.M., and Mundschutz, S., (2018a*), Numerical modelling of an Alaska 1964-type tsunami at the Canadian Coast Guard Base in Seal Cove, British Columbia*. Can. Tech. Rep. Hydrogr. Ocean Sci. 321; 978-0-660-24928-5.

Fine, I.V., Thomson, R.E., Lupton, L.M., and Mundschutz, S., (2018b), *Numerical modelling of a Cascadia Subduction Zone tsunami at the Canadian Coast Guard Base in Seal Cove, British Columbia*. Can. Tech. Rep. Hydrogr. Ocean Sci. 322; 978-0-660-25113-4.

Gao, D. (2016), *Defining Megathrust Tsunami Sources at Northernmost Cascadia Using Thermal and Structural Information*. Master of Science Thesis, School of Earth and

Ocean Sciences, The University of Victoria; https://dspace.library.uvic.ca/handle/1828/7435

Hausfather, Z. and Peters, G.P. (2020), Emissions – the 'business as usual' story is misleading, *Nature*, 577, 618-620.

Imamura, F. (1996), Review of tsunami simulation with a finite difference method. In: *Long-Wave Run-up Models* (Eds. H. Yeh, P. Liu, and C. Synolakis), World Scientific, Singapore, pp. 25–42.

Imamura, F., Yalciner, A.C., and Ozyurt, G. (2006), *Tsunami Modelling Manual (TUNAMI Model)*; http://www.tsunami.civil.tohoku.ac.jp/hokusai3/J/projects/manual-ver-3.1.pdf

James, T.S., Henton, J.A., Leonard, L.J., Darlington, A., Forbes, D.L., and Craymer, M. (2014). *Relative Sea-level Projections in Canada and the Adjacent Mainland United States*; Geological Survey of Canada, Open File 7737, 72 p. doi:10.4095/295574.

James, T.S., Henton, J.A., Leonard, L.J., Darlington, A., Forbes, D.L., and Craymer, M. (2015). *Tabulated Values of Relative Sea-Level Projections in Canada and the Adjacent Mainland United States*, Geological Survey of Canada, Open File 7942, 81 p. doi:10.4095/297048.

James, T.S., Robin, C., Henton, J.A., and Craymer, M. (2021). *Relative Sea-Level Projections for Canada Based on the IPCC Fifth Assessment Report and the NAD83v70VG National Crustal Velocity Model*, Geological Survey of Canada, Open File 8764, 1 .zip file, https://doi.org/10.4095/327878.

Johnson, J.M., Satake, K., Holdahl, S.R., and Sauber, J. (1996), The 1964 Prince William Sound earthquake – joint inversion of tsunami waveforms and geodetic data, *Journal of Geophysical Research*, 101 (B1), 523-532.

Lander, J.F. (1996), *Tsunamis Affecting Alaska*, 1737-1996. USDC/NOAA, Boulder, CO, USA, 195 p.

LeBlond, P.H., Dunbar, D., and Murty, T.S. (1989), Maximum tsunami amplitudes and associated currents on the coast of British Columbia, *Science of Tsunami Hazards*, 7(1). 3-44.

Lemmen, D.S., Warren, F.J., James, T.S., and Mercer Clarke, C.S.L., editors (2016), *Canada's Marine Coasts in a Changing Climate*; Government of Canada, Ottawa, ON, 274p.

Leonard, L.J. and Bednarski, J.M. (2014), Field survey following the 27 October 2012 Haida Gwaii tsunami. *Pure and Applied Geophysics*, 171, 3467-3482; doi: 10.1007/s00024-014-0792-0.

Leonard, L.J., Rogers, G.C., and Mazotti, S., (2014), Tsunami hazard assessment of Canada, *Natural Hazards*, 70, 237-274.

Liu, P. L.-F., Woo, S-B., and Cho, Y-S. (1998), *Computer programs for tsunami propagation and inundation*. Technical report, Cornell University.

Matheron, G. (1963), Principles of geostatistics. *Economic Geology*, 58, 1246–1266.

Meinshausen, M. et al. (2011), The RCP greenhouse gas concentrations and their extensions from 1765 to 2300 (open access), *Climatic Change*, 109(1–2), 213–241; doi:10.1007/s10584-011-0156-z

Moss, R. et al. (2008). *Towards New Scenarios for Analysis of Emissions, Climate Change, Impacts, and Response Strategies*. Geneva: Intergovernmental Panel on Climate Change, 132 p.

Myers, E.P. and Baptista, A.M. (2001), Analysis of factors influencing simulations of the 1993 Hokkaido Nansei-Oki and 1964 Alaska Tsunamis. *Natural Hazards*, 23 1-28; https://doi.org/10.1023/A:1008150210289

Ng, M.K.-F., LeBlond, P.H., and Murty, T.S. (1991), Simulation of tsunamis from great earthquakes on the Cascadia Subduction Zone, *Science*, 250, 1248–1251.

NOAA (2017), British Columbia, 3 arc-second MSL DEM. https://www.ngdc.noaa.gov/dem/squareCellGrid/download/4956. Last access on 11.10.2017.

Oppenheimer, M. and Glavovic, B. (Lead authors) (2019*), Sea Level Rise and Implications for Low Lying Islands, Coasts and Communities. Chapter 4. In: IPCC Special Report on the Ocean and Cryosphere in a Changing Climate (SROCC)*, https://www.ipcc.ch/reports/

Prince Rupert Daily News (1964), Newspaper articles for March 30 – April 7, 1964.

Rabinovich, A.B. and Stephenson, F.E. (2004), Longwave measurements for the coast of British Columbia and improvements to the tsunami warning capability, *Natural Hazards,* 32(3), 313-343.

Rabinovich, A.B., Thomson, R.E., and Stephenson, F.E., (2006), The Sumatra tsunami of 26 December 2004 as observed in the North Pacific and North Atlantic oceans*, Surveys in Geophysics*, 27, 647-677.

Rabinovich, A.B., Thomson, R.E., and Fine, I.V., (2013), The 2010 Chilean tsunami off the west coast of Canada and the northwest coast of the United States, *Pure and Applied Geophysics*, 170, 1529-1565, doi: 10.1007/s00024-012-0541-1.

Rabinovich, A.B., Thomson, R.E., Lupton, L.M., and Mundschutz, S. (2019a), *Historical Tsunamis at the Seal Cove and Victoria Canadian Coast Guard Stations, British Columbia*. Can. Tech. Rep. Hydrogr. Ocean Sci. 325, Fisheries and Oceans Canada, Institute of Ocean Sciences, Sidney, BC.

Rabinovich, A.B., Thomson, R.E., Krassovski, M.V., Stephenson, F.E., and Sinnott, D.C. (2019b), Five great tsunamis of the 20th century as recorded on the coast of British Columbia, *Pure and Applied Geophysics*, 176 (7), 2887-2924; doi: 10.1007/s00024-019-02133-3.

Rabinovich, A.B. and Thomson, R.E. (2020), *Effect of Global Sea Level Rise over the near, Intermediate and Long-Term on Extreme Longwave Motions on IOS (Patricia Bay) and PBS (Nanaimo)*, Unpublished report, Fisheries and Oceans Canada, Institute of Ocean Sciences, Sidney, BC.

Robin, C.M.I., Craymer, M., Ferland, R., James, T.S., Lapelle, E., Piraszewski, M., and Zhao, Y. (2020), *NAD83v70VG: A New National Crustal Velocity Model for Canada*; Geomatics Canada, Open File 0062, 1. zip file. https://doi.org/10.4095/327592

Rogelj, J., Meinshausen, M., and Knutti, R. (2012), Global warming under old and new scenarios using IPCC climate sensitivity range estimates, *Nature Climate Change*, Vol.2, p. 248–253; doi:10.1038/NCLIMATE1385.

Satake, K., Shimazaki, K., Tsuji, K., and Ueda, K. (1996), Time and size of a giant earthquake in Cascadia earthquake inferred from Japanese tsunami records of January 1700, *Nature*, 379, 246–249.

Spaeth, M.G. and Berkman, S.C., (1967), *The Tsunami of March 28, 1964, as Recorded at Tide Stations*, ESSA Technical Report C&GS 33, Rockville, Md, 86 p.

Stephenson, F.E., Rabinovich, A.B., Solovieva, O.N., Kulikov, E.A., and Yakovenko, O.I., (2007), *Catalogue of Tsunamis, British Columbia, Canada: 1700-2007*. Preprint. Shirshov Inst. Oceanology, RAS, Moscow, 134 p.

Stephenson F.E. and Rabinovich, A.B. (2009), Tsunamis on the Pacific coast of Canada recorded in 1994-2007, *Pure and Applied Geophysics* 166(1/2), 177-210.

Suito, H. and Freymueller, J.T. (2009), A viscoelastic and afterslip post seismic model for the 1964 Alaska earthquake. *Journal of Geophysical Research*, 114, B11404, doi:10.1029/2008JB005954.

Suleimani, E.N. (2011), *Numerical Studies of Tectonic and Landslide-Generated Tsunamis Caused by the 1964 Great Alaska Earthquake*, University of Alaska Fairbanks, Ph.D. Thesis, 181 p.

Suleimani, E.N., Nicolsky, D.J., and Koehler, R.D. (2013), *Tsunami Inundation Maps of Sitka, Alaska*, Report of Investigations 2013-3, State of Alaska, Department of Natural Resources, Division of Geological and Geophysical Surveys, Fairbanks, AK, 76 p. doi:10.14509/26671.

Thomson, R. E. (1981), *Oceanography of the British Columbia Coast*. Can. Special Pub. Fish. Aquat. Sci., 56. Ottawa, 291 p.

Thomson, R.E., Bornhold, B.D., and Mazzotti, S. (2008), *An Examination of the Factors Affecting Relative and Absolute Sea Level in Coastal British Columbia*; Can. Tech. Rep. Hydrogr. Ocean Sci. 260, 49 p.; http://www.dfo-mpo.gc.ca/Library/335209.pdf

Thomson, R., Fine, I., Rabinovich, A., Mihály, S., Davis, E., Heesemann, M., and Krassovski, M. (2011), Observation of the 2009 Samoa tsunami by the NEPTUNE-Canada cabled observatory: Test data for an operational regional tsunami forecast model, *Geophysical Research Letters*, 38, L11701, doi:10.1029/2011GL046728.

Wang, K., Wells, R., Mazzotti, S., Hyndman, R.D., and Sagiya T. (2003), A revised dislocation model of interseismic deformation of the Cascadia Subduction Zone, *Journal of Geophysical Research*, 108(B1), doi:10.1029/2001JB001227.

Wang, K., and Tréhu, A.M. (2016), Invited review paper: Some outstanding issues in the study of great megathrust earthquakes—The Cascadia example, *Journal of Geodynamics*, 98, 1-18.

Wang, K., Thomson R.E., Rabinovich, A.B., Fine, I.V., and Insua, T.L. (2020), The 2018 Alaska-Kodiak tsunami off the west coast of North America: A rare midplate tsunamigenic event. *Pure and Applied Geophysics*, 177(3), 1347-1378; doi.org/10.1007/s00024-019-02427-x.

Wang, P-L., Engelhart, S.E., Wang, K., Hawkes, A.D., Horton, B.P., Nelson, A.R., and Witter, R.C. (2013), Heterogeneous rupture in the Great Cascadia earthquake of 1700 inferred from coastal subsidence estimates. *Journal of Geophysical Research,* 118, 2460-2473.

Weart, S. (2011), *International Cooperation: Democracy and Policy Advice (1980s). The Discovery of Global Warming*. American Institute of Physics.

Weyant, J., Azar, C., Kainuma, M. et al. (2009), *Report of 2.6 Versus 2.9 Watts/m2. RCPP Evaluation Panel (PDF)*. Geneva, Switzerland: IPCC Secretariat.

Whitmore, P.M. (1993), Expected tsunami amplitudes and currents along the North American coast for Cascadia Subduction Zone earthquakes, *Natural Hazards*, 8, 59–73.

Wigen, S.O. (1983), Historical studies of tsunamis at Tofino, Canada, in *Tsunamis – Their Science and Engineering*, edited by K. Iida and T. Iwasaki, Terra Sci. Publ. Comp., Tokyo, Japan, 105-119.

Wigen, S.O., and White, W.R.H. (1964), *Tsunami of March 27-29, 1964, West Coast of Canada*, Dept. Mines Techn. Surv., Victoria, BC, Canada, 12 p.

Witter, R.C., Zhang, Y.J., Wang, K. et al. (2013), Simulated tsunami inundation for a range of Cascadia megathrust earthquake scenarios at Bandon, Oregon, USA, *Geosphere*, 9(6), 1783-1803, doi:10.1130/GES00899.1